

ULTRA-WIDEBAND SOA FIBRE LASER

NOR AHYA BINTI HASSAN

**DISSERTATION SUBMITTED IN FULFILLMENT
OF
THE REQUIREMENTS FOR THE DEGREE OF
MASTER OF SCIENCE**

**DEPARTMENT OF PHYSICS
FACULTY OF SCIENCE
UNIVERSITY OF MALAYA
KUALA LUMPUR**

2015

UNIVERSITI MALAYA

ORIGINAL LITERARY WORK DECLARATION

Name of Candidate: **NOR AHYA BINTI HASSAN** I/C/Passport No: **860405-23-6688**

Registration/Matric No.: **SGR090096**

Name of Degree: **MASTER OF SCIENCE**

Title of Project Paper/Research Report/Dissertation/Thesis ("this Work"):

"ULTRA-WIDEBAND SOA FIBER LASER"

Field of Study: **PHOTONICS**

I do solemnly and sincerely declare that:

- (1) I am the sole author/writer of this Work,
- (2) This Work is original,
- (3) Any use of any work in which copyright exists was done by way of fair dealing and for permitted purposes and any excerpt or extract from, or reference to or reproduction of any copyright work has been disclosed expressly and sufficiently and the title of the Work and its authorship have been acknowledged in this Work,
- (4) I do not have any actual knowledge nor do I ought reasonably to know that the making of this work constitutes an infringement of any copyright work,
- (5) I hereby assign all and every rights in the copyright to this Work to the University of Malaya ("UM"), who henceforth shall be owner of the copyright in this Work and that any reproduction or use in any form or by any means whatsoever is prohibited without the written consent of UM having been first had and obtained,
- (6) I am fully aware that if in the course of making this Work I have infringed any copyright whether intentionally or otherwise, I may be subject to legal action or any other action as may be determined by UM.

(Candidate Signature)

Date:

Subscribed and solemnly declared before,

Witness's Signature

Date:

Name **PROFESSOR DR HARITH AHMAD**

Designation

Witness's Signature

Date:

Name **PROFESSOR DR SULAIMAN WADI HARUN**

Designation

ABSTRACT

A comprehensive study has been conducted on an ultra-wideband semiconductor optical amplifier (SOA) for the generation of ultra-wideband fibre lasers of various attributes throughout this dissertation. The fundamental characteristics of the ultra-wideband SOA such as the gain and noise figure (NF) are successfully investigated by utilizing the conventional method of measurement and described in the earlier part of the thesis. A result of high gain with small NF drawbacks and coverage of three communication bandwidth regions of more than 120 nm, of short (S-) band, conventional (C-) band and long (L-) band is achieved. The ultra-wide band coverage of the telecommunication bandwidth has made the ultra-wideband SOA a promising candidate to reduce dependency on the costly rare earth doped fibres that dominates the communication industry nowadays. The characterization technique of double-pass configuration of the ultra-wideband SOA also has attained attractive results on gain and NF values. This characterization is crucial in later experiments regarding ultra-wideband SOA fibre laser generation.

The ultra-wideband fibre lasers are realized by utilizing three experimental configurations; by using arrayed-waveguide grating (AWG), by using three wavelength selective filters of fibre Bragg gratings (FBGs), and by applying nonlinear effect in the optical fibre of stimulated Brillouin scattering (SBS) effect. The method using AWG produces a 16-channel system of an ultra-wideband multi-wavelength SOA fibre laser. The occurrence of a single wavelength signal of every S-, C- and L-band simultaneously for every selected channel has been the main highlight of this laser configuration. Other than that, this configuration also has the favourable factor of wavelength tunability within the aforementioned bandwidth range.

The method that deploys three FBGs, representing S-, C- and L-band as the wavelength selective filters, produces three simultaneous signal wavelengths with high average signal-to-noise ratio (SNR) at the maximum drive current of ultra-wideband SOA. The proposed system would find many applications where a wide-band and stable laser source is crucial, such as in communications and sensing. The third method deployed is by applying nonlinear effects into a high nonlinear fibre of dispersion compensating fibre (DCF). This experimental configuration yields three sets of multi-wavelength laser comb of S-, C- and L-band simultaneously, with about 0.08 nm wavelength spacing (equal to 10 GHz in frequency frame) in each wavelength comb. This system has the advantage of the ability to supply many wavelength signals at one time, which is highly demanded in the dense wavelength division multiplexing (DWDM) system application.

All the three ultra-wideband SOA fibre laser systems are tested for stability tests of 70 minutes duration running time. This is to prepare for a stable fibre laser system into the network applications.

ABSTRAK

Suatu kajian yang terperinci tentang penguat semikonduktor optikal (SOA) berjalur ultra-lebar telah dijalankan dengan bertujuan untuk menghasilkan laser gentian berjalur ultra-lebar dengan pelbagai pencirian. Ciri-ciri asas SOA berjalur ultra-lebar seperti nilai kuatan dan angka hingar (NF) telah berjaya dikenalpasti pada bahagian awal tesis, dengan menggunakan teknik pengukuran konvensional. Hasil nilai kuatan tinggi dengan nilai NF yang rendah, yang merangkumi kesemua tiga jalur komunikasi pendek (S-), konvensional (C-) dan panjang (L-) telah dicapai. Rangkuman jalur telekomunikasi ultra-lebar telah menjadikan SOA berjalur ultra-lebar sebagai calon yang amat sesuai untuk menggantikan kegunaan gentian berdopan nadir-bumi yang berkos tinggi, yang mendominasi industri komunikasi hari ini. Teknik pencirian konfigurasi laluan-sekali ganda SOA berjalur ultra-lebar telah memperoleh hasil nilai kuatan dan NF yang memberangsangkan. Pencirian ini amat penting di dalam eksperimen seterusnya untuk menghasilkan gentian laser SOA berjalur ultra-lebar.

Gentian laser berjalur ultra-lebar dihasilkan dengan tiga teknik konfigurasi eksperimen; dengan menggunakan parutan pandu gelombang tersusun (AWG), dengan menggunakan tiga penapis gelombang terpilih iaitu gentian parutan Bragg (FBG), dan dengan mengaplikasikan kesan tak-linear kepada gentian optik iaitu kesan Brillouin dirangsang (SBS). Cara pertama menggunakan AWG telah menghasilkan sebuah sistem gentian laser multi-gelombang SOA berjalur lebar yang mempunyai 16 saluran. Penghasilan satu isyarat gelombang di setiap jalur S-, C- dan L- secara serentak, pada setiap saluran telah menjadi kemuncak utama dalam eksperimen ini. Selain itu, konfigurasi ini juga mempunyai sifat gelombang boleh laras dalam lingkungan kawasan lebar-jalur yang telah disebutkan.

Cara seterusnya yang menggunakan tiga FBG untuk setiap jalur S-, C- dan L- sebagai penapis gelombang terpilih, telah menghasilkan tiga isyarat gelombang dengan purata SNR yang tinggi pada arus panduan tertinggi SOA. Sistem yang dicadangkan akan dapat digunakan dengan meluas kerana berkepentingan dalam penghasilan sumber laser yang stabil dan berjalur lebar, seperti dalam komunikasi ataupun sensing. Cara ketiga adalah dengan mengenakan kesan tak-linear kepada medium gentian bersifat tak-linear yang tinggi iaitu gentian penanggungan penyebaran (DCF). Konfigurasi eksperimen ini menghasilkan tiga set laser multi-gelombang pada jalur S-, C- dan L- secara serentak, dengan jarak gelombang kira-kira 0.08 nm (bersamaan 10 GHz dalam rangka frekuensi) di setiap set. System ini mempunyai kelebihan untuk membekalkan banyak isyarat gelombang pada satu masa, dimana ia amat diperlukan di dalam kegunaan system pemultipleksan gelombang padat (DWDM).

Kestabilan ketiga-tiga gentian laser SOA berjalur-lebar telah diuji dengan menjalankan ujian kestabilan selama 70 minit. Ini adalah untuk menyediakan system gentian laser yang stabil ke dalam kegunaan rangkaian.

ACKNOWLEDGEMENTS

Alhamdulillah robbil ‘alameen,

All praises to Almighty Allah, The Lord of the world and its content, The Magnificent, and The Most Merciful.

My gratitude goes to my supervisors; Prof. Dr. Harith bin Ahmad and Prof. Dr. Sulaiman bin Wadi Harun, for their never ending support and helps during the challenging process of the research works, as well as the process of completing this dissertation. Without their helpful advices and encouragement, none of the research and dissertation could be successfully realized.

Special and heartfelt appreciation goes to my beloved parents, Mr. Hassan Darisoon and Mrs. Halimahton Ahmad for their incomparable love and kind understanding, as well as being my backbones and my persistent supporters through the ups and downs of the completing process of the research and this dissertation. Without their continuous encouragement and faith in my ability, I may never be able to finish, thus to successfully complete my Masters Degree studies in any way.

Last but not least, I also would like to thank my peer friends in the Photonics Research Centre of University of Malaya (PRC UM) for the helps and patience during the laboratory works, etc. Many thanks to Dr. Mohd Zamani Zulkifli whom had always be my mentor during the conduction of research, and the accomplishment of this dissertation.

Thank you very much.

CONTENTS

Original Literary Work Declaration	i
Abstract	ii
Abstrak	iv
Acknowledgements	vi

CHAPTER 1 : INTRODUCTION

1.1	Fibre Optics Communication	1
1.2	Bandwidth Demand in the Wavelength Division Multiplexing (WDM) System	2
1.3	SOA Based Ultra-Wideband Source	3
1.4	Research Objectives	6
1.5	Research Methodology	6
1.6	Thesis Overview	9

CHAPTER 2 : THEORETICAL BACKGROUND

2.1	Introduction	14
2.2	Semiconductor Optical Amplifier (SOA) and Its Structure	15
2.3	Principles of Amplification in SOA	19
2.3.1	Spontaneous and Stimulated Transition Rates	23
2.3.2	Carrier Density Rate Equations	25
2.3.3	Small Signal Gain	27
2.3.4	Saturation Current, Saturation Power & Bandwidth	29
2.3.5	Noise Figure and Amplified Spontaneous Emission (ASE)	31
2.3.6	Polarization Dependent Gain Effect	33
2.4	Applications of Ultra-Wideband SOAs	34
2.4.1	Ultra-Wideband SOA Fibre Laser	34

2.5	Wavelength Selective Filtering	36
2.5.1	Fibre Bragg Gratings (FBGs)	37
2.5.2	Arrayed-Waveguide Gratings (AWGs)	39
2.6	Nonlinear Effects in Optical Fibres	41
2.6.1	Stimulated Brillouin Scattering (SBS)	42
2.7	Summary	44

CHAPTER 3 : CHARACTERIZATION OF ULTRA-WIDEBAND SOA

3.1	Introduction	51
3.2	Ultra-Wideband SOA Characterization	52
3.2.1	Alphion SAS26p Ultra-wideband SOA and Experimental Setup	54
3.2.2	Amplified Spontaneous Emission of Ultra-Wideband SOA	56
3.2.3	Ultra-Wideband SOA Gain Bandwidth	57
3.2.4	Small Signal Gain and Gain Saturation Effect	60
3.2.5	Noise Figure of Ultra-Wideband SOA	61
3.2.6	Polarization Dependent Gain Effect of Ultra-Wideband SOA	64
3.2.7	High Gain S-Band SOA with Double Pass Configuration	67
3.3	Summary	71

CHAPTER 4 : ULTRA-WIDEBAND SOA FIBRE LASER GENERATION

4.1	Introduction	76
4.2	Cavity Configurations of SOA Fibre Laser	78
4.3	Ultra-Wideband Switchable SOA Fibre Laser	79
4.3.1	120nm Wideband Switchable SOA Fibre Laser	79
4.4	Multi-Wavelength SOA Fibre Laser	90
4.4.1	Ultra-Wideband SOA Fibre Laser by Using FBGs	90
4.4.2	Multi-Wavelength SOA Brillouin Fibre Laser	96

4.5	Summary	103
-----	---------	-----

CHAPTER 5 : FUTURE WORKS AND CONCLUSION

5.1	Future Works	112
-----	--------------	-----

5.2	Conclusion	113
-----	------------	-----

Appendix 1: Ultra-wideband SOA Data Sheet

Appendix 2: Publications

CHAPTER 1

INTRODUCTION

1.1 : Fibre optics communication

Communications can be broadly defined as the transfer of information from one point to another. In optical fibre communications, this transfer is achieved by using light as the information conveyer. Optical communication systems started two centuries ago when the French engineer Claude Chappe invented the “optical telegraph” in 1790s, which was then followed by the Photophone by Alexander Graham Bell in 1880 [1]. Several people persevered in experimenting with optical communications, including an American Telephone & Telegraph Corp engineer, Norman R. French, who then succeeded and patented the idea of communicating by sending light through pipes in the 1930s [1]. Nobody took optical communications seriously until Theodore Maiman demonstrated the first laser in 1960 [1], for which the first trials were done by sending the laser light through the air. However, it was later found to be not a very good transmission medium due to fog, rain, snow and haze that could block signals, as well as other problems which contribute to the degrading of communication signal.

Fibre optics communications on the other hand is based on the important physics principle that light in a glass medium can carry more information over longer distances than electrical signals can carry in a copper or coaxial medium or radio frequencies through a wireless medium. The glass fibre, combined with improved system electronics, enables fibre to transmit digitized light signals hundreds of kilometres without amplification. Due to few transmission losses, low interference and high bandwidth

potential, optical fibre is an almost ideal transmission medium. It was in 1970, when Corning Incorporated scientists Drs. Robert Maurer, Donald Keck and Peter Schultz created a fibre with attenuation of less than 20dB/km and it was the purest glass ever made at the time. The three scientists' work is recognized as the discovery that led the way to the commercialization of optical fibre technology, which then led to a tremendous advancement for the technology in terms of performance, quality, consistency, and applications. The basic idea of fibre optics communication systems consist of a transmitter, optical fibre and a receiver.

1.2 Bandwidth demand in the wavelength division multiplexing (WDM) system

Due to the increasing demand for data bandwidth that is powered by the tremendous development of the internet, the shifting to optical networking from the existing electrical networking has become the primary focus in this new era of communication. The main advantage of optical fibres is that they can carry high-bandwidth signals over much longer distances than copper. *Bandwidth* is defined by the signal-transmission capacity over a time, and this is highly dependent on the type of signals, the transmitter and receiver, as well as the transmission medium [2]. In other words, bandwidth decides how much information the signal carries over time within a certain length of transmission.

Wavelength division multiplexing (WDM) is a fibre optic transmission technique that employs light wavelengths to transmit data parallel-by-bit or serial-by-character. It is a system where optical multiplexing technology is used to increase bandwidth over existing fibre networks. The system works by combining and transmitting multiple data signals from different sources simultaneously at different wavelengths on the same fibre. Early WDM systems were based on the two low-loss wavelength regions of 1310 nm and

1550 nm, which are generally known as the wideband WDM regions [3]. Research in the beginning of the 1990s brought the development of narrowband WDMs, where 2 to 8 channels are spaced at intervals of about 400 GHz in the 1550 nm window [3, 4]. A system with fewer active wavelengths and larger channel spacings that is used in metropolitan networks is known as coarse WDM (CWDM), whilst a system with larger number of active wavelengths and smaller channel spacings is known as dense WDM (DWDM). The CWDM systems commonly have a spacing of 20 nm or 2500 GHz between channels, covering wavelength from 1310 nm to 1610 nm.

DWDM technology continues to develop in recent years, and current systems have over 20 wavelength channels in a transmission stream. In order to provide many densely spaced channels, DWDM uses temperature-stabilized lasers to maintain the centre wavelength and narrow band filters. For a channel spacing of approximately 0.8 nm, a typical frequency of 100 GHz is achieved, as specified by the international telecommunication union (ITU). Although systems with a capacity of 128 wavelengths on a single fibre are already in the research environment since the early of 21st century, the limits however are still not exactly known [5, 6]. Other than the fact that the CWDM systems cover a broader bandwidth than the DWDM systems do, these system also only require relatively inexpensive un-cooled DFB laser diodes instead of costly temperature-controlled laser sources. The fact that the CWDM's signal wavelengths are further spaced from each other gives an overall advantage to the DWDM systems which are highly capable in providing greater capacity over the same fibre.

1.3 SOA based ultra-wideband source

Semiconductor optical amplifiers (SOAs) are essentially compact devices designed to amplify passing optical signals like EDFAs or other doped fibre amplifiers.

Whilst the doped fibre amplifiers require an optical power of certain wavelengths, e.g. 980 nm or 1480 nm, to generate the stimulated emission process that operates the amplifier, the SOAs however need external electrical current to inject the semiconductor medium to provide a gain; this is defined by amplification per unit length. In this regards, the SOAs are basically laser diodes with very low optical feedback [7]. The first study of SOA itself was carried out around time of the semiconductor laser diodes invention in 1960s, thus there are many similarities observed in the basic operation of those two.

In the early development, SOAs were based on the GaAs homojunction which operated at low temperatures. The emergence of double heterostructure devices spurred more investigation on the SOAs application in optical communication systems. Prior research on SOAs done by Zeidler and Personic in the 1970's was then followed by a more crucial study on the device design and modelling on the 1980's [8]. At first, the studies focused on the AlGaAs SOAs that operate in the 830 nm range, whilst InP/InGaAsP SOAs that operated in 1.3 μm and 1.55 μm designs were done later in the same year. The true-travelling wave SOAs were then realized in line with the advancement of anti-reflection coating technology. This led to further development on the SOA structures, which were designed based on the anti-reflection coated semiconductor laser diodes [9]. These devices, however, exhibited highly gain sensitive polarization due to their asymmetrical waveguide structure, and were improved by utilizing more symmetrical waveguides into the SOAs. The small size of the devices, capability of providing large optical gain, large third-order nonlinearities, and to other functions, have useful benefits in a system [10]. Due to their wide gain spectrum and the viability to be integrated with other optical devices, SOAs emerged as important components for optical networks, especially in the long haul area of optical communication [11]. Moreover, the dominant inhomogeneous broadening property exhibited by the SOAs has been the most important advantage over the conventional

erbium-doped fibre amplifiers (EDFAs) in generating multiple laser output powers in room temperature, thus reducing the effect of mode competition [12-14]. The utilization of SOAs as the gain medium in fibre laser generation has brought forth the realization of the multi-wavelength fibre laser system at normal room temperature [15-17].

In recent years, experiments on attaining SOA-based fibre laser have been carried out [18-21]. However, the band region of the fibre laser systems obtained are limited to the conventional band of communication, which ranges from 1530 nm to 1565 nm wavelength, with the currently used SOAs in telecom systems operating at signal wavelength near 1.3 μm or 1.5 μm . Due to this situation, much research has been exerted to further expand the available transmission band region, mainly to the short band (S-band) of 1460 nm to 1525 nm and to the long band (L-band) of 1570 nm to 1620 nm, by using doped-fibres. Other than the erbium-doped fibre (EDF) which produces amplification in the conventional C-band region and in the L-band region with the condition the EDF having a longer length, thulium- and praseodymium-doped fibre (TDF and PDF) also have amplification potential in the S-band and O-band (1310 nm) regions respectively. These two types of fibre are not in significant commercial use because of their impractical handling limitation. Bismuth-based erbium-doped fibre (Bi-EDF) on the other hand is an alternative to achieve amplification in the L-band region by using a shorter length of EDF.

To date, the only way to supply ultra-wideband gain bandwidth for fibre lasers and amplifiers is by combining different type of doped-fibres into a laser cavity system. For example, embedding a suitable length of EDF, TDF and Bi-EDF in a system configuration is necessary in order to achieve an ultra-wideband of S-, C- and L-band fibre laser or amplifier. The practice of using so many doped fibres to produce a single system of laser sources is indeed very costly and bulky. Moreover, in regards to the

homogeneous broadening property exhibited by the doped-fibres, a multi-wavelength laser source system is far from being realized due to the mode competition effect. Thus, the ultra-wideband SOA is the only eligible candidate to solve this matter. The compact design and the inhomogeneous broadening property that are manifested by the SOA, as well as their lower cost compared to the doped-fibres, have put the SOA as the best option to realize effective ultra-wideband laser sources and amplifiers, and hence this option will be exploited in this research project.

1.4 Research objectives

The primary objectives of this study is to generate a single wavelength in each of three bands of communication; short (S-), conventional (C-) and long (L-) band.

The second objective of this study is to realize a 100 nm range ultra-wideband fibre laser system with a switchable characteristic throughout three band regions of S-, C- and L-band.

The third objective of this study is to attain a stable and dense (with 0.08 nm wavelength spacing) multi-wavelength fibre laser system.

All three objectives will be realized by utilizing an ultra-wideband semiconductor optical amplifier (SOA) as the gain medium. All the steps taken in generating the ultra-wideband SOA fibre laser systems will be discussed in the next part of this chapter.

1.5 Research methodology

To conduct the experiments, the first thing to perform is literature review and acquire an understanding of the theory and the operating principles of SOA. After

completing the reviews, a characterization experiment on SOA is then conducted in order to understand the behaviour of the gain and noise figure (NF) of the gain medium. The results of the gain and NF characteristics are then observed and analysed through each band of S-, C- and L-bands. Aside from the width of the transmitted band of the ultra-wideband SOA, the effect on polarization dependent gain (PDG) will also be verified and analysed. A double pass configuration has also been tested in the study and a publication resulting from this work has been achieved, as listed in Appendix 2.

The next process is to optimize the proposed designs for fibre laser generation. There have been 3 publications on ultra-wideband fibre laser generation by using the ultra-wideband SOA, and these are also listed in Appendix 2 of this thesis. Many techniques developed in this dissertation have also been applied in the area of S-band regions by other members of the research group.

The methodology of the study engaged in this research project is elaborated in Figure 1.1.

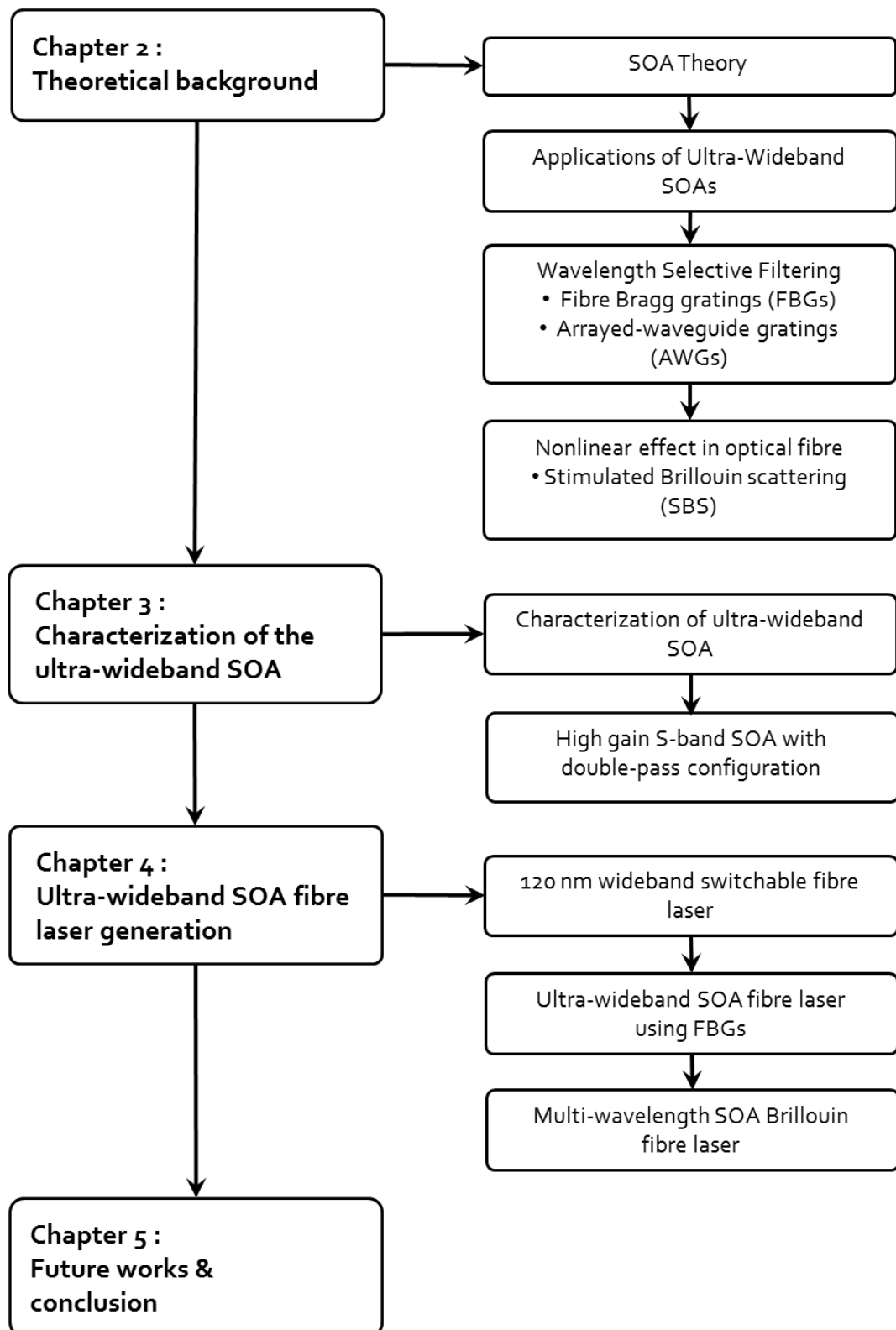


Figure 1. 1 Research methodology of this project study.

1.6 : Thesis overview

This dissertation consists of five chapters. The first chapter will propose a brief introduction to optical fibre technology and its deployment to telecommunication systems in order to assist in solutions to the increasing demand in capacity of network applications. An introduction to the semiconductor optical amplifier (SOA) as a compact and cost-effective gain medium will also be explained in this chapter. Chapter 2 will focus on the theoretical understanding of the physical principles that are utilized throughout the experiments. Thorough theoretical explanations about the amplification processes in the SOA, as well as other optical principles used in the experiments, will be given in this chapter in order to provide further knowledge regarding the proposal of generating ultra-wideband multi-wavelength fibre lasers. Such principles used include wavelength filtering mechanisms of fibre Bragg gratings (FBGs) and arrayed-waveguide grating (AWG), and nonlinear optics of the stimulated Brillouin scattering (SBS) effect.

Chapter 3 will manifest the characterization of the ultra-wideband SOA used in the experiments. The characterization will be performed for the gain and noise figure (NF) measurements for all wavelengths in the range of S-, C- and L-bands, as well as the amplified spontaneous emission (ASE) of the SOA. Other measurements such as small signal gain and saturation effect of the SOA, and polarization gain dependent (PDG) effect will also be done in the characterization experiments. A double-pass configuration will also be demonstrated in order to observe the gain bandwidth behaviour of the ultra-wideband SOA, as referred to number 3 of my journal publication list in Appendix 2.

Chapter 4 of this thesis will demonstrate the generation of ultra-wideband SOA fibre lasers. There are three experiments will be discussed in this chapter in order to achieve the objectives of generating multi-wavelength fibre lasers that cover three bands of S-, C- and L-band. The first two methods will involve the wavelength filtering

mechanisms by utilizing the FBGs and AWGs, whilst the third method will use the nonlinear optic effect of the SBS. The design and architecture of the setups will be thoroughly considered such that the results achieved have significant advantages over those of much previous research. Optimal results are attained by controlling the cavity loss and optimizing the output power emitted by the ultra-wideband SOA, as elaborated in Chapter 4 of this thesis. The significant achievement of obtaining multi-wavelength fibre laser on each S-, C- and L-band has been the main focus in this project for means of meeting the increasing demand in network systems capacity. On the whole, the homogeneous broadening property of the SOA is observed to be the main enabling factor to produce such broad bandwidth for stable, multiple wavelengths fibre laser, with the issue of mode competition is eliminated, in comparison to that obtained when using the conventional erbium-doped fibre amplifier (EDFA).

Lastly, chapter five of this thesis will detail future works and some applications of the generated ultra-wideband SOA fibre lasers. This chapter will also conclude the findings of the research in relation to fulfilling the demand in the network traffic capacity.

REFERENCES

1. J. Hecht, "City of Light: The Story of Fibre Optics", Oxford University Press, New York, 1999.
2. J. Hecht, "Understanding Fibre Optics", 4th Edition, Prentice Hall, USA, 2002.
3. Kavintheran A/L Thambiratnam, "A Multi-wavelength Source based on Sagnac Loop and Semiconductor Optical Amplifier", Master of Science Thesis, University of Malaya, 2007.
4. D. Derickson, "Fibre Optics Test and Measurement", Prentice Hall Inc. 1998.
5. Kartalopoulos, Stamatios. V, "Introduction to DWDM Technology: Data in a Rainbow", IEEE Press, New York, 1999.
6. Mohd Zamani Zulkifli, "Study of S-Band Optical Amplifiers and Its Applications", Doctor of Philosophy Thesis, University of Malaya, 2012.
7. M. J. Connelly, "Semiconductor Optical Amplifiers", Kluwer Academic Publishers, Dordrecht, 2002.
8. J. C. Simon, "GaInAsP Semiconductor Laser Amplifiers for Single-Mode Fibre Communications", IEEE/OSA J. Lightwave Technology, Vol. 5, 1286-1295, 1987.
9. C. E. Zah, C. Caneau, F. K. Shokoohi, S. G. Menocal, F. Favire, L. A. Reith, T. P. Lee, "1.3 μm GaInAsP Near-Travelling-Wave Laser Amplifiers Made by Combination of Angled Facets and Antireflection Coatings", Electronics Letters, Vol. 24, pp. 1275-1276, 1988.
10. B. Dagens, A. Labrousse, R. Brenot, B. Lavigne, M. Renaud, "SOA-Based Devices for All-Optical Signal Processing", OFC Proc. ThX1, pp. 582-583, 2003.
11. J. Jennen, H. de Waardt, G. Acket, "Modelling and Performance Analysis of WDM Transmission Links Employing Semiconductor Optical Amplifiers", Light Wave Technology, Vol. 19, pp. 1116-1124, 2001.

12. Ana Carrasco-Sanz, Sonia Martí'n-Lo'pez, Miguel González-Herrá'ez, Pedro Corredera, Mari'a Luisa Hernanz, "Synthesis of Optical Standard Frequencies in the S C and L Telecommunication Bands by Use of Four-Wave Mixing in Semiconductor Optical Amplifiers", *Optics Communications*, 264, pp. 135-141, 2006.
13. D. N. Wang, F. W. Tong, X. Fang, W. Jin, P. K. A. Wai, J. M. Gong, *Optics Communications*, 228, pp. 295, 2003.
14. H. Ahmad, K. Thambiratnam, S. W. Harun, A. H. Sulaiman, S. N. Aziz, "A Compact Dual-Wavelength Ring Laser Using A Semiconductor Optical Amplifier and Arrayed Waveguide Grating", *Optoelectronics and Advanced Materials – Rapid Communications*, 2(1), 1, 2008.
15. N. Pleros, T. Houbavlis, G. Theophilopoulos, K. Vlachos, C. Bintjas, H. Avramopoulos, "SOA-Based Multi-wavelength Laser Sources", *Fibre and Integrated Optics*, 23, 263-274, 2004.
16. Z. Zhang, J. Wu, K. Xu, X. Hong, J. Lin, "Tunable Multi-Wavelength SOA Fibre Laser with Ultra-Narrow Wavelength Spacing Based On Nonlinear Polarization Rotation", *Optics Express*, Vol. 17, No. 19, pp. 17200-17205, 2009.
17. M. Z. Zulkifli, H. Ahmad, N. A. Hassan, M. H. Jemangin, S. W. Harun, "An Ultra-Wideband Tunable Multi-Wavelength Brillouin Fibre Laser based On A Semiconductor Optical Amplifier and Dispersion Compensating Fibre in a Linear Cavity Configuration", *Quantum Electronics*, Vol. 41, No. 7, pp. 602-605, 2011.
18. H. Ahmad, K. Thambiratnam, A. H. Sulaiman, N. Tamcek, S. W. Harun, "SOA-Based Quad-Wavelength Ring Laser", *Laser Physics Letters*, Vol. 5, No. 10, pp. 726-729, 2008.

19. S. W. Harun, K. Thambiratnam, A. H. Sulaiman, S. N. Aziz, H. Ahmad, "SOA-Based Triple-Wavelength Ring Laser", The Open Applied Physics Journal, Issue 1, pp. 1-3, 2008.
20. N. V. Pedersen, K. B Jakobsen, M. Vaa, "Mode-Locked 1.5 μm Semiconductor Optical Amplifier Fibre Ring", Journal of Lightwave Technology, Vol. 15, No. 5, pp. 833-838, May 1996.
21. S. Kim, J. Kwon, S. Kim, B. Lee, "Multiplexed Strain Sensor using Fibre-Grating Tuned Fibre Laser with Semiconductor Optical Amplifier", IEEE Photonics Technology Letter, Vol. 13, No. 4, pp. 350-1, 2001.

CHAPTER 2

THEORETICAL BACKGROUND

2.1 : Introduction

This chapter starts the theoretical background by introducing the semiconductor optical amplifier (SOA) as the gain medium that provides an ultra-wideband transmission within the experiments. This overview includes analysing the structure of the SOA and the types of material used to produce such criterion as inhomogeneous broadening to the SOA, thus making the device attractive for multi-wavelength fibre laser generation. A detailed discussion then follows about the amplification principle of the SOA, covering the stimulated and spontaneous emission transition rates, and carrier density rate equations. The small signal gain, the saturation current, the saturation power and the transmission bandwidth of the SOA are also discussed in this section. A subsequent section will elaborate on the noise figure (NF) and the amplified spontaneous emission (ASE) of the SOA, which are other important parameters in establishing the performance of the SOA. A brief description on the important phenomenon involved in the amplification process such as *spontaneous absorption*, *spontaneous emission* and *stimulated absorption* will be discussed in between sections to provide more understanding within the subject topics.

To complete the theoretical background, this chapter also has a brief discussion about the optical principle of the wavelength filtering mechanism involved in this thesis, namely those of fibre Bragg gratings (FBGs) and arrayed waveguide gratings

(AWGs). Last but not least, a succinct explanation about stimulated Brillouin scattering (SBS) effect is also included in the final part of this chapter.

2.2 : Semiconductor optical amplifier (SOA) and its structure

A semiconductor optical amplifier (SOA) is designed to amplify light signals under suitable operating conditions. It is a compact optoelectronic device that is driven electronically by injecting an external current, to which allows for amplification to signals that pass through it. The compactness of the SOA has made it more viable than the EDFA in terms of incorporation into network systems, even though both devices have comparable gain characteristics. The compactness of SOA can save up to 50% of space together with a cost effectiveness as compared to the EDFA system.

Basically, SOA is a device that provides optical gain based on inversion in the semiconductor medium when it is electronically pumped, such that the p-n junction structure creates a spatial region of optical inversion [1]. In the general case of a semiconductor laser, the optical field in the SOA is confined within an optical waveguide that is an integral part of the structure [1]. The SOA generally functions as a gain block within an optical system. Due to its development in tandem with the semiconductor laser, the SOA shares similar characteristics by being compact and easily integrated with other elements into photonics integrated circuits (PICs) [1].

SOA structure

The vital factor regarding production of SOA is the structure of the SOA. The best structure of SOA offers an optimum gain even at low injection current. Since the development of SOA is in tandem with that of the semiconductor laser diode, SOA is basically built with a semiconductor laser diode structure albeit with low reflectivity

facets. In the early development of SOAs, the gain attained by the SOA was very sensitive to polarization effects. This sensitivity was due to the asymmetrical waveguide structures in the SOA [2, 3], and the devices were not viable for commercial use until 1989 when the fabrication of true travelling-wave SOAs was finally realized [4-7]. Low polarization gain sensitivity SOA has been produced by developing more symmetrical waveguide structures of the SOA [8], with the consequence of SOA being utilized in optical communication networks. This breakthrough has been the starting point of the SOA to be developed along with the advanced semiconductor materials, device fabrication, antireflection coating technology, packaging and photonic integrated circuits [4, 5, 9-11].

The basic design of the modern SOA has evolved from the early era of its development [4], in parallel with the advancement of the anti-coating technology, as well as the development from the homostructure to heterostructure semiconductor devices. A semiconductor-based gain medium is placed between the input and output facets of an SOA. Both the input and output facets are coated with anti-reflection coating to prevent back-reflection when light passes through the gain medium for amplification via the optical fibre that is connected to each input and output facet. Other than conducting the injection current to the gain material, the semiconductor material itself restricts the light signal within only the active region in order to improve efficiency and reduce loss. A typical SOA has about 0.6 - 2.0 mm length of active medium, in which a propagating signal is amplified via the stimulated emission process from the electron-hole pairs recombination, and this intrinsic gain medium is sandwiched between p- and n-claddings that form a double heterogeneous structure [12-14]. The heterogeneous interface is formed when the cladding regions have higher bandgap energies than the active region and hence create a lower refractive index than

that of the active region [4, 15, 16]. The difference of the refractive index obeys Snell's law of refraction, which results in the propagating signal being trapped within only the active region so to obtain maximum gain. This feature improves the SOA efficiency by preventing injected carriers being diffused through the SOA by exploiting the bandgap energy difference. Such confinement of the passing signal and injected carriers can also be attained by embedded waveguides due to the advanced and refined modern fabrication processes [17].

The next crucial aspect that defines the SOA is the optical coupling, which is meant to guide the propagating light from the fibre to the active region. Since the mode field diameter (MFD) of a propagating signal in a single mode fibre is usually about $9.3\text{ }\mu\text{m}$, whilst the active region is approximately a hundredfold smaller [18], the optical coupling is very important. The light signal needs to be coupled so that not to leak out to the cladding regions and cause high loss to the SOA. Optical coupling requires the SOA to possess cleaved facets with anti-reflection coating, or be suitably modified at its input and output ends in order to achieve an almost zero reflectivity [4, 19, 20]. The presence of resonance and ripple in the gain spectrum can be reduced by using the low reflectivity facets, and this is a crucial factor for the gain characteristic of the SOA.

Figure 2.1 shows a schematic diagram of a basic SOA, in which the active region in the device imparts gain to an input signal. The energy source that facilitates the occurrence of gain is provided by the external current that is injected to the active region. There is a waveguide embedded in order to confine the propagating signal wave to the active region, although, because of the weak optical confinement, some of the signal will escape into the surrounding lossy cladding regions [4]. The amplification process produces additive noise that accompanies the output signal, and

it cannot be entirely avoided. The reflective facets of the amplifier cause ripples to occur in the gain spectrum, though these can be reduced by using angled facet connectors.

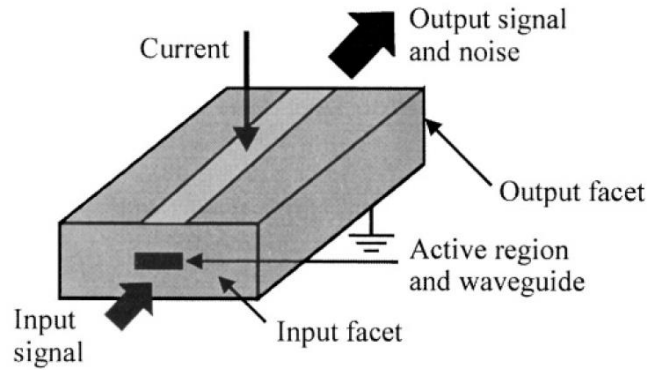


Figure 2. 1 Schematic diagram of an SOA [4].

SOAs can be classified into two main types as displayed in Figure 2.2. The first basic SOA type is the Fabry-Perot SOA (FP-SOA). The reflective cleaved facets at both ends of the FP-SOA cause light passing through the active region to reflect several times, with a portion of the amplified light leaving the cavity. The FP-SOA has a similar principle of operation to that of the Fabry-Perot laser [21]. The process of the multiple reflections explains the exhibition of ripples in the gain spectrum of the FP-SOA as referred to Figure 2.2. The second basic type of SOA is the travelling-wave SOA (TW-SOA). Unlike the FP-SOA, the TW-SOA is essentially an active medium with no reflective facets at its ends, which results in negligible reflections and causes an input signal to be amplified by travelling directly through the active region of the SOA [21]. The smooth gain spectrum produced by a TW-SOA is as shown in Figure 2.2. Anti-reflection coatings can be used to decrease the facet reflectivity to at most a 10^{-3} fraction [4]. The TW-SOA is distinguished to be less sensitive than the FP-SOA to fluctuations in bias current, temperature and signal polarization [4].

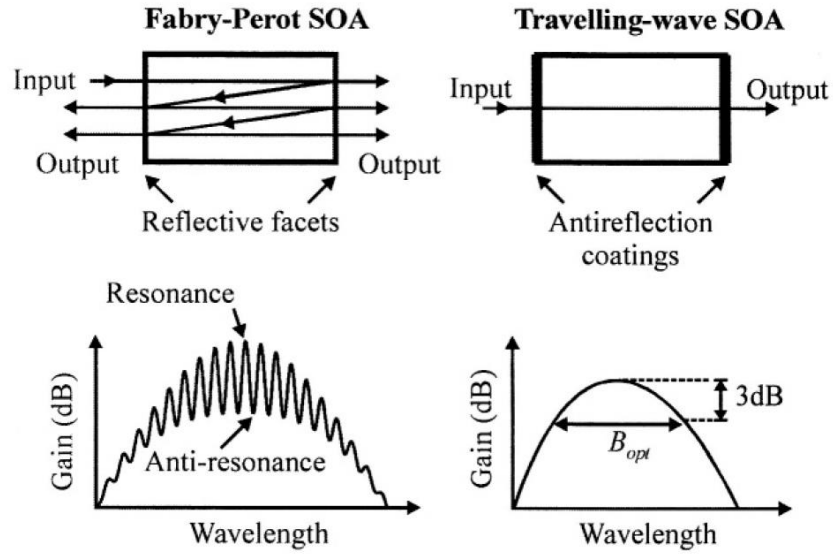


Figure 2. 2 Basic types of SOA and associated gain spectra. An ideal TW-SOA has a smooth gain spectrum. The FP-SOA gain spectrum exhibits ripples caused by reflections at the end facets. The gain ripples are exaggerated here for clarity [4].

2.3 : Principles of amplification in SOA

In this thesis, the type of SOA used in all experiments is the TW-SOA. A laser diode controller controls the SOA in order to supply external forward bias current to the semiconductor active medium in the SOA. The external current source injects electrons (which are more commonly referred to as carriers) into the active region of the SOA. The carriers are then excited from the low energy states of the valence band (VB) to the higher energy states of the conduction band (CB) of the active region material. This excitation process leaves holes in the VB and increases the number of electron in the CB. Essentially, there are three basic radiative mechanisms that can occur in the semiconductor [4]. These mechanisms are, as shown in Figure 2.3,

spontaneous emission, stimulated emission and stimulated absorption. Note that the figure refers to two discrete energy levels of energy band and type of material.

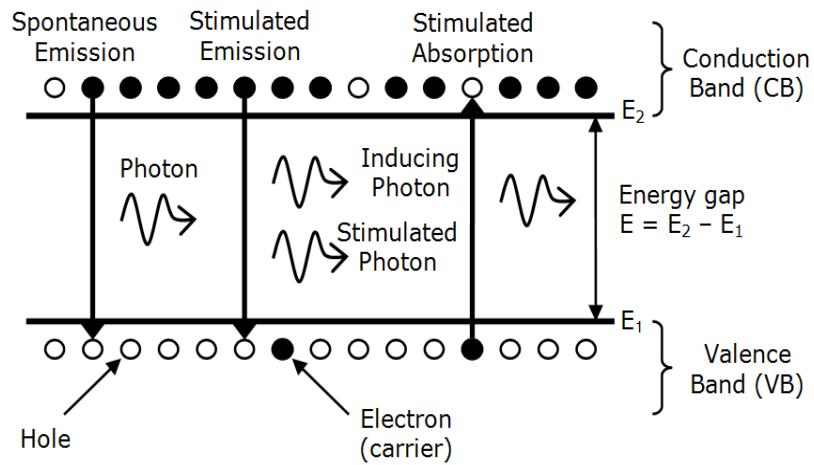


Figure 2. 3 Spontaneous and stimulated processes in a two level system [4].

When a carrier is stimulated from the lower energy states of the VB to the higher energy states of the CB by an incident photon with sufficient energy, a stimulated absorption occurs. This process is however a loss process because the incident photon is annihilated at the end of the process [4].

A stimulated recombination of a carrier in the CB with a hole in the VB occurs when a photon of light with suitable energy is incident on the semiconductor. Such a recombination process yields energy in the form of a photon of light that is identical to the inducing photon in terms of phase, frequency and direction. The inducing photon and the new stimulated photon are in coherence with each other and they both have similar values of energy. Note that both the original (inducing) photon and the stimulated photon can create additional replica stimulated photons and thus increase the stimulated transition occurrences in the system, since this process is a chain process. To increase the probability of stimulated emission to occur, the carrier population in the CB must exceed the carrier population in the VB. This phenomenon

is called population inversion since the higher energy level contains more number of carriers than the lower energy level. In order to achieve population inversion, the injection current to the semiconductor medium must be sufficiently high. When the occurrence of stimulated emission is greater than the stimulated absorption, the semiconductor will exhibit optical gain [4].

The existence of noise in the SOA cannot be avoided, so there is no means to realize a noiseless SOA. The underlying reason is a non-zero probability per unit time of a spontaneous recombination of CB carriers with VB holes, with a consequent emission of photons having random phase and random direction. These spontaneously emitted photons travel in a wide range of frequencies, which are considered as noise that causes a decrease in the population of the carrier in CB that is otherwise available for optical gain. Since spontaneous emission is a result of the amplification process, it can never simply be dismissed. Although the intensity of the inducing radiation affects the rate of the stimulated processes (a higher intensity of the inducing radiation promotes a higher rate of the stimulated processes), the spontaneous emission is absolutely independent of inducing radiation intensity.

The basic concept of the SOA operation has been discussed thus far. The electron carrier transitions between the CB and the VB is crucial to ensure an efficient performance of the SOA in order to realize optical gain. It is noted that the behaviour of the electron transitions is influenced by the semiconductor material used as the active medium in the SOA.

The amplification principle in the SOA is based on stimulated emission of photons. The arrival of a photon in an excited medium assists the generation of a second photon with identical wavelength, phase and polarization [1]. Essentially, the new quantum of light is generated by the recombination of an electron with a hole in

the valence band. This indicates that the wavelength of the amplified photons is determined totally by the band structure of the semiconductor material used in the SOA. The range of energy of the emitted photons depends on the bandgap energy as shown in Figure 2.4. A larger bandgap energy results in shorter wavelength emission, whilst the smaller bandgap energy results in longer wavelength emission.

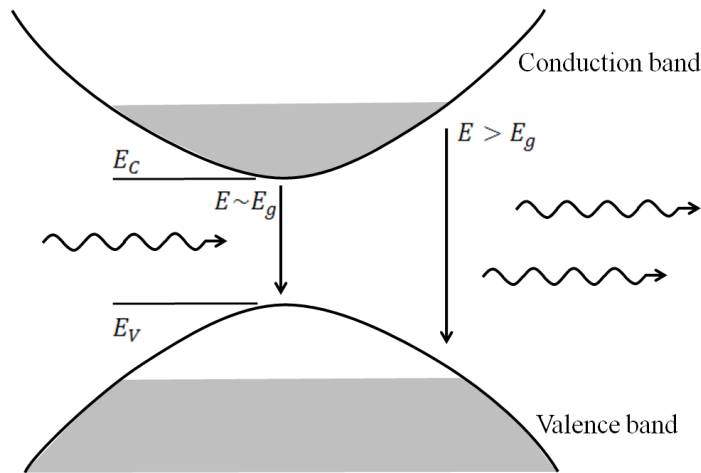


Figure 2. 4 Stimulated emission of photons as a result of population inversion. Recombination of electrons and holes close to the band edge results in emission of photons with an energy close to that of the band gap, while recombination of carriers from higher occupied states within the bands produces photons with a shorter wavelength of emission¹.

To achieve amplification, a population inversion must be present. A population inversion is when the number of carriers in the excited state level is larger than the number of carriers in the ground state level. If a population inversion is not achieved, the emitted photons would be readily reabsorbed by the high number of carriers in the

ground state level. An electrical pumping is used via applying a forward current to a semiconductor diode in order to attain this inversion [1].

2.3.1 : Spontaneous and stimulated transition rates

The gain properties of the SOA are directly related to the processes of spontaneous and stimulated emission in the semiconductor medium of the SOA. The relationship can be quantified by considering a system of energy levels, E_1 and E_2 , with energy $E_2 > E_1$ associated with a particular physical system. Let N_1 and N_2 be the average number of atoms per unit volume of the system characterized by the energies respectively. When a certain atom has energy E_2 , there will be a finite probability per unit time that the atom will undergo a transition from E_2 to E_1 , during which it will emit a photon. The spontaneous carrier transition rate per unit time from level 2 to level 1 is given by [4]

$$r_{21}|_{\text{spont}} = A_{21}N_2 \quad (2.1)$$

where A_{21} is the spontaneous transition parameter for level 2 to level 1 transition. Stimulated transitions can occur alongside the spontaneous emission thus, the transition rate for such transition from level 2 to level 1 is given by

$$r_{21}|_{\text{stim}} = B_{21}\rho(\nu)N_2 \quad (2.2)$$

where B_{21} is the stimulated transition parameter for level 2 to level 1 transitions and $\rho(\nu)$ is the incident energy density and frequency ν . On the other hand, the rate of stimulated carrier absorption from level 1 to level 2 by photons with energy $h(f) = E_2 - E_1$ can be written as

$$r_{12} = B_{12}\rho(\nu)N_1 \quad (2.3)$$

where B_{12} is the stimulated absorption parameter for level 1 to level 2 transition.

Through quantum mechanical considerations [22, 23], it can be shown that

$$B_{12} = B_{21}$$

$$\frac{A_{21}}{B_{21}} = \frac{8\pi n_r^3 h \nu^3}{c^3} \quad (2.4)$$

where n_r is the material refractive index and c is the speed of light in vacuum.

Substituting (2.4) into (2.2) gives

$$r_{21}|_{stim} = \frac{A_{21}c^3\rho(\nu)N_2}{8\pi n_r^3 h \nu^3} \quad (2.5)$$

For the case of a stimulating radiation is monochromatic at frequency ν , then the stimulated transition rate from level 2 to level 1 is

$$r_{21}|_{stim} = \frac{A_{21}c^3\rho_\nu l(\nu)N_2}{8\pi n_r^3 h \nu^3} \quad (2.6)$$

where ρ_ν is the energy density (J/m^3) and $l(\nu)$ is the normalized transient line-shape, in which

$$\int_{-\infty}^{\infty} l(\nu) d\nu = 1 \quad (2.7)$$

$$I_\nu = \frac{c}{n_r} \rho_\nu \quad (2.8)$$

c , n and ρ_ν can be written as the inducing field intensity, I_ν (W/m^2) so that equation (2.6) can now be written as

$$r_{21}|_{stim} = \frac{A_{21}c^2l(\nu)I_\nu N_2}{8\pi n_r^2 h\nu^3} \quad (2.9)$$

From this the material gain coefficient g_m , can be derived as [8]:

$$dP_\nu = (r_{21}|_{stim} - r_{12})h\nu A dz$$

$$\frac{dP}{dz} = (r_{21}|_{stim} - r_{12})h\nu A$$

$$= g_m(\nu)P_\nu \quad (2.10)$$

where $g_m = \frac{A_{21}c^2l(\nu)(N_2-N_1)}{8\pi n_r^2 h\nu^3}$. Thus, it can be seen that in order to achieve positive gain in the SOA, a population inversion of $N_2 > N_1$ must exist (with all other parameters being constant) between level 2 and level 1. In the case of $N_2 < N_1$, there is negative gain in the SOA, i.e. the signal photons will undergo stimulated absorption. Furthermore, the derivation also indicates that the occurrence of spontaneous emission (A_{21}) is an inherent part of the optical gain process and cannot be avoided [24]. Therefore, it is impossible, even theoretically, to create a fully lossless SOA.

2.3.2 : Carrier density rate equations

The amplification in the SOA is highly dependent on the number of carriers or electrons in the heterojunction structure of the semiconductor medium as discussed in the previous part of this chapter. Such a number of carriers, which is also known as *carrier density*, $\frac{dn(z)}{dt}$ is controlled by the bias current of the SOA. The density of the carriers per volume at position z in the SOA can be expressed by the following rate equation

$$\begin{aligned} \frac{dn(z)}{dt} = & \frac{I}{qdLW} - R(n) - \frac{\Gamma}{dW} \left\{ \sum_{k=1}^{N_s} g_m(v_k, n) [Ns_k^+(z) + Ns_k^-(z)] \right\} \\ & - \frac{2\Gamma}{dW} \left\{ \sum_{j=0}^{N_m-1} g_m(v_j, n) [N_j^+(z) + N_j^-(z)] \right\} \end{aligned} \quad (2.11)$$

where I represents the bias current injected into the SOA, d is the thickness of the active region of the SOA, q is the electronic charge, L is the length of the waveguide active region, W is the width of the active region in the SOA, and Γ is the confinement factor. The Ns_k^+ and Ns_k^- symbols represent the photon rates in the positive and negative z direction respectively, whilst N_j^+ and N_j^- represent the photon rates at positive and negative z direction with a particular polarization respectively. The v_k and v_j symbols on the other hand denote the frequencies of each respective term.

In equation (2.11), it is assumed that all the injected current is able to pass through the active region i.e. none into the surrounding InP regions [4]. The bias current is assumed to have a uniform distribution across the active region width [4]. The density rate equation is expressed basically by four factors of mechanisms. The first positive term of $\frac{I}{qdLW}$ indicates the addition of carriers to the active region from the bias current. These injected carriers are then depleted by various mechanisms occurring within the amplifier [4]. The second term indicates the radiative and non-radiative recombination mechanisms [4] for which the carrier leakage from the active region into surrounding InP regions is assumed to be negligible [25]. The third and fourth terms on the equation denote radiative recombination of carriers associated with the amplified signal and ASE, which are also regarded as losses in the gain medium. Γ is the confinement factor and is used to designate the recombination mechanisms applies to carriers confined to the gain medium [24]. The factor of two in the equation is in regards of the fact that spontaneously emitted photons can exist in one of two

mutually orthogonal polarizations; transverse-electric (TE) or transverse-magnetic (TM) polarities.

2.3.3 : Small signal gain

The most important operation of the SOA is its ability to amplify incoming light signals. This ability of the SOA is known as the gain of the SOA, and can be typically given as either its intrinsic gain or its fibre-to-fibre gain [4]. The intrinsic gain, G , is simply the ratio of the power of the signal at the input facet to the power of the signal at the output facet. The fibre-to-fibre gain includes the input and output coupling losses of the SOA. This fibre-to-fibre gain can be calculated as the ratio of the output signal P_{out} to the input signal P_{in} so that

$$G(\nu) = \frac{P_{out}}{P_{in}} \quad (2.12)$$

The amplification energy imparted to the propagating signal by the SOA originates from the bias current as described in section 2.2. As well as the fibre-to-fibre gain factor and injection current, the SOA gain is also wavelength dependent on the passing signal. The small signal gain of an SOA at an optical frequency of f can be written as [26]

$$G(f) = \frac{(1 - R_1)(1 - R_2)G_s}{(1 - \sqrt{R_1 R_2} G_s)^2 + 4\sqrt{R_1 R_2} G_s \sin^2\left[\frac{(f - f_o)L}{v}\right]} \quad (2.13)$$

where G_s is the single-pass amplifier gain, R_1 and R_2 are the reflectivity of the input and output facets, f_o is the center frequency and v is the velocity of the light when travelling in the SOA gain medium (v can be obtained by the ratio of the speed of light

in air, approximately c , to the refractive index of the material, n , so that $v = \frac{c}{n}$ [27]).

The SOA gain medium and facets form a reflective cavity, giving rise to resonant frequencies which occur when the \sin^2 factor is 0 and in turn will cause minimum gain for the SOA. The single pass gain, G_s , can be measured in terms of the material gain coefficient, confinement factor Γ , absorption coefficient α and active region length L as [4, 5]

$$G_s = \exp[(\Gamma g_m - \alpha)L] \quad (2.14)$$

Equation (2.14) can be simplified by taking the reflectivity factors to be identical (as in the case of most SOA designs) so that $R_1 = R_2 = R$. This yields

$$G(f) = \frac{(1 - R)^2 G_s}{(1 - R G_s)^2 + 4 R G_s \sin^2 \left[\frac{(f - f_o)L}{v} \right]} \quad (2.15)$$

Equation (2.15) is the general formula for calculating the small signal gain in an SOA and is applicable to the FP-SOA where the reflectivities are of concern. In a TW-SOA, the reflectivities have no discernible effect on the gain of the SOA and therefore, $R_1 = R_2 = R = 0$, and equation (2.15) can be reduced to $G(\omega) = G_s$.

Another factor that can affect the SOA gain is the input signal power. This is because as the signal power increases, the gain of the SOA decreases due to gain saturation [27]. The relationship between the input signal power dependent gain, $G(p)$ and the input signal power can be given as

$$G(p) = G_0 \exp \left[\frac{(G - 1)P_{out}}{G P_{sat}} \right] \quad (2.16)$$

G is given as in equation (2.12) and P_{sat} is obtained from the saturation power of the SOA.

Using these equations, we are thus able to predict the small signal gain for the SOA under varying drive currents, input wavelengths and input powers. However, these equations are only true for certain conditions [4]. Typically, SOAs can exhibit an unsaturated gain of between 8 dB to as high as 29 dB [28], but these equations become invalid as the drive current and input signal power increases. In the case of the bias current, the gain increases as the bias current is increased until the saturation current point, after which there is no longer any additional gain regardless of the increase in the drive current [11, 29]. In the same manner, significant gain is imparted to low-power input signals, but the gain decreases as the input signal power increases until the point of saturation power [4, 5, 11]. Furthermore, the wavelength of the signal that the SOA can amplify is also limited to the SOA bandwidth [4, 5, 11]. As such, optical amplification only takes place if specific criteria are met, and the general equations of Section 2.2.4 are invalid. The next section will examine the limitations that the drive current, signal power and wavelength impose on the SOA's gain.

2.3.4 : Saturation current, saturation power & bandwidth

The maximum gain an SOA can impart is limited by the maximum bias current that can be injected into the SOA active medium, and the input signal that can be amplified by the SOA is dependent on its power and wavelength.

Although equation (2.11) indicates that increasing the SOA bias current will increase the SOA gain as a result of additional excited electrons [4], this is only true for bias currents below the saturation current. Above the saturation current, there is no

longer any increase in the gain of the SOA even if the SOA current is increased. This occurs due to the semiconductor nature of the SOA; more and more carriers are displaced from the VB to the CB as the injection current is increased [30, 21]. However, only a certain amount of carriers can exist in the CB as there are only a finite number of energy states in the CB for the carriers to occupy, and the maximum number of carriers in turn determines the maximum gain that the SOA can impart. Above the saturation current, excess carriers can no longer flow through the semiconductor active medium, and are instead converted to heat which must be vented, in order for the SOA not to overheat and fail.

The gain saturation parameter of an SOA determines the maximum amount of gain that an SOA can impart based on the power of the input signal. Although equations (2.13) and (2.14) indicate that a signal of any power will always be amplified, in reality the gain of the SOA is limited by the input signal saturation power. This is because the material gain coefficient is dependent on the signal frequency and power [4], such that

$$g(f, P) = \frac{g(f)}{1 + \frac{P}{P_{sat}}} \quad (2.17)$$

From (2.17), the material gain coefficient can be seen to be dependent on the input signal power. As the input power increases, the material gain coefficient begins to decrease until half the maximum material gain coefficient is obtained when the signal is full saturated. The reason for this is the high number of photons in the input signal fully depleting the carriers in the CB through recombination with VB holes, leaving no more electrons to recombine even if the number of external photons is increased [29]. From the material gain coefficient, the gain can be computed to be

$$G_s = 1 + \left(\frac{P_{sat}}{P_{in}} \right) \ln \frac{G_s^{max}}{G_s} \quad (2.18)$$

where G_s^{max} is G_s at ω_o and P_{sat} is the saturation power. The saturation power is defined as the signal power at which the gain of the SOA is half (3dB) the small-signal gain.

The usable wavelength range of the SOA is given by the bandwidth of the SOA. By definition, the bandwidth of the SOA is the frequency range at which the gain is half the maximum value, coinciding with the SOA saturation power. The bandwidth of the SOA can be obtained (2.15), in which the gain is reduced by a factor of 2 [27] to yield

$$BW = \Delta f = (f - f_0) = \left(\frac{v}{L} \right) \sin^{-1} \frac{(1 - RG_s)}{[2\sqrt{(RG_s)}]} \quad (2.19)$$

where v is the speed of the signal in the SOA cavity as given by $v = \frac{c}{n}$. Hence, the saturation current, saturation power and bandwidth can be combined to set the operational limits of the SOA to provide a more realistic theoretical model.

2.3.5 : Noise figure and amplified spontaneous emission (ASE)

As well as the gain and saturation limits, another important parameter in determining the performance of the SOA is its noise figure. The noise figure of an SOA shows how much noise the SOA adds to a signal and therefore how much a passing signal deteriorates. Therefore, an SOA with a gain that is as high as possible and NF that is as low as possible is always sought after.

The noise figure of an optical amplifier is defined as the ratio of the input's to output's signal-to-noise ratio. This parameter is useful in quantifying the performance of an optical amplifier, and is generally given by [27]

$$NF = \frac{\left(\frac{S}{N}\right)_i}{\left(\frac{S}{N}\right)_o} \quad (2.20)$$

where $\left(\frac{S}{N}\right)_i$ is the input signal-to-noise ratio and $\left(\frac{S}{N}\right)_o$ is the output signal-to-noise ratio. In the case of the SOA, the noise figure can be expressed more specifically in terms of the SOA gain and ASE power as [31, 32]

$$NF = \frac{1}{G} + \frac{P_{ASE}}{Gh\nu\Delta\nu} \quad (2.21)$$

where h is Planck's constant, ν is the signal frequency, and $\Delta\nu$ is the bandwidth. An important point to note from equation (2.21) is that the SOA noise figure is inversely proportional to the SOA gain; thus as the gain increases the noise figure will decrease. The ASE power, P_{ASE} , is a result of carriers that spontaneously decay from the upper energy level to the lower energy level of the SOA, in the process releasing photons that have random phases and directions. Although these photons fall within the same frequency range as the signal, their random phase and direction does not contribute to amplifying the passing signal, and instead generate noise. The average peak ASE power can be obtained by the formula [27]

$$P_{ASE} = 2n_{sp}h\nu G\Delta\nu \quad (2.22)$$

The factor of 2 in equation (2.22) is due to the fact that the ASE will propagate equally in both the forward and backward directions, and thus the ASE power measured at

either end of the SOA is only half of the total ASE power generated [33]. The spontaneous emission factor, n_{sp} , of the SOA is related to the ratio of carriers still in the upper level to the carriers that have already decayed spontaneously, and is given by [27]

$$n_{sp} = \frac{N_2}{N_2 - N_1} \quad (2.23)$$

In typical optical amplifier operations, the ASE is usually a detrimental effect. Forward or co-propagating ASE will generate noise in the receiver that will deteriorate the system performance [27], while backward or counter-propagating ASE will deplete the population inversion available for signal amplification, affecting the SOA's gain performance. However, in this thesis the ASE is a sought after effect, as the ASE will be used in conjunction with a PMF-SLM to form the multi-wavelength source.

2.3.6 : Polarization dependent gain effect

Generally, the gain of an SOA depends on the polarization state of the input signal. The dependency is in regards of several factors including the waveguide structure, the polarization dependent nature of anti-reflection coatings and the gain material. Cascaded SOAs boost this polarization dependence. Two mutually orthogonal polarization modes, the transverse electric (TE) and transverse magnetic (TM) modes, characterize the amplifier waveguide. The input signal polarization state usually lies somewhere between these two extremes. The gain $G_{TE/TM}$ polarization sensitivity of an SOA is defined as the magnitude of the difference between the TE mode gain G_{TE} and TM mode gain G_{TM} .

$$G_{TE/TM} = |G_{TE} - G_{TM}| \text{ (dB)} \quad (2.24)$$

2.4 : Applications of ultra-wideband SOAs

2.4.1: Ultra-wideband SOA fibre laser

Fibre lasers play an important role in providing laser sources into WDM and DWDM optical network systems. Properties such as narrow linewidth, high output power, compactness, low threshold power and wide tunability have made the fibre laser favoured for network applications. Additional advantages of ultra-wide fibre laser bandwidth can be achieved as a result of the work described in this thesis, thus increasing viability for DWDM network applications. Fibre lasers can be grouped into two types, namely linear cavity or ring cavity; Fabry-Perot cavity is also known as a linear cavity fibre laser [34]. The illustration is as stated in Figure 2.5.

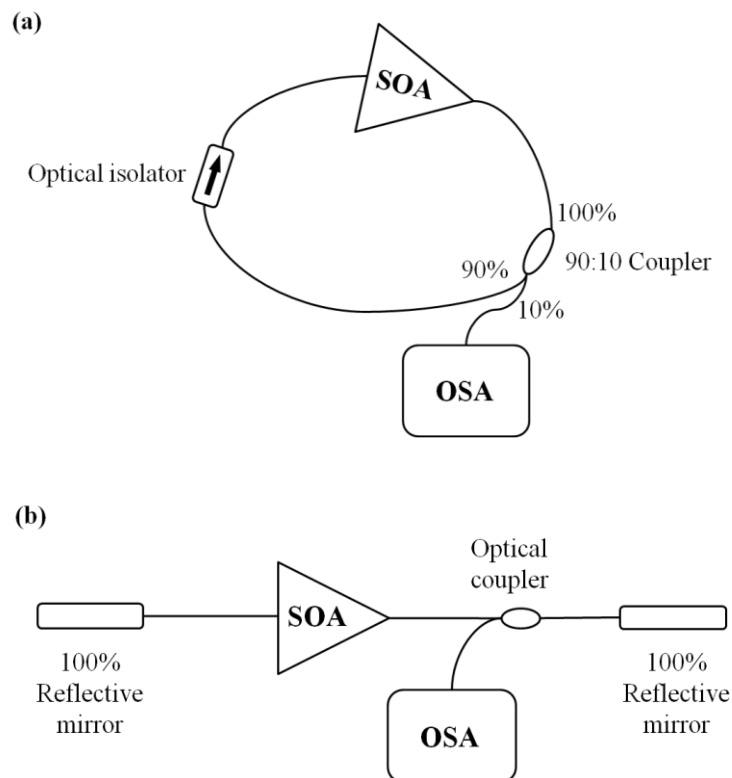


Figure 2. 5 Types of fibre laser cavities: (a) Ring cavity fibre laser, (b) Linear cavity fibre laser.

Both types of cavities deploy an optical amplifier as the gain medium. It can be seen for the ring cavity, that the output port is looped back into the input port of the SOA to create a ring resonator effect. An optical coupler is used to tap out a small portion of the output laser power to be analysed by the OSA. Conversely, the linear cavity fibre laser is generated by attaching each input and output port of the SOA with a highly reflective mirror. The laser output is tapped out via an optical coupler and subsequently analysed by use of the OSA.

Fibre lasers characteristic

The crucial factors on determining the performance of fibre lasers are the output power, side-mode-suppression ratio (SMSR), tunability and stability. A sufficiently high pump power is needed for a population inversion to occur until the energy of the system reaches the lasing threshold and consequently emit laser output. A lasing is actually generated when a small-signal gain coefficient is larger than its loss coefficient. A reliable yet stable fibre laser usually attains at least -20 dBm of output peak power, and higher output power improves performance.

The SMSR measurement is critical to evaluate the degree of the fibre laser output power. SMSR is defined as the difference of the main longitudinal mode intensity with the maximum side mode intensity by ‘comparing’ the power of the laser output mode with its siding mode, the SMSR can be expressed by the following equation (2.25).

$$\begin{aligned}
 SMSR (dB) &= 10 \log \left(\frac{I_{main}}{I_{side}} \right) \\
 &= I_{main}(dBm) - I_{side}(dBm)
 \end{aligned} \tag{2.25}$$

To attain high values of SMSR means fibre lasers attain good performance. A typical SMSR value for a conventional laser diode is about 40 dB, thus, for a well performing laser to be obtained, it is essential to achieve an SMSR value as high as possible and preferably with a minimum value of 40 dB. The effect of high SMSR fibre lasers can be seen by the reduction in crosstalk in the WDM networks whilst such lasers act as transmitters [35].

In order to allow for wavelength selection of the fibre laser, laser tunability is important. A wide range attained will be advantageous in many applications especially in DWDM communication system as a transmitter, in spectroscopy and in sensor applications; particularly in temperature and displacement detectors.

Another crucial factor of making the fibre laser viable to DWDM applications is the good stability performance of the fibre laser output power over time. The stability test is important so as to ensure that the fibre laser system operates well over significant period of time without any power deterioration, and thus minimize operating cost.

2.5: Wavelength selective filtering

The basic concept of a wavelength selective filtering component lies in blocking all the other propagating wavelengths whilst allowing only one particular wavelength to be transmitted. There are two types of wavelength selective filtering utilized in the scope of the work of this dissertation; fibre Bragg gratings (FBGs) and arrayed waveguide gratings (AWGs). Each type implements different optics principle to select and filter particular wavelength to be used in the optical resonator.

Such filters are called *fibre gratings* because the refractive index variations scatter light passing through the fibre; this effect is similar to how grooves etched in

bulk optical devices, called *diffraction gratings*, scatter light hitting their surfaces [36]. However both processes depend on the wavelength of light.

In this section of the thesis, a brief theory and operation principle of the multi-wavelength fibre laser generation by employing two wavelength selective filtering mechanisms, as stated above, is discussed to provide understanding within the topics.

2.5.1 : Fibre Bragg gratings (FBGs)

Bragg grating is essentially a periodic variation of the refractive index of the fibre core along the length of a fibre [38]. The principal property of FBGs is that they reflect light in a narrow bandwidth that is centred about the Bragg wavelength λ_B , which is given by

$$\lambda_B = 2n_{eff}\Lambda \quad (2.26)$$

where Λ is the spatial period (or pitch) of the periodic variation and n_{eff} is the effective refractive index for light propagating in a single mode, usually the fundamental mode of a monomode optical fibre. The wavelength in the material has to be twice the length of the grating period [37]. The refractive index variations are formed by exposure of the fibre core to an intense optical interference pattern of ultraviolet light [38]. This process is photosensitivity, which refers to a permanent change in the index of refraction of the fibre core when exposed to light with characteristic wavelength and intensity that depend on the core material [39]. Photosensitivity was discovered by Hill et. al in 1978 at the Communications Research Centre in Canada (CRC) [40, 41].

As the Bragg wavelength λ_B is reflected back by the grating period inside the fibre, other wavelengths are transmitted through the grating period. It is obvious that the centre wavelength selected by the FBG is highly dependent on the uniformly-spaced grating period inscribed in the fibre core of the FBG, and the grating sections have an increased refractive index from that of the rest of the core [36]. The reflected wavelength is scattered by the refractive index difference in the core by what is called the Bragg scattering. The Bragg scattering however is not precisely the same as scattering from a diffraction grating, but it does selectively reflect a narrow range of wavelengths [38]. The principle is that, every time when the light hits a region of higher refractive index, a bit is scattered backwards. If the wavelength matches the spacing of the high-index zones in the fibre, the waves scattered from each high-index zone interfere constructively, producing strong reflection. The FBG is considered as a low loss passive device which can easily be coupled to any fibre configuration. The ability of the FBG to select one or more wavelengths is important in wavelength division multiplexing, or where pump and signal wavelengths must be combined or separated [36]. An overview showing the principle aspects of FBG is depicted in Figure 2.6.

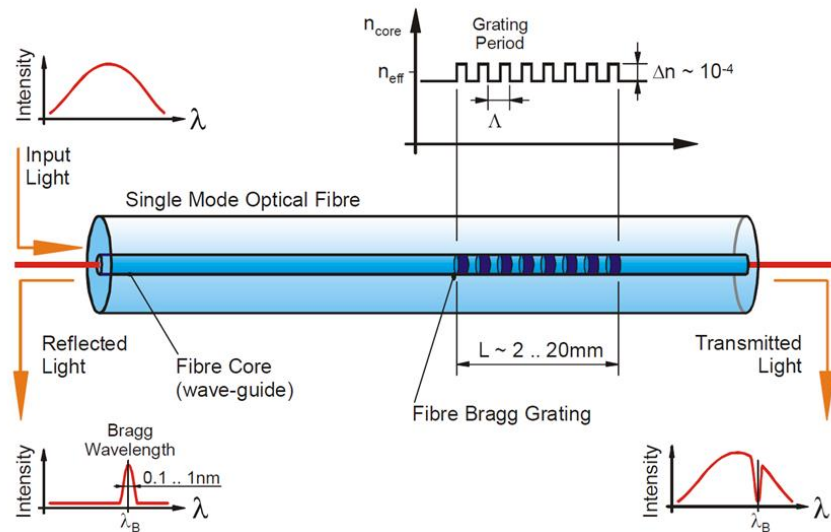


Figure 2. 6 Fibre Bragg grating [50]

Each of the grating planes will scatter the light traveling along the core of the optical fibre in accordance to Bragg condition. However, if the Bragg condition is not satisfied, the reflected light from each of the subsequent planes becomes progressively out of phase and then will eventually be cancelled out [42]. Basically, light that is not coincident with the Bragg wavelength resonance will experience very weak reflection at each of the grating planes because of the index mismatch; this reflection accumulates over the length of the grating. When the Bragg condition is satisfied, the contributions of reflected light from each grating plane add constructively in the backward direction to form a back-reflected peak with a centre wavelength defined by the grating parameters [42].

The ability to filter a narrow range of wavelength has made the FBG the most preferred wavelength selector for fibre-based applications. The 3 dB bandwidth recorded is typically 1.0 nm, and the reflectivity varies from about 80% to 99%, as according to the properties provided by the manufacturer. Even though FBGs are known to serve as a wavelength selective element, they however cannot be tuned independently. Other than applying physical changes to the FBG, additional components are required for the FBG to be tuned, or the reflected wavelength to be altered in order to achieve tunability.

2.5.2 : Arrayed waveguide gratings (AWGs)

Arrayed waveguide gratings (AWGs) multiplexers/demultiplexers are planar devices which are based on an array of waveguides with both imaging and dispersive properties [42]. This device is capable of multiplexing a large number of wavelengths into a single optical fibre, thereby increasing the transmission capacity of optical networks considerably via the process of ‘splitting’ or ‘slicing’ wavelengths. The

device operates based on the fundamental principle of optics that light waves of different wavelengths interfere linearly with each other. In this regard, if each channel in an optical communication network makes use of light of a slightly different wavelength, then the light from a large number of these channels can be carried by a single optical fibre at the transmission end, and also can be used as demultiplexers to retrieve individual channels of different wavelengths at the receiving end of an optical communication network.

As depicted in Figure 2.7, the AWG is deployed to split the incident beam into multiple batches, usually 16 and 24 channels, with a minimum insertion loss of about 3dB. The AWG images the field in an input waveguide onto an array of output waveguides in such a way that the different wavelength signals present in the input waveguide are imaged onto different output waveguides [42].

An AWG consists of N transmitter/receiver waveguides, two focusing object/image planes, and arrayed waveguides with a constant path length difference ΔL between neighbouring waveguides. When an input beam is launched through the transmitter waveguide and enters the free propagation region (FPR) of the object plane, the beam is automatically diverged into the input aperture of the arrayed waveguides and is no longer confined laterally at this point. The coupled beam then propagates through the individual array waveguides towards the output aperture, and then towards the image plane. The length of the array waveguides is chosen such that the optical path length difference between adjacent waveguides equals an integer multiple of the central wavelength, λ_c , of the demultiplexer [36]. As for the λ_c , the fields in the individual waveguides arrive at the output aperture with equal phase (mod. 2π), and thus the field distribution at the input aperture is reproduced at the output aperture [43]. With equal amplitude and phase distribution, the divergent beam at the input aperture

is transformed into a convergent one whilst the input field at the object plane gives rise to a corresponding image at the centre of the image plane. By linearly increasing the lengths of the array waveguides, the spatial separation of different wavelengths is attained, which thus introduces a wavelength-dependent tilt of the outgoing beam that is associated with a shift of the focal point along the image plane. To achieve distinctly different wavelengths at each output ports, the receiver waveguides are placed at appropriate positions along the image plane.

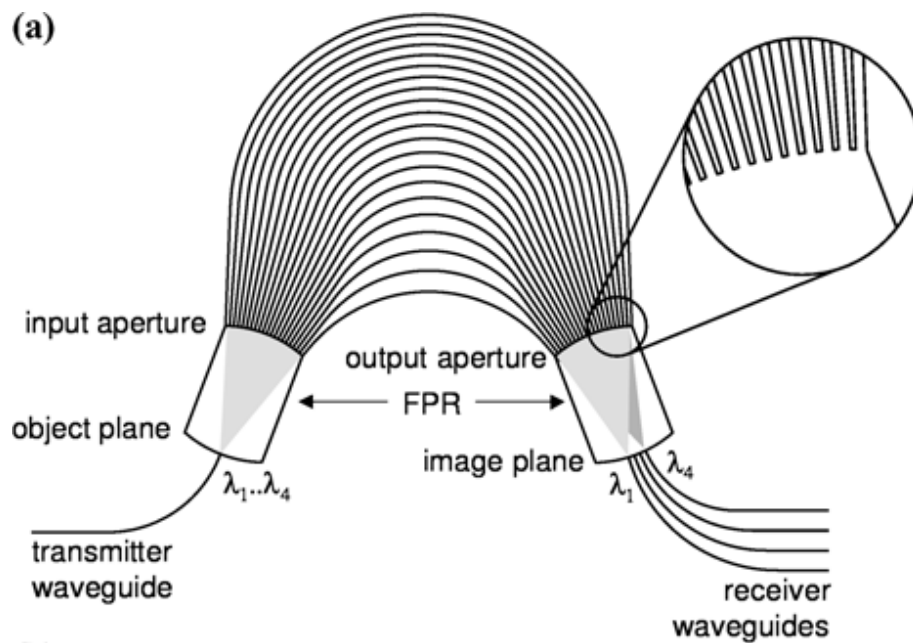


Figure 2. 7 (a) Geometry of an AWG demultiplexer, (b) beam focusing geometry in the free propagation region.

2.6: Nonlinear effects in optical fibres

There are two types of nonlinearities classifications. The first originates from the scattering effects in the fibre medium due to the interaction of light waves with phonons in the silica medium, which is also known as molecular vibration. Such

nonlinearity produces two main effects, known as stimulated Brillouin scattering (SBS) and stimulated Raman scattering (SRS). The second type of nonlinearities effects occur because of the dependency of the optical power on the refractive index. Such changes in the refractive index of the silica fibre, also known as Kerr Effect, can be explained by the change of the refractive index Δn in proportion to the optical intensity I . This phenomenon exhibits itself in three different effects depending on the type of the input signal; self-phase modulation (SPM), cross-phase modulation (XPM) and four wave mixing (FWM) [44].

In scattering effects, energy gets transferred from one light wave to another wave of a longer wavelength (or lower energy) [45]. The energy emitted upon the transfers is then absorbed by the molecular vibrations, or phonons, in the medium. However, the type of phonon involved is different for SBS and SRS. Generally, the two waves involved in the effects are the pump wave and the Stokes wave; which are described as the incident light, and the scattered light with acoustic wave generated through an electrostriction process, respectively [47]. As the pump wave propagates in the fibre, it loses its power, and this results in a power gain for the Stokes wave. In the case of SBS, the pump wave is the signal wave while the Stokes wave is the unwanted wave that is generated due to the scattering process [45].

2.6.1 : Stimulated Brillouin scattering (SBS)

Brillouin scattering arises from the interaction of light with propagating density waves or acoustic phonons [46]. The stimulated Brillouin scattering is essentially described by a nonlinear interaction between two types of waves: the pump wave and the Stokes wave [47]. Electrostriction is the phenomenon wherein material density increases in response to the intensity of an applied optical field [48]. The phenomenon

produces density-fluctuations in a fibre medium by increasing the material disorder, which in turn modulates the linear refractive index of the medium and results in an electrostrictive-nonlinearity [46, 48]. Brillouin scattering can be understood via scattering of a Brillouin pump photon by an acoustic phonon, which is a unit of energy and momentum for the acoustic or sound wave produced through the electrostriction [47], and can also be described simply as a moving Bragg grating that reflects the pump light to the opposite direction of propagation, and is Doppler-shifted to a slightly lower optical frequency [34]. The basic principle of the SBS effect is shown in Figure 2.8:

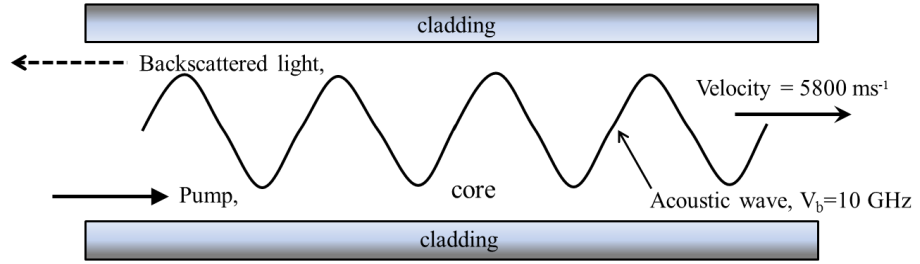


Figure 2. 8 Basic principle of stimulated Brillouin scattering effect.

The backscattered light also experiences gain from the forward-propagating signals, and so contributes to depletion of signal power. The Doppler shift experienced by the frequency of the scattered light is given by

$$v_B = \frac{2nV_s}{\lambda} \quad (2.27)$$

where n is the refractive index of the fibre core, whilst V_s is the velocity of sound wave (phonon) in the medium [49]. For instance, for a wave of wavelength 1550 nm that propagates in a silica based fibre, the acoustic wave velocity gives a Brillouin frequency shift of about 11 GHz when V_s is equals to 5800 ms⁻¹. The low threshold

and the large Brillouin gain traits of the SBS effect have made it interesting to DWDM network applications.

2.7 : Summary

This chapter comprehensively discusses the ultra-wideband semiconductor optical amplifier (SOA) and its applications, including the essential operating principles and usage in the realization of ultra-wideband fibre lasers. The beginning part of the chapter explains the brief features of SOA in optical fibre communication utilization. The best structure of SOA shall have the lowest loss-of-light signal that is coupled to the SOA, so as to avoid light leakage to the cladding regions. Cleaved facets with anti-reflection coating are the most eligible candidate to surpass the limitation, and have improved to achieve almost zero reflectivity at this time. There are two basic types of SOAs that are distinguished based on the reflectivity facets at both ends; Fabry-Perot and travelling-wave SOA. The difference of the two types of the SOA can be distinguished by the output spectrum emitted, as observed in the optical spectrum analyser (OSA).

The next section of the chapter is the theoretical understanding of the amplification operations of the SOA. The three essential radiative processes of spontaneous emission, stimulated emission and stimulated absorption are elaborated for further understanding. Both the spontaneous and stimulated emissions are understood to be yielding energies when they take place, hence making conditions likely for amplification. The stimulated absorption however is a loss process because the incident photon is annihilated at the end of the process. To attain amplification, a condition known as population inversion must be achieved. Characteristics of the SOA could be further explained by understanding the small signal gain concept of the SOA

along with the saturation current and power of the SOA. In order to determine the quality of amplification of an SOA, the noise figure and the amplified spontaneous emission theories are explained in the following part of this chapter, as well as the polarization dependent gain (PDG) effect that often causes output power fluctuations of the SOA. Two forms of fibre laser, namely linear cavity fibre laser and ring cavity fibre laser, are also introduced in this section.

Lastly, the final section of this chapter elaborates three methods of ultra-wideband fibre laser generation. The first two methods are associated with the wavelength filtering mechanisms of each AWG and FBGs. The final part of this section describes briefly the nonlinearity effect that occurs in optical fibres and the stimulated Brillouin scattering (SBS) effect. This final part is important as it gives a preliminary idea about one of the nonlinear effects in optical fibres.

REFERENCES

1. J. M. Wiesenfeld, L. H. Spiekman, "Chapter 19: Semiconductor Optical Amplifiers" in "Handbook of Optic volume V: Atmospheric Optics, Modulators, Fibre Optics, X-Ray and Neuron Optics", 3rd Edition, pp. 19.1-19.10, McGraw-Hill Companies, United States of America, 2010.
2. I. P. Kaminow, R. E. Nahoray, M. A. Pollack, L. W. Stulz, J. C. Dewinter, "Single-Mode CW Ridge-Waveguide Laser Emitting at 1.55 μ m", Electronics Letter, Vol. 15, No. 23, pp. 763-765, 1979.
3. R. J. Nelson, N. K. Dutta, "Review of InGaAsP/InP Laser Structure and Comparison of Their Performance", review of Semiconductors and Semimetals, Academic Press, New York, 1985.
4. M. J. Connelly, "Semiconductor Optical Amplifiers", Kluwer Academic Publishers, Dordrecht, 2002.
5. N. K. Dutta, Q. Wang, "Semiconductor Optical Amplifiers", Springer, Verlag, 2002.
6. C. E. Zah, R. Bhat, S. G. Menocal, N. Andreadakis, F. favire, C. Caneau, M. A. Koza, T. P. Lee, "1.55 μ m GaInAsP angled-Facet Flared-Waveguide Travelling-Wave Laser Amplifiers", Photonics Technology Letters, Vol. 2, No. 1, pp. 46-47, 1990.
7. I. Cha, M. Kitamura, H. Honmou and I. Mito, "1.5 μ m Band Travelling-Wave Semiconductor Optical Amplifier with Window Facet Structure", Electronics Letters, Vol. 26, No. 2, pp. 124-125, 1990.
8. B. Mersali, G. Gelly, A. Accard, J. L. Lafrayette, P. Doussiere, M. Lambert, B. Fernier, "1.55 μ m High-Gain Polarization-Insensitive Semiconductor Travelling

- Wave Amplifier with Low Driving Current”, *Electronics Letters*, Vol. 26, No. 2, pp. 124-125, 1990.
9. M. O’Mahony, “Semiconductor Laser Optical Amplifiers for Use in Future Fibre Systems”, *Journal of Lightwave Technology*, Vol. 5, No. 4, pp. 531-544, 1988.
 10. P. G. Eliseev, V. V. Luc, “Semiconductor Optical Amplifiers: Multifunctional Possibilities, Photoresponse and Phase Shift Properties”, *Pure Applied Optics*, Vol. 4, No. 4, pp. 295-313, 1995.
 11. A. E. Kelly, C. Michie, C. Tombling, I. Andonovic, “High Performance semiconductor Optical Amplifiers”, *Optical Fibre Comm. Conference*, Vol. 2, pp. 3, 2004.
 12. W. P. Dumke, “Interband Transitions and Maser Action”, *Physics Review*, Vol. 127, No. 5, pp. 1559-1563, 1962.
 13. H. Kroemer, “A Proposed Class of Heterojunction Injection Lasers”, *Proceeding IEEE*, Vol. 51, pp. 1782-1783, 1963.
 14. H. Kroemer, “Heterostructure Bipolar Transistors and Integrated Circuits”, *Proceeding IEEE*, Vol. 70, No. 1, pp. 13-25, 1982.
 15. A. F. Qasrawi, N. M. Gasanly, “Refractive Index, Static Dielectric Constant, Energy Band Gap and Oscillator Parameters of Ga₂SeS Single Crystals”, *Physica Status Solidi (A)*, Vol. 204, No. 9, pp. 3165-3169, 2007.
 16. J. Hashimoto, K. Koyama, T. Katsuyama, Y. Tsuji, K. Fujii, K. Yamazaki, A. Ishida, “1.3 μ m GaInNAs Bandgap Difference Confinement Semiconductor Optical Amplifiers”, *Japan Journal of Applied Physics*, Vol. 45, pp. 1635-1639, 2006.
 17. F. Xia, J. Wei, V. Menno, S. R. Forrest, “Monolithic Integration of a Semiconductor Optical Amplifier and a High Bandwidth P-I-N Photodiode

- using Assymetric Twin-Waveguide Technology”, *Photonics Technology Letters*, Vol. 15, No. 3, pp. 452-454, 2003.
18. E. Yablonovitch, “Photonic Band-Gap Structures”, *J. Opt. Soc. Am. B*, Vol. 10, No. 2, pp. 283-297, Claifornia, 1993.
 19. M. Ilyas, H. T. Mouftah, “The Handbook of Optical Communication Networks”, CRC Press, 2003.
 20. F. R. Barbosa, C.Coral, J. R. Caumo, A. Flacker, “Hermetically Packaged semiconductor Optical Amplifier for Application in Singlemode Fibre Systems”, *SBMO International Microwave Conference/Brazil*, Vol. 1, pp. 129-134, 1993.
 21. D. K. Mynbaev, L. L. Scheiner, “Fibre-Optic Communications Technology”, Prentice Hall, New Jersey, 2001.
 22. Y. Suematsu, A. R. Adams, “Handbook of Semiconductor Lasers and Photonic Integrated Circuits”, Chapman and Hall, London, 1994.
 23. A. Yariv, “Quantum Electronics”, Wiley, New York, 1989.
 24. Kavintheran A/L Thambiratnam, “A Multi-wavelength Source based on Sagnac Loop and Semiconductor Optical Amplifier”, Master of Science Thesis, University of Malaya, 2007.
 25. M. J. Adams, J. V. Collins, I. D. Henning, “Analysis of Semiconductor Lasers Optical Amplifiers”, *IEEE Proceedings*, Vol. 132, No. 1, pp. 58-63, 1985.
 26. Y. Yamamoto, “Characteristics of AlGaAs Fabry-Perot Cavity Type Laser Amplifiers”, *Quantum Electronics*, Vol. 16, No. 10, pp. 1047-1052, 1980.
 27. D. K. Mynbaev, L. L. Scheiner, “Fibre-Optic Communications Technology”, Prentice Hall, New Jersey, 2001.
 28. A. E. Kelly, I. F. Lealman, L. J. Rivers, S. D. Perrin, M. Silver, “Low Noise Figure (7.2dB) and High Gain (29dB) Semiconductor Optical Amplifier with a

- Single Layer AR Coating”, *Electronics Letters*, Vol. 33, No. 6, pp. 536-537, 1997.
29. E. Comforti, C. M. Gallep, S. H. Ho, A. C. Bordonalli, S.M. Kang, “Carrier Reuse with Gain Compression and Feed-Forward Semiconductor Optical Amplifiers”, *Trans. Microwave Theory and Tech.*, Vol. 50, pp. 77-81, 2002.
 30. M. Quillec, “Materials for Optoelectronics”, Springer, 1996.
 31. S. W. Harun, P. Poopalan, H. Ahmad, “Gain Enhancement in L-band EDFA through a Double-Pass Technique”, *Photonic Technology Letters*, Vol. 14, No. 3, pp. 296-297, 2002.
 32. Product Note 71452-1, EDFA Testing with Interpolation technique”, Agilent Technologies, USA, 2000.
 33. D. Marcuse, “Principle of Optical Fibre Measurements”, Academic Press, New York, 1981.
 34. Mohd Zamani Zulkifli, “Study of S-Band Optical Amplifiers and Its Applications”, Doctor of Philosophy Thesis, University of Malaya, 2012.
 35. Amirah binti Abd. Latif, “The Generation of Dual-Wavelength Fibre Lasers and Their Applications”, Doctor of Philosophy Thesis, University of Malaya, 2013.
 36. J. Hecht, “Understanding Fibre Optics”, Prentice Hall, 4th Edition, 2002.
 37. J. Roths, C. Sudan, R. Kuttler, C. Gerz, “High Precision, Low-Cost Interrogation System for Fibre Bragg Grating Sensors”, *DGaO Proceedings*, 2005.
 38. K. O. Hill, “Chapter 9: Fibre Bragg Gratings” in “Handbook of Optic volume IV: Fibre Optics and Nonlinear Optics”, 2nd Edition, pp. 9.1-9.12, McGraw-Hill Companies, United States of America, 2001.
 39. A. Othonos, K. Kalli, D. Pureur, A. Mugnier, Fibre Bragg Gratings in “Wavelength Filters in Fibre Optics” Springer Series in Optical Sciences, Vol. 123, pp. 189-269, 2006.

40. K. O. Hill, Y. Fujii, D.C. Johnson, et al., "Photosensitivity in Optical Waveguides: Application to Reflection Filter Fabrication," *Applied Physics Letter*", Vol. 32, No. 10, pp. 647-649, 1978.
41. B. S. Kawasaki, K. O. Hill, D. C. Johnson, et al., "Narrow-Band Bragg Reflectors in Optical Fibers", *Optics Letters*, Vol. 3, No. 8, pp. 66-68, 1978.
42. Abdul Hadi Sulaiman, "SOA-Based Fibre Ring Laser", Masters of Science Thesis, University Malaya, 2009.
43. X. J. M. Leijtens, B. Kuhlow, M. K. Smit, *Arrayed Waveguide Gratings in "Wavelength Filters in Fibre Optics" Springer Series in Optical Sciences*, Vol. 123, pp. 125-187, 2006.
44. S. P. Singh, N. Singh, "Nonlinear Effects in Optical Fibers: Origin, Management and Applications", *Progress In Electromagnetic Research (PIER)*, Vol. 73, pp. 249-275, 2007.
45. R. U. Kale, P. M. Ingale, R. T. Murade, "Comparison of SRS & SBS (Non Linear Scattering) In Optical Fibre", *International Journal of Recent Technology and Engineering (IJRTE)*, Vol. 2, Issue 1, pp. 118-122, March 2013.
46. A. B. Ruffin, "Stimulated Brillouin Scattering: An Overview of Measurements, System Impairments, and Applications", NIST-SOFM 2004.
47. Mohammadreza Rezadadeh Shirazi, "Multiwavelength Brillouin Fiber Lasers", Doctor of Philosophy Thesis, University of Malaya, 2009.
48. S. P. Singh, R. Gangwar, N. Singh, "Nonlinear Scattering Effects in Optical Fibers", *Progress In Electromagnetic Research, PIER* 74, pp. 379-405, 2007.
49. G. Keiser, "Optical Fibre Communications", 4th Edition, McGraw-Hill International Edition, 2010.
50. J. Roths, C. Sudan, R. Kuttler, C. Gerz, "High Precision, Low-Cost Interrogation System for Fibre Bragg Grating Sensors", *DGaO Proceedings*, 2005.

CHAPTER 3

CHARACTERIZATION OF ULTRA-WIDEBAND SOA

3.1 : Introduction

In this thesis, three methods of generating a fibre laser based on an ultra-wideband semiconductor optical amplifier (SOA) as the gain medium are proposed; fibre Bragg gratings (FBGs) as a wavelength selective filtering component, 16-channels arrayed waveguide grating (AWG) to create a switchable fibre laser system, and stimulated Brillouin scattering (SBS) effect to produce a 0.08nm wavelength spacing multi-wavelength fibre laser system. The ultra-wideband SOA will operate as the gain medium that is responsible for generating the ASE spectrum needed by the respective fibre laser systems. The three stated methods will ‘process’ the amplified spontaneous emission (ASE) spectrum into the multiple wavelength laser output. In order to obtain the desired results of the three methods of ultra-wideband multi-wavelength fibre laser generation, the characteristics of the ultra-wideband SOA is first investigated. As stated in chapter 2, the ASE has biggest influence in the efficiency of the ultra-wideband SOA performance as it is related to gain pattern. The investigation then continues by determining the gain and noise figure performance of the semiconductor gain medium, together with its polarization dependent gain effect on both gain and noise figure.

3.2 Ultra-wideband SOA characterization

Due to its nature of optical amplifier basis, the SOA is expected to amplify the power level of any optical signals that pass through it. This contributes to the importance of gain and noise figure characteristics of the SOA so that to determine the efficiency of a particular SOA. Gain is defined as the ability of the SOA to amplify optical signals that pass through it, whilst noise figure refers to the noise contributed to the optical signal by the SOA itself [1]. The quality of a certain signal is dependent on the number of SOAs deployed in a single fibre transmission line. This is due to the fact that noise increases with every insertion of the SOA into the fibre transmission line, whereas the higher the number of SOAs deployed in series into a certain fibre transmission line, the higher the noise accumulated in the system [2]. Consequently, the gain should be attained as high as possible whilst the noise figure penalty should be optimized to be as low as possible in order to accomplish optimum operation.

The function of the SOA varies by certain location in a network. There are three different applications of SOA depending on the placement of it in a network; post-amplifier (or booster amplifier), in-line amplifier, and pre-amplifier [3]. Post-amplifier which is also known as booster amplifier, has the function to increase a relatively high power input signal prior to transmission, and hence it is inserted right after the transmitter. Since the optical signal travels quite a long distance before reaching the receiver (i.e. > 100 km for a long haul link network [1]), the power level of the optical signal is very prone to attenuation. In order to sustain the power level of the optical signal transmitted, an in-line amplifier needs to be inserted in between the transmitter and the receiver. A series of an in-line amplifiers (constructed by many SOAs put in series with a certain distance between them) can be used to mitigate the power attenuation by reinstating the power level of the optical signal, as well as preserving its original signal spectrum [2, 4].

Thus, it is crucial for the SOAs used in the construction of the in-line amplifier to have high gain, high output power and a low noise figure [1]. On the contrary, a pre-amplifier is used to increase the power level of an incoming signal prior to conventional reception and demodulation, so as to increase receiver sensitivity and hence to increase the link power budget [3]. The crucial characteristic of an SOA used as a pre-amplifier is to have a very low noise figure so as to minimize the penalty on the output signal quality. Figure 3.1 shows the configuration of the post-amplifier or booster amplifier, in-line amplifier and pre-amplifier in a particular transmission network system.

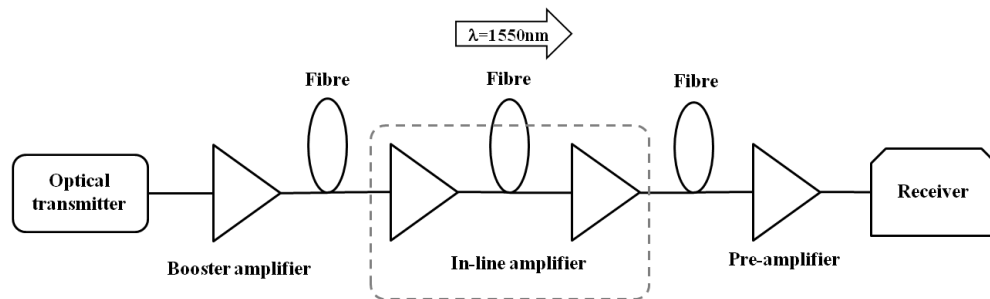


Figure 3. 1 The placement configuration of the three types of amplifiers in a transmission network

In this chapter, the amplification performance of the SOA is first characterized by observing its gain, NF and polarization dependence gain. The capability of the SOA to manage ultra-wideband amplification is also determined by observing the gain bandwidth of the SOA, which is discussed in the later part of this chapter. The ultra-wideband amplification covers the range of the telecommunication bands of the conventional (C-) band of 1530 nm to 1565 nm, as well as expanding it to the short (S-) band and long (L-) band of 1460 nm to 1525 nm and 1570 nm to 1620 nm wavelength range respectively.

3.2.1 Alphion SAS26p ultra-wideband SOA and experimental setup

The ultra-wideband SOA used in this research is the SAS26p model from Alphion Corporation as shown in Figure 3.2. Alphion claims that the SOA operates in the wavelength range of 1460 nm to 1620 nm which wholly covers the short (S-), conventional (C-) and long (L-) band [5]. The SOA is fabricated by implementing the quantum dot technology so as to provide an ultra-wide band ASE functionality to the system. The maximum drive current of the ultra-wideband SOA is about 600 mA [6]. The operating temperature of the ultra-wideband SOA is maintained to not exceed 70°C by using the TEC cooler whilst the storing temperature should be in the range of -40°C to 85°C. The thermistor current must not exceed 5 mA whilst the TEC current and TEC voltage maximum values are 1.8 A and 3.4 V respectively. It is critical to ensure that all the absolute maximum ratings of the device are strictly abided, in order to avoid any permanent damage to the module. Hence, a laser diode driver equipped with a TEC cooler is used to drive the SAS26p SOA model, and is mounted on a specially designed solid block aluminium casing with the purpose to instantly unlock the heat extraction from the SOA during operation.

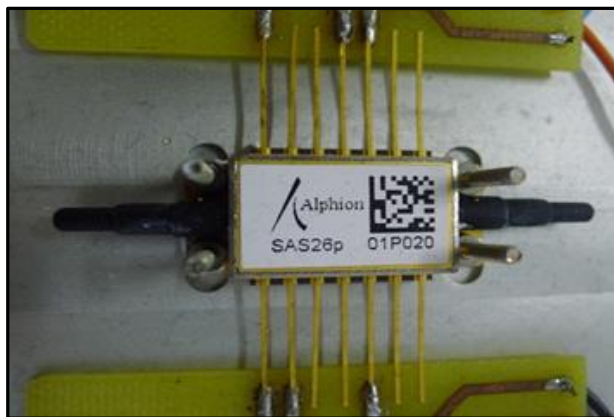


Figure 3. 2 SAS26p SOA model by Alphion Corporation

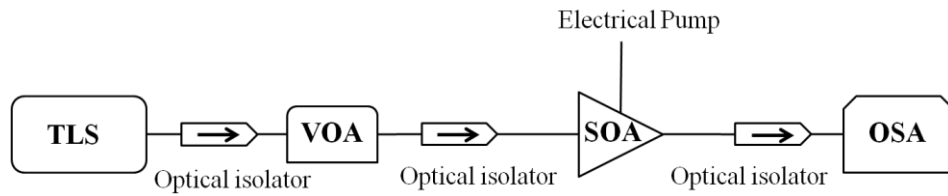


Figure 3. 3 Experimental setup of an ultra-wideband amplifier by using SOA as the gain medium

Figure 3.3 shows the experimental setup to investigate the gain and noise figure (NF) pattern of the SOA by first determining its amplified spontaneous emission (ASE) pattern. The electrical pump controls the drive current of the SOA which is driven by an ILX Laser Diode Controller. When sufficient current is injected to exceed the threshold current to the SOA, an ASE signal emitted from SOA is forced to propagate in unidirectional path by the optical isolator, and subsequently analysed via the optical spectrum analyser (OSA) (Ando AQ6317C) with a 0.02 nm resolution. The ultra-wideband SOA is driven by an ILX Laser Diode Controller at an optimum drive current of 390 mA, while a Yokogawa AQ2211 Tunable Laser Source (TLS) with a tunability range of 1400 nm to 1670 nm and a resolution of 0.001 nm is used to provide the ultra-wideband input signal. To control the input power emitted by the TLS, a variable optical attenuator (VOA) is placed after the TLS. An optical isolator is immediately placed in sequence, in order to force the signal to propagate in a unidirectional path and also to prevent any back-reflected signals that can cause damage to the TLS. Finally, the amplified signal exits the SOA and enters another optical isolator for analysis via the OSA.

3.2.2 Amplified spontaneous emission of ultra-wideband SOA

Spontaneous emission occurs in an excited medium without the existence of an input signal. In a semiconductor, the injection of the drive current contributes to the spontaneous recombination of electron-hole pairs that causes the spontaneous emission to occur. Within the occupied states of the semiconductor bands, the spontaneous emission occurs in a certain range of wavelength, within every spatial direction [7]. As discussed in Chapter 2 of this thesis, stimulated emission is another type of emission that is possible to occur in the system. Some fractions of the spontaneously emitted photons will stimulate the emissions of new coherent photons, which then results in the rise of ASE. Since the ASE is well known as the source of noise in the SOA [7], it is crucial to determine the optimum drive current of the SOA so as to attain the desired gain, as well as minimizing the noise figure penalty. Figure 3.4 shows the ASE spectra of the ultra-wideband SOA at various drive currents.

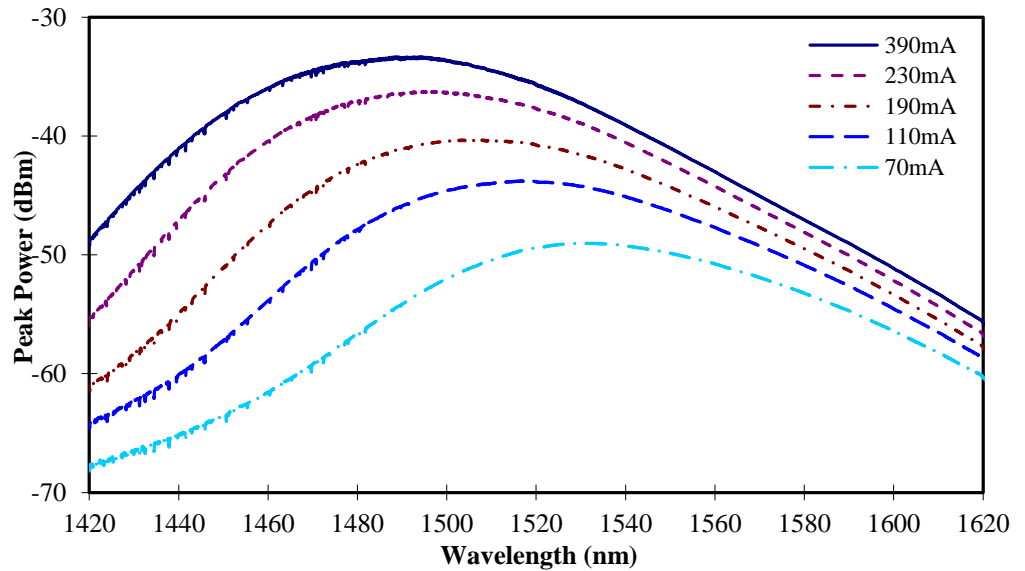


Figure 3. 4 ASE spectrums with variation of drive current effect.

As shown in Figure 3.4, the ASE spectra cover a wide-band range from 1420 nm to 1600 nm transmission wavelength. The ASE power level is observed to be increasing as the drive current is varied from 70 mA to 390 mA. This is attributed to the increase of the population inversions subsequent to the increase of drive current. It is also observed that the ASE spectrum shifts to a shorter wavelength as the injected current increases. This is attributed to more of the higher states in the band being filled as the current is increased, and so extends the amplification region to a shorter wavelength [7]. Recombination of carriers from higher occupied states within the bands produces photons with a shorter wavelength.

3.2.3 Ultra-wideband SOA gain bandwidth

The next essential study of the ultra-wideband SOA is to determine the gain bandwidth of the optical amplifier. To characterize the gain bandwidth, two sets of experiment are conducted; injecting a low and high input signal power of -30 dBm and 0 dBm into the amplifier setup. The wavelength of the input signal is varied throughout the triple band of S-, C- and L-bands of 1460 nm until 1600 nm to tweak the gain and the noise figure (discussed in the next section 3.2.4) performance for the particular wavelength of transmission. The experimental setup is as shown in the earlier Figure 3.3.

Figure 3.5 (a) shows the gain pattern attained at a wavelength range of 1460 nm until 1600 nm for a low input power of -30 dBm characterization. It is observed that the gain bandwidth obtained for the low input signal power is about 140 nm wide. It can be seen that most of the higher gain values are attained at the S-band region that lies in the range of 1460 nm to 1520 nm. In the shorter wavelength of S-band region of 1460 nm to 1475 nm, the gain is observed to be increasing linearly from 17.17 dB to 21.72 dB. For the middle wavelength range of the S-band, a gradual increase in the gain pattern is

observed within the 1480 nm to 1500 nm wavelength with a gain value of 22.03 dB to 23.53 dB. A slight dwindle in the gain value at wavelength 1495 nm is mostly due to the polarization dependent gain (PDG) effect which will be discussed further in this chapter. In the longer wavelength range of the S-band (1505 nm to 1525 nm), a gradually descending pattern of the gain values is observed from 22.84 dB to 20.96 dB. As for the C-band region of 1530 nm to 1565 nm, a linear decrease in the gain value is seen from 20.56 dB to 14.1 dB. A persistent decrement of the gain value is monitored towards the longer wavelength of L-band region. The lowest attained gain value is recorded to be 7.71 dB at 1600 nm wavelength.

The gain results for the high input power signal of 0 dBm are as shown in Figure 3.5 (b). In the wavelength region of S-band, the gain shows a linear increment from 1460 nm to 1500 nm with the gain value of 6.96 dB to 9.62 dB. As for the longer S-band wavelength, an almost flat gain is observed. This almost flat gain pattern is extended to the C-band region, which is in the wavelength range of 1505 nm until 1560 nm, with the gain values varied from 9.72 dB to 9.19 dB. Towards the longer wavelength of 1565 nm to 1600 nm, it can be seen that the gain value is gradually decreasing. The smallest gain achieved is at wavelength 1600 nm with the value of 6.04 dB.

The low input power signal gain pattern is observed to be slightly following the ASE pattern of the ultra-wideband SOA, whilst the high input power signal gain test of 0 dBm is observed to be experiencing a Gaussian-like type of gain profile. This is primarily a consequence of the saturation gain effect of the input signal. The saturation gain effect will be further discussed in the next section.

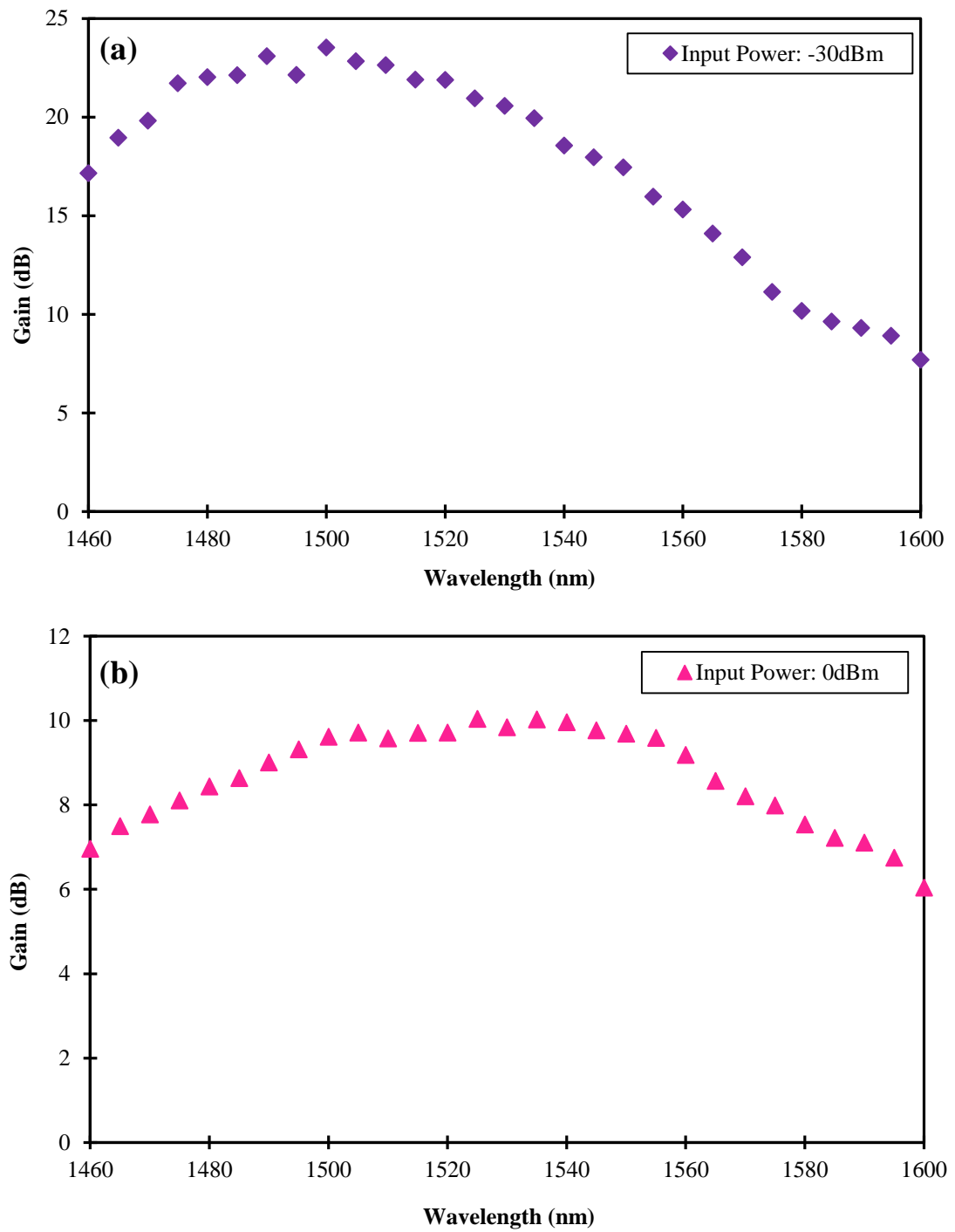


Figure 3. 5 Gain performances for different input wavelength with constant input power of (a) low input power -30 dBm, (b) high input power 0 dBm.

3.2.4 Small-signal gain and gain saturation effect

In laser amplifiers, a small signal gain is defined as the gain obtained for an input signal which is so weak that it does not cause any gain saturation [1, 3]. In this chapter, several tests are conducted to characterize the small signal gain and the saturation effect for each transmission region of the S-, C- and L-bands. By fixing the signal wavelength to 1500 nm for S-band, 1550 nm for C-band and 1580 nm for L-band, the tests are conducted by shooting a varied set of input power signals to the amplifier setup. The input power signals are varied from as low as -40 dBm to as high as 5 dBm. The results of the small signal gain and the saturation effect tests are as shown in Figure 3.6.

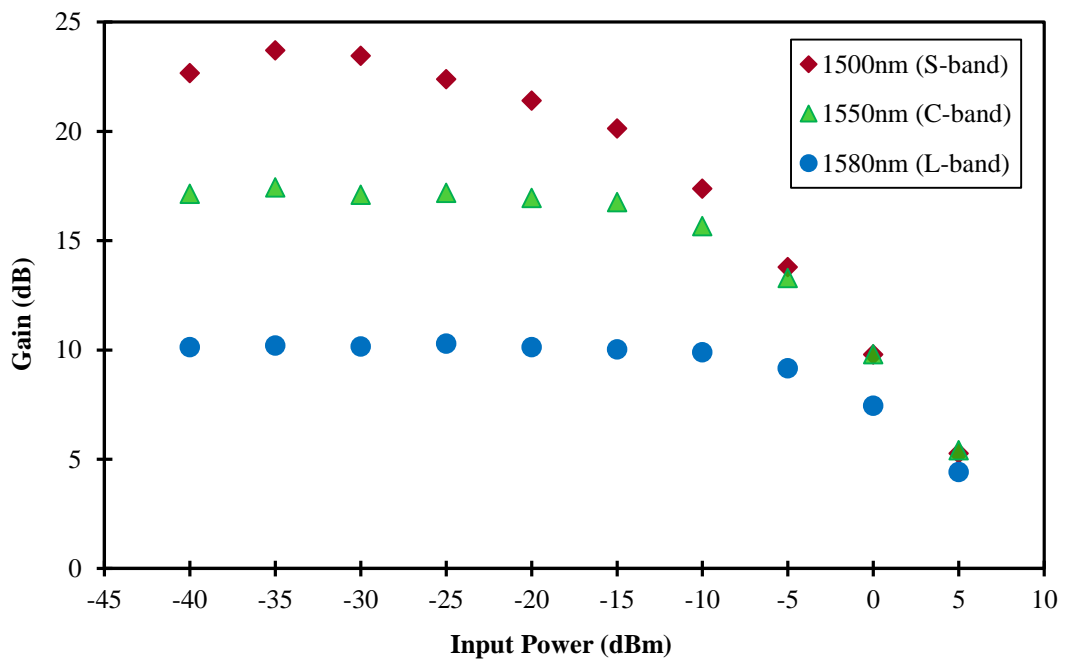


Figure 3. 6 Gain results of the input power signal variation tests for S-, C- and L-bands.

Referring to Figure 3.6 above, the wavelength of 1500 nm attains the highest gain value of 23.71 dB at -35 dBm input signal power. The increase in input signal power then leads to a decrease in gain value for the same input signal wavelength of 1500 nm. The

lowest gain value of 5.27 dB is observed at the highest input signal power of 5 dBm. For 1550 nm signal wavelength, a different pattern of gain results is observed. An almost flat gain shape at the lower power of input signals (from -40 dBm to -15 dBm) is obtained, before a steep negative slope is observed at the higher power range of the input signal. It is observed that the highest gain achieved is 17.44 dB at a -35 dBm input signal power, while the lowest gain is 5.41 dB for a high input signal power of 5 dBm. A similar case of gain pattern is observed for the 1580 nm input signal wavelength. The gain pattern is seen to be almost flattened at the lower input signal range of -40 dBm to -10 dBm, before descending gradually as the input power signal is increased. The highest gain achieved is at input power signal -35 dBm with 10.2 dB whilst the lowest gain is 4.42 dB at 5 dBm input power signal. The average gain at the lower input power signal of -40 dBm to -10 dBm range are about 21.59 dB, 16.89 dB and 10.12 dB for 1500 nm, 1550 nm and 1580 nm signal wavelengths respectively. From the figure, it can also be determined that the 3 dB input signal saturation powers are observed to be -18.0 dBm for 1500 nm, -7.5 dBm for 1550 nm and 0.5 dBm for 1580 nm input signal wavelength. It can be concluded that the 3 dB saturation input powers increase for longer wavelengths of operation.

3.2.5 Noise figure of ultra-wideband SOA

The next important part of characterizing the ultra-wideband SOA is the noise figure (NF) characterization. As well as determining the gain of each band region of transmission, the NF observation needs to be analyzed in order to attain maximum performance of the SOA. NF is briefly introduced as a measure of how much a device (in this case, an amplifier) degrades the signal-to-noise ratio (SNR). In Figure 3.7, the NF performance for two types of input power signal throughout the triple bands of S-, C- and L-bands (from 1460 nm to 1600 nm) is shown. Figure 3.7 (a) shows the NF performance

of low input signal power of -30 dBm, whilst Figure 3.7 (b) shows the NF performance of high input signal power of 0 dBm.

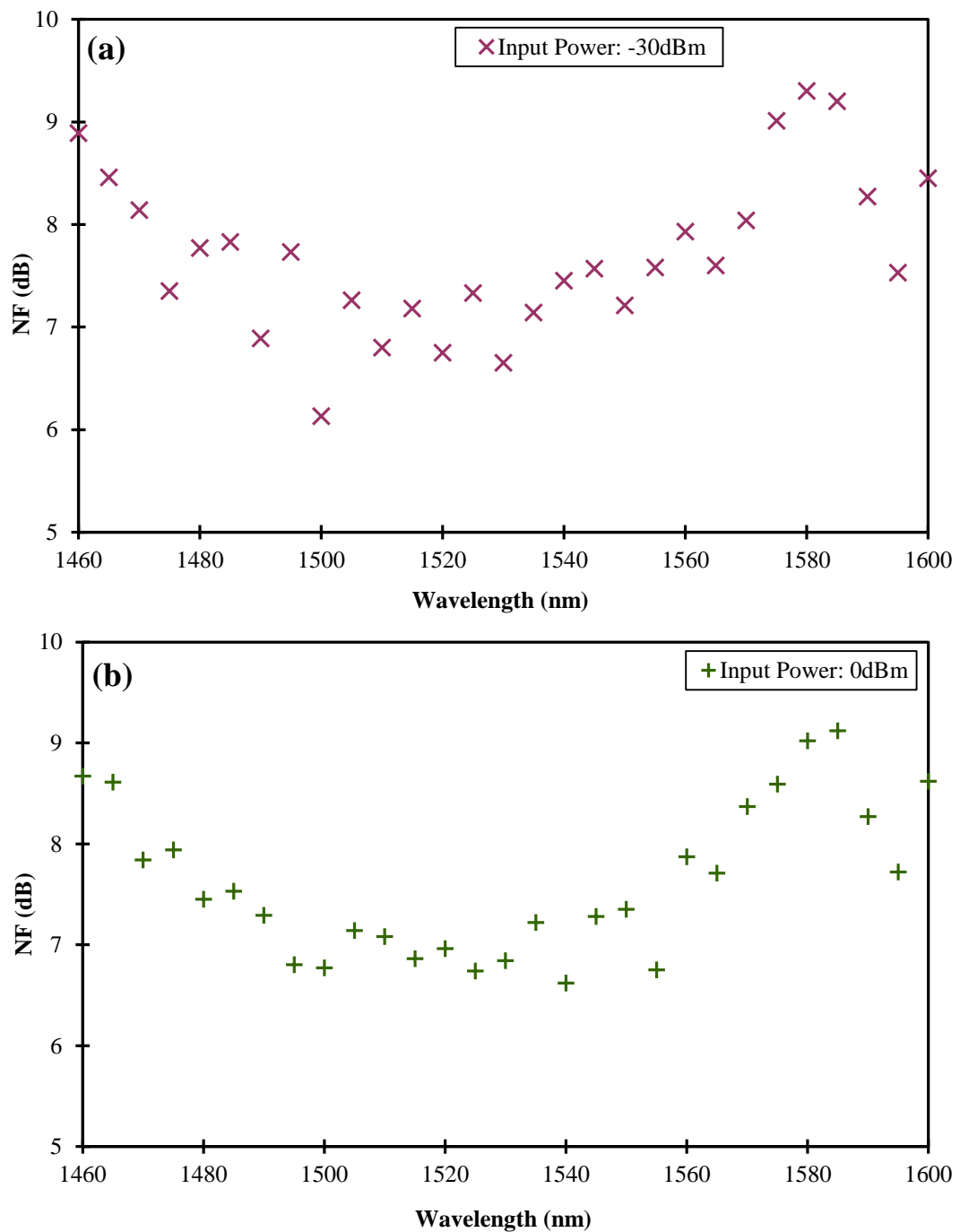


Figure 3. 7 NF performances for different input wavelength with constant input power of (a) low input signal power -30 dBm, (b) high input signal power 0 dBm.

In Figure 3.7 (a), the NF pattern for input signal power -30 dBm is observed to experience small fluctuations in the values. This results from the polarization dependent gain (PDG) effect of the ultra-wideband SOA. The effect on PDG could be minimized by using polarization maintaining fiber (PMF) on the whole resonator configuration, which unfortunately will increase the cost of the proposed system [15, 16]. More discussion on the PDG effect will take part later in this chapter. At wavelength 1500 nm (S-band), the lowest value of NF of 6.13 dB is obtained. However, the NF values increase towards the longer wavelength, as the 1550 nm (C-band) NF is about 7.21 dB and the 1580 nm (L-band) NF is about 9.3 dB. The maximum value of noise extinction ratio is recorded to be about 1.60 dB. A lower value of NF attained in the 1500 nm to 1560 nm region is mainly due to a limitation of the operating wavelength range of the isolator used (which is in C-band region) in the experiment. The maximum noise extinction ratio for the low input signal power is about 0.40 dB.

The next characterization is conducted by varying the input signal power from as low as -40 dBm to as high as 5 dBm for a fixed centre wavelength of each band : S-band (1500 nm), C-band (1550 nm) and L-band (1580 nm). The results are as plotted in Figure 3.8. It can be seen that the NF pattern for each centre wavelength is different from others. For wavelength 1500 nm and 1550 nm, there are significant fluctuations in the NF values observed. However, the NF trend for centre wavelength 1580 nm shows an almost flattened NF values for different input signal powers. The NF values vary from 8.92 dB to 9.15 dB, whilst the 1500 nm and 1550 nm NFs vary from 6.35 dB to 7.8 dB and from 7.23 dB to 8.09 dB respectively. The fluctuations are mainly a consequence of the PDG effect which is considered as a property of most semiconductor optical amplifiers.

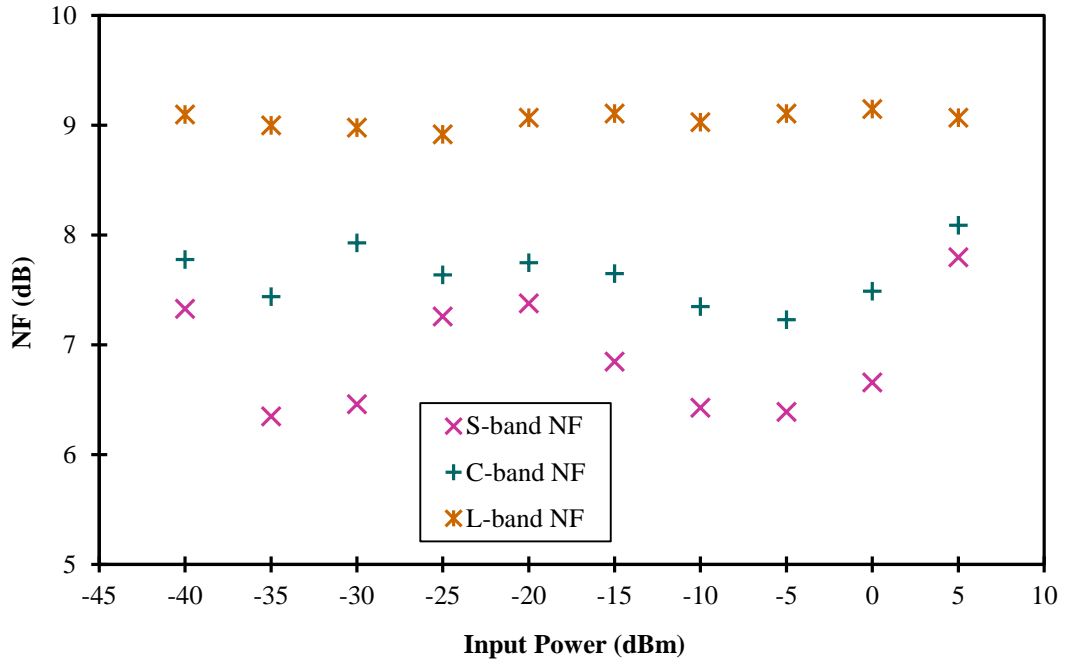


Figure 3. 8 The NF performance in input signal power variation for three centre wavelength of S-band (1500 nm), C-band (1550 nm) and L-band (1580 nm).

3.2.6 Polarization dependent gain effect of SOA

The final part of the characterization of the ultra-wideband SOA is the PDG effect. It is well known that most SOAs are very sensitive to input signal polarization state; thus a completed characterization is crucial in order to determine the polarization effect on the gain performance of the ultra-wideband SOA.

The experimental setup shown in Figure 3.9 is basically similar with the earlier experimental setup of Figure 3.3, except for the existence of a polarization controller (PC) which is attached to both the input and output ports of the ultra-wideband SOA. The test is conducted by adjusting the PC to achieve maximum and minimum values of output powers. The difference of the maximum and the minimum values of the output powers

are then recorded and plotted in a graph in order to observe a pattern. The tabulated PDG test graph is as shown in Figure 3.10.

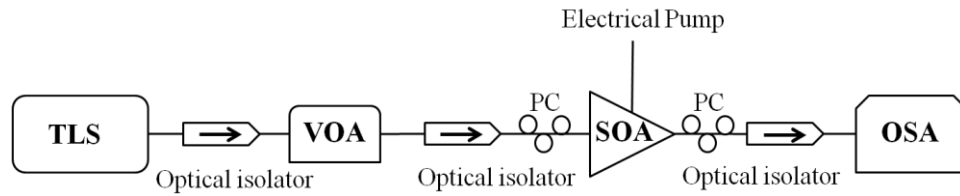


Figure 3. 9 Experimental setup of PDG effect test of the ultra-wideband SOA.

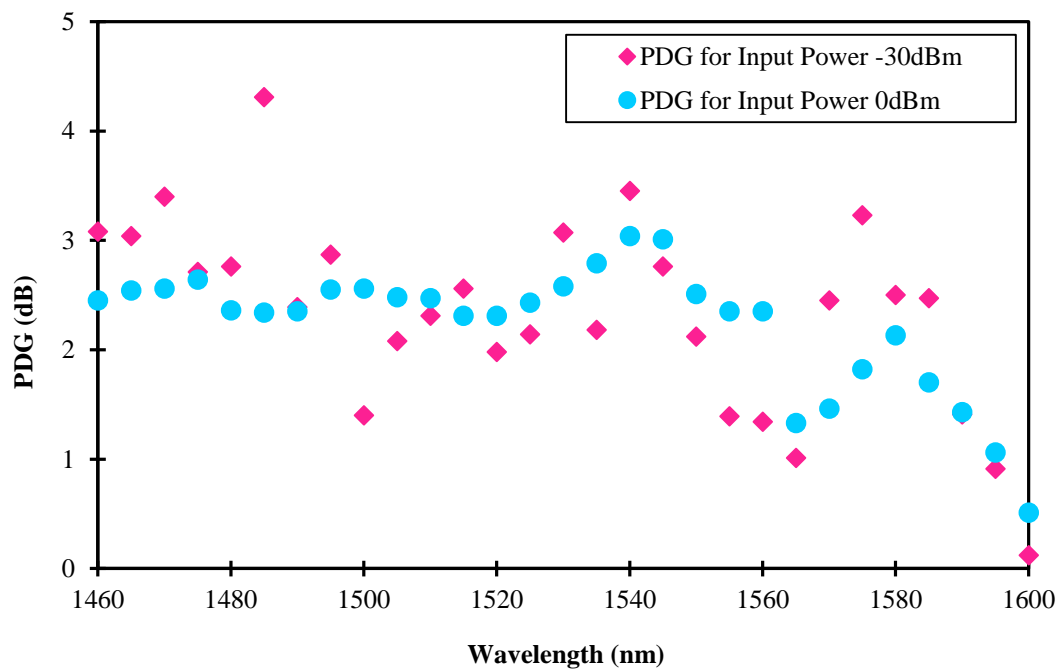


Figure 3. 10 The PDG results for variation of input signal power of -30 dBm (low) and 0 dBm (high) across input signal wavelength ranges from 1460 nm until 1600 nm.

According to Figure 3.10, the maximum PDG attained by the low input signal power of -30 dBm is about 4.31 dB at wavelength 1485 nm, while about 3.04 dB maximum PDG is attained for high input signal power of 0 dBm at 1540 nm wavelength.

For the low input signal power of -30 dBm, the PDG of wavelength 1500 nm is calculated to be 1.4 dB while the PDG at 1550 nm and 1580 nm are recorded as 2.12 dB and 2.5 dB respectively. For high input signal power, the PDG recorded for wavelengths 1500 nm, 1550 nm and 1580 nm are 2.56 dB, 2.51 dB and 2.13 dB respectively. The graph of Figure 3.10 also shows that the PDG results of the low input signal power (-30 dBm) have more fluctuations compared to the high input signal power (0 dBm) PDG results. The cause for the high fluctuations is mainly due to the higher ASE level obtained at low input signal power, which results in a higher sensitivity to the polarization effect that is mainly affected by the type of optical fibre used to construct the laser resonator.

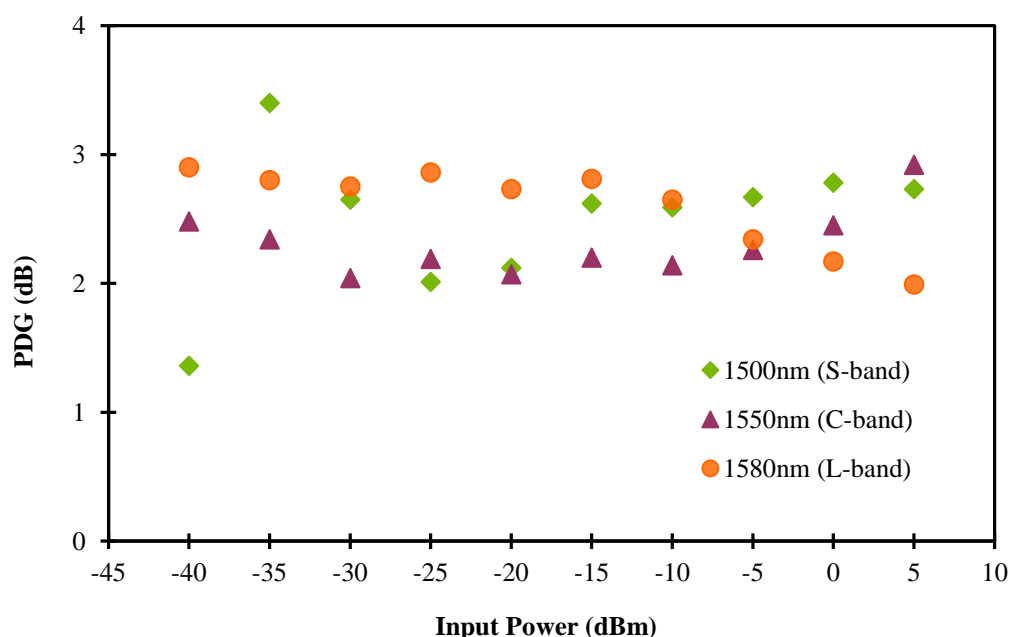


Figure 3. 11 PDG test results with variation of input signal power for S-, C- and L-bands centre wavelength.

Figure 3.11 shows the PDG test results against input signal power variation. By conducting three sets of PDG tests with three different centre wavelengths of 1500 nm (S-band), 1550 nm (C-band) and 1580 nm (L-band), the input signal power is varied from

-40 dBm to 5 dBm. For the 1500 nm centre wavelength, the maximum PDG is recorded to be about 3.4 dB at the input signal power of -35 dBm. This is the highest value of maximum PDG for all three centre wavelengths, since the 1550nm and the 1580 nm obtain only about 2.92 dB and 2.9 dB maximum PDG, for 5 dBm and -40 dBm input signal powers respectively. The S-band centre wavelength of 1500 nm PDG results are observed to experience a considerable fluctuation throughout the changes of input signal power compared to the C-band and L-band centre wavelengths results. This is mainly due to the high ASE level that causes higher sensitivity of polarization in this wavelength region.

3.2.7 High gain S-band SOA with double-pass configuration

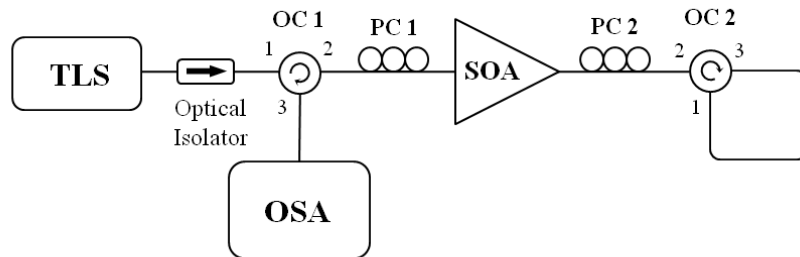


Figure 3. 12 Experimental setup of the high-gain S-band in a double-pass configuration.

Figure 3.12 above shows the experimental setup of the high-gain S-band SOA in a double-pass configuration. The setup consists of an ultra-wideband SOA as the gain medium. The ultra-wideband SOA is driven by an ILX laser diode controller at a drive current of 460 mA, whilst a Yokogawa AQ2211 tunable laser source (TLS) with a tunability range of 1440 nm to 1530 nm and a resolution of 0.001 nm is used to provide the S-band input signal [8]. An optical isolator is placed immediately after the TLS to

force the signal to propagate in a unidirectional path and also prevent any back-reflected signals that can cause damage to the TLS [8]. The S-band signal generated from the TLS first travels to port 1 of the first optical circulator (OC1), where it then continues via port 2 towards the polarization controller and onwards to the SOA [8]. The use of the polarization controller is to provide a means to optimize the gain [8]. The amplified signal will then exit the SOA and enter another polarization controller, after which it enters the second optical circulator (OC2) where port 1 and port 3 are connected, which functions as a 'mirror' [8]. This back-reflected amplified signal will then be re-amplified by the SOA and is subsequently emitted at port 3 of OC1 (entering OC1 at port 2) and analysed via an optical spectrum analyser (OSA) [8]. For the case of single pass configuration, there are no optical circulators that function as 'mirrors', unlike in the double-pass [8]. The signal is instead measured directly after the SOA as shown in Figure 3.3.

The comparison of the ASE spectra of the SOA in the single-pass and double pass configuration can be seen in Figure 3.13. It is observed that the power level of the ASE is about -24 dBm at wavelength 1500 nm, with the drive current of 460 mA. For an identical condition, the single-pass configuration only manages to yield about -32 dBm of ASE power level, which is calculated to be 8 dB less than the double-pass configuration [8]. A distinct shape difference of the ASE also can be observed from the respective figure. It can be seen that the double-pass configuration is slightly concentrated at the longer transmission wavelength region that fits well in the L-band regions; whilst the single-pass ASE disperses over a wider transmission wavelength range [8]. This phenomenon is influenced by the inhomogeneous broadening property of the SOA material gain, InGaAsP [8].

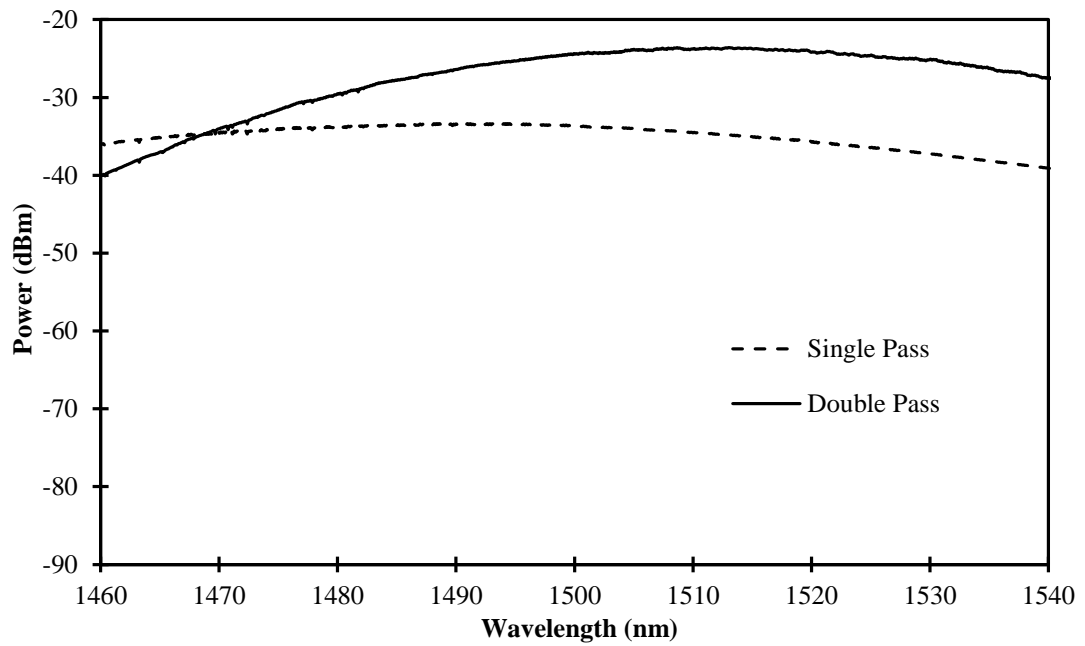


Figure 3. 13 ASE spectra comparison between the single-pass and double-pass configuration setup when 460 mA drive current is applied to the SOA.

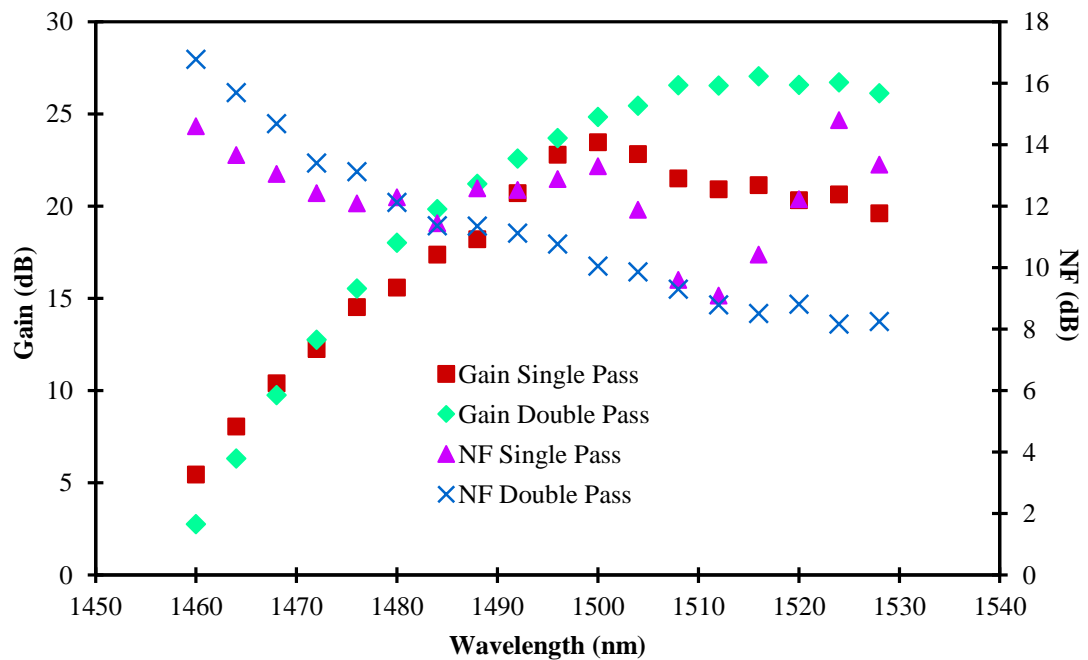


Figure 3. 14 Gain and noise figure performance at various input wavelength for -30 dBm input signal power.

The gain and NF performance of both single-pass and double-pass configuration against input wavelength variation is as shown in Figure 3.14. The input signal power is fixed at -30 dBm for the experiment. The initial gain values of both the single-pass and double-pass systems are almost similar, with the difference between gains achieved by the two systems amounting to approximately 2 to 3 dB up to an input wavelength of 1500 nm [8]. However, at longer wavelengths the gain of the single-pass system drops, whereas the gain of the double-pass system continues to increase to a maximum value of 27.06 dB at a wavelength of 1516 nm, an improvement of 6.01 dB over that of the single-pass configuration. This gain performance can be explained from the ASE spectra of the two systems given in Figure 3.13. The NF of the single-pass system fares better from 1480 nm until 1520 nm in comparison to the double-pass system that has a better NF from 1460 nm to 1480 nm. The NF for the single-pass configuration at 1490 nm is about 11 dB and reduces to 8 dB at around 1520 nm [8]. Normally, the NF of an SOA is quite high at around 15 dB, and as such the values obtained can be considered a good achievement [8]. The fluctuating NF of the double-pass system at the longer wavelength region is attributed to the PDG effect in the SOA [8]. Other than that, the SOA characteristics of gain and NF of different input signal powers of -40 dBm to -5 dBm (simulating low to high powered input signals) are also measured at a fixed wavelength of 1500 nm.

In Figure 3.15, it is observed that the double-pass configuration shows higher gain performance with respect to the single-pass configuration, having a maximum gain of 31.07 dB at an input signal power of -40 dBm, which is measured to be 6.7 dB higher than the maximum gain of the single-pass configuration at this condition. It can also be observed that the gain of the double-pass always exceeds the gain for the single-pass system as the signal power is increased. However, when reaching a higher input signal power of -5 dBm, the gain trends tend to merge together which is mostly affected by the saturation [8]. The NF values are measured to be an average of 10 dB for the single-pass

system with various input signal powers, which is somewhat similar with the double-pass system NF values of about 8 to 9 dB [8]. On the whole, this specific SOA could function as a good alternative for obtaining high gain amplification in the S-band region [8]. The lack of corresponding for the gain value of the input signal power of -30 dBm at wavelength 1500 nm of Figure 3.15 with the results in Figure 3.14 is largely due to the PDG effect that usually occurs in most types of SOAs [9-14], and this can be minimized by the careful adjustment of the polarization controllers [8]. The reported PDG characteristic is as discussed previously in section 3.2.6. The value of the PDG effect can be larger for the double-pass configuration.

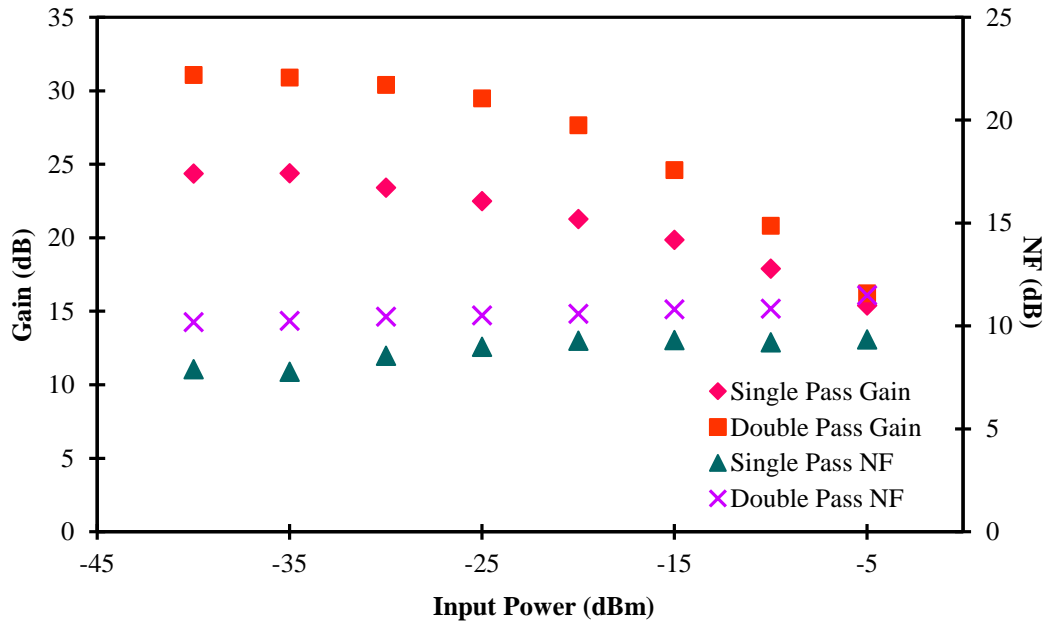


Figure 3. 15 Gain and NF performance against different input powers at a wavelength of 1500nm.

3.3 Summary

In this chapter, the characteristics and behaviour of the ultra-wideband SOA have been studied extensively. The capability of the ultra-wideband SOA to emit an ASE

spectrum starting from 1460 nm to 1600 nm, which covers the short (S-band), conventional (C-band) and long (L-band), has been observed thoroughly, and experiments have been conducted to characterize the gain and noise figure properties of the ultra-wideband SOA.

The first step of the SOA characterization involves implementing various drive current to the SOA in order to observe the response of the ASE spectrum via the OSA. The ASE spectrum of the SOA is observed to be shifted to the shorter wavelength as the drive current is increased from 70 mA to 390 mA, and hence a wider bandwidth of emission is attained, which represents a significant advantage for an optical amplifier to provide such a wide bandwidth of emission just by using a single chip. The gain test experiment is first started by varying the input wavelength from 1460 nm to 1600 nm with fixed input powers of -30 dBm and 0 dBm which correspond to the low-signal and high-signal gain. For low-input signal of -30 dBm, the centre wavelength of the S-band region of 1500 nm attains about 23.53 dB gain, whilst the centre wavelength of C- and L-bands of 1550 nm and 1580 nm achieves about 17.46 dB and 10.18 dB gain values respectively. It is also observed that the gain achieved at each centre wavelengths of the S-, C- and L-band region are about 9.62 dB, 9.69 dB and 7.54 dB gain respectively for the 0 dBm input signal power measurement. The fluctuations of gain is higher at low input signal compared to the high input signal which is mostly because of the PDG effect on SOA. At 1500 nm, the maximum gain measured at input signal power -35 dBm is about 23.71 dB gain, compared to 17.44 dB and 10.2 dB achieved by each of 1550 nm and 1580 nm wavelength. At high input signal power, all bands show an almost similar gain value with the maximum of about 5.27 dB for 1500 nm, 5.41 dB for 1550 nm and 4.42 dB for 1580 nm.

The NF value of the SOA is then measured with the same set of gain characterization tests. The average NF value observed is about 7.70 dB at input signal power of -30 dBm, whilst the pattern shows higher NF at the longer band region of 1570 nm to 1600 nm with an average NF of about 8.54 dB. Fluctuations of the NF values are observed within all the three bands, and these are due to the PDG effect affecting by the SOA. For a higher input signal power of 0 dBm, the average NF is calculated to be about 7.62 dB within 1460 nm to 1600 nm wavelength range. At a lower input signal power of -40 dBm to -10 dBm, the average NF values for each wavelength are observed to be 6.87 dB for 1500 nm, 7.65 dB for 1550 nm, and 9.03 dB for 1580 nm.

The PDG effect characterization is done by adjusting the PCs that are attached at the input and output port of the ultra-wideband SOA to achieve maximum and minimum gain of the SOA with various parameters. The average PDG is calculated to be 2.33 dB for -30 dBm input signal power and 2.22 dB for a 0 dBm input signal power. On the other hand, for the various input signal powers of -40 dBm to 5 dBm with fixed signal wavelengths of 1500 nm, 1550 nm and 1580 nm, the average value of the PDG for each wavelength is 2.49 dB, 2.31 dB and 2.60 dB respectively. The biggest PDG fluctuation occurs at a lower input signal of -40 dBm until -10 dBm at wavelength 1500 nm with the average PDG of 2.39 dB.

In the final section of this chapter, an improvement of the S-band gain is demonstrated by applying a double pass configuration to the setup. The high gain amplifier proposed covers the S-band region of 1480 nm to 1520 nm with a gain value of 31.07 dB at input signal power of -40 dBm at signal wavelength of 1500 nm, whilst the NF value at wavelength 1480 nm to 1520 nm is measured and improved to 8 dB, from the previous value achieved by the single pass configuration of 11 dB.

REFERENCES

1. Kavintheran A/L Thambiratnam, "A Multi-wavelength Source based on Sagnac Loop and Semiconductor Optical Amplifier", Master of Science Thesis, University of Malaya, 2007.
2. M. J. O' Mahony, "Semiconductor Laser Optical Amplifiers for Use in Future Fibre Systems", J. Lightwave Technology, Vol. 6, No. 4, pp. 531-544, 1988.
3. M. J. Connelly, "Semiconductor Optical Amplifiers", Kulwer Academic Publishers, Dordrecht, 2004.
4. A. Mecozzi, "Soliton Transmission Control with Semiconductor Amplifiers", Optics Letters, Vol. 20, No. 15, pp. 1616-1618, 1995.
5. Alphon SAS26p 01P020, Alphon SA_H Devices Operating Specifications, Alphon Corporation, New Jersey, USA.
6. SAS26p PON Amplifier, Semiconductor Optical Amplifier Application Catalog.
7. J. M. Wiesenfield, L. H. Spiekman, Semiconductor Optical Amplifiers In "Handbook of Optics Volume V (3rd Edition), (pp. 19.5), United States of America, McGraw-Hill.
8. H. Ahmad, M. Z. Zulkifli, N. A. Hassan, A. A. Latif, S. W. Harun, "High Gain S-Band Semiconductor Optical Amplifier with Double-Pass Configuration", Laser Physics, Vol. 21, No. 7, 2011.
9. O. Liboiron-Ladouceur, K. Bergman, M. Boroditsky, M. Brodsky, "Polarization-Dependent Gain in SOA-Based Optical Multistage Interconnection Networks", Journal of Lightwave Technology, Vol. 24, No. 11, November 2006.
10. N. Antoniadis, K. C. Reichmann, P. P. Iannone, N. J. Frigo, A. M. Levine, I. Roudas, "The Impact of Polarization-Dependent Gain on the Design of Cascaded Semiconductor Optical Amplifier in CWDM Systems", IEEE Photonics Technology Letters, Vol. 18, No. 20, October 2006.

11. B. F. Kennedy, S. Philippe, F. Surre, A. L. Bradley, D. Reid, P. Landais, "Investigation of Polarization Dependent Gain Dynamics in a Bulk SOA", *Optics Communications* 272, pp. 490-495, 2007.
12. R. M. Jopson, G. Eisenstein, M. S. Whalen, K. L. Hall, U. Koren, J. R. Simpson, "A 1.55- μm Semiconductor-optical Fiber Ring Laser", *Applied Physics Letters*, Vol. 48, pp. 204, 1986.
13. Z. Zhang, J. Wu, K. Xu, X. Hong, J. Lin, "Tunable Multiwavelength SOA Fiber Laser with Ultra-narrow Wavelength Spacing based on Nonlinear Polarization Rotation", *Optics Express*, Vol. 17, No. 19, September 2009.
14. H. Awad, A. Atieh, T. J. Hall, "Polarization-dependent Gain and State of Polarization Effects on Linewidth of Semiconductor Fiber Ring Lasers", *Microwave and Optical Technology Letters*, Vol. 50, Issue 1, pp. 31-34, January 2008.
15. R. Ulrich, "Polarization stabilization on single-mode fiber", *Applied Physics Letters*, Vol. 35, pp. 840-842, Dec 1979.
16. J. Noda, K. Okamoto, Y. Sasaki, "Polarization-Maintaining Fibers and Their Applications", *Journal of Lightwave Technology*, Vol. LT-4, No. 8, pp. 1071-1089, August 1986.

CHAPTER 4

ULTRA-WIDEBAND SOA FIBRE LASER GENERATION

4.1 : Introduction

As traffic capacity becomes increasingly filled due to the development of communications technology, such as mobile phones, tablets, etc, which contributes to usage of the telecommunication bandwidth, the demand for a wider transmission bandwidth is continuous. Research has been rendered extensively to expand the current transmission bandwidth of the conventional (C-) band by utilizing various methods of generation to explore various promising types of gain medium. These gain mediums include the rare-earth doped fibre such as erbium-doped fibre, thulium-doped fibre, erbium-ytterbium doped fibre, and bismuth-erbium doped fibre, as well as optical amplifiers and the nonlinear amplification of Raman amplifiers [1]. Since erbium-doped fibre amplifiers (EDFAs) only support amplification in the C-band region, additional deployment of other type of amplifiers or doped fibres into the fibre resonator is needed in order to realize the desired ultra-wide gain bandwidth. However, such deployment is inapplicable for commercial use because of bulky size and cost ineffectiveness, as each band region needs different fibre amplification material to emit their wavelength range. Other alternatives have been put forward to eliminate such problems, and research has found that the semiconductor optical amplifier (SOA) could be a suitable candidate for its small size and low cost factor, following from the development of quantum dot (QD) technology in semiconductors that arose in the late 90's [2, 3]. A paper by Z. G. Lu et. al. indicates that the quantum dot SOA (QD-SOA)

is much better than quantum-well SOA (QW-SOA) in terms of optical spectral bandwidth, temperature sensitivity and output power stability [3]. As compared to the erbium-doped fibre (EDF), the dominant behaviour of inhomogeneous broadening of the SOA has become the main advantage, as it contributes to multiple simultaneous wavelengths emission and leads to the realization of simple and compact multi-wavelength fibre lasers governed by SOA.

As discussed from previous chapters, three basic components of optical communication networks are transmitter (or signal source), transmission medium and receiver. In order to realize efficient network systems, all the basic components must be ensured to be in excellent performance. For the transmitter that acts as the source of the signal, the main factors to emphasize when choosing such components are the laser beam quality and stability. The laser beam quality includes consideration of the power level, the full-width half-maximum (FWHM) and the signal-to-noise ratio (SNR) of the laser beam. Other than that, the stability and the width of the covering wavelength band are also important factors to be considered. The utilization of discrete wavelength semiconductor laser diodes as the signal source in the most recent optical communication systems is mainly because of the good quality and the better stability of the laser beam. The rise of dense wavelength division multiplexing (DWDM) systems has rendered semiconductor laser diode unsuitable for the task: the expense of discrete wavelength sources required to operate such systems would be impractical, particularly in light of the fact that channel spacings of the DWDM systems have increased from 100, 50 and most recently 12.5 GHz [4, 5]. Hence, the current limitations of network capacity are still an unresolved issue as the DWDM systems are hardly used to their full capacity.

Research and development of fibre lasers has been pro-actively undertaken throughout recent years. Fibre lasers have been discovered to be the most effective alternative to the distributed feedback (DFB) laser diode as a signal source. This is due to manifold advantages, particularly in terms of wavelength tunability and the ability to generate multiple output wavelengths from a single source [6], which significantly lessens the cost per wavelength. With the wide range of fibre lasers applications such as sensing [7, 8] and frequency generation [9, 10] to name but a few, utilization of fibre lasers is promoted over distributed feedback (DFB) laser diodes.

In this chapter, the generation of an ultra-wideband multi-wavelength fibre laser (MWFL) by utilizing an ultra-wideband SOA is demonstrated and studied via three methods of production. All the three methods are designed and demonstrated thoroughly in the lab to ensure optimum results and repeatable experiments. The first method is by using three fibre Bragg gratings (FBGs) with different wavelengths as the wavelength filters, the second is by using an arrayed waveguide gratings (AWGs) selective wavelength channel, and the third is by using a 7.7 km dispersion compensating fibre (DCF) as the nonlinear gain medium, which allows for a stimulated Brillouin scattering (SBS) effect in the Brillouin fibre laser method. These three methods of ultra-wideband fibre laser generation have been carried out through several trials of experiments in order to attain optimum results in the production of an ultra-wideband wavelength channel that covers the three important band region in telecommunication of S, C and L-bands.

4.2 : Cavity configurations of SOA fibre laser

The generation of fibre lasers requires one of two feasible configuration setups; Fabry-Perot or linear cavity, or ring cavity designs. The two designs are

distinguishable by the existence of reflectors in the configuration setup. The Fabry-Perot or the linear cavity fibre lasers are designed by attaching two reflectors at both input and output ends of the gain medium. Some examples of reflectors are fibre Bragg gratings (FBGs) and optical circulators of the same operating wavelength range as the intended lasing wavelength. On the contrary, ring cavity designs are constructed by looping back the laser output from the gain medium into itself. The generated wavelengths then pass through the gain medium numerous times, which in turn leads to lasing. Advantages, such as narrow linewidths and the ability to generate multiple lasing wavelengths with very close spacings have made fibre lasers to be considered highly suitable as a laser source, as well as use in optical sensing and spectroscopy [11].

4.3 : Ultra-wideband switchable SOA fibre laser

4.3.1 : 120nm wideband switchable SOA fibre laser

The first method of the ultra-wideband multiwavelength fibre laser (MWFL) generation experiment conducted in this thesis involves use of a 1×16 arrayed waveguide grating (AWG) as the wavelength filter. The switchable fibre laser resonator consists of an ultra-wideband SOA, a 16-channel AWG and two optical channel selectors (OCSs) connected in a ring cavity configuration. The ASE emitted from the SOA propagates into the 1×16 AWG, which then slices the ASE output spectrum into 16 different wavelength channels. Because of the broad output of ASE spectrum emitted by the SOA, which covers the whole three bands of S-, C- and L-bands, each of the 16 channels of the AWG will contain a set of three wavelength signals of S-, C- and L-bands. This feature is due to the diffraction effect experienced

by the AWG used. Each individual wavelength will diffract and focus at different angles at the AWG output plane in accordance with equation [11]

$$\theta_m \approx \frac{N_{eff}}{N_f} \frac{\Delta L - m\lambda_g}{d_a}$$

where θ_m is the tilt angle, ΔL is the optical path difference, $\lambda_m = \frac{\lambda}{N_{eff}}$, m is an integer (diffraction order), d_a is the pitch between the array waveguide, and N_{eff} and N_f are the effective refractive indices in the waveguide array and in the free propagation region respectively [13]. The AWG is actually optimized for C-band region operation, ranging from 1530.56 nm to 1542.34 nm wavelengths, but when the broadband source (S-, C- and L-bands) is transmitted through the AWG, a set of three wavelength components of S-, C- and L-bands will be attained in each channel. This occurs because the multiple diffraction orders now include $m - 1$, m , and $m + 1$, which satisfy the condition of $\theta_{m-1} = \theta_m = \theta_{m+1}$ for different wavelengths [13]. Note that θ_{m-1} is for L-band, θ_m is for C-band and θ_{m+1} is for S-band [13]. Even though the AWG is designed to be operating only in the C-band, the set of the three diffraction orders focus at the same spot, and result in them being emitted together in a single output channel. These 16 AWG output channels are connected to the 16 output channels of the 1×16 optical switch of a commercial unit (ANDO AQ3540), which is referred as optical channel selector (OCS1). The optical switch has a switching speed of 500 ms⁻¹ between channels and a transmission bandwidth ranging from 1200 nm to 1650 nm [13], which covers the experimental bandwidth of this experiment.

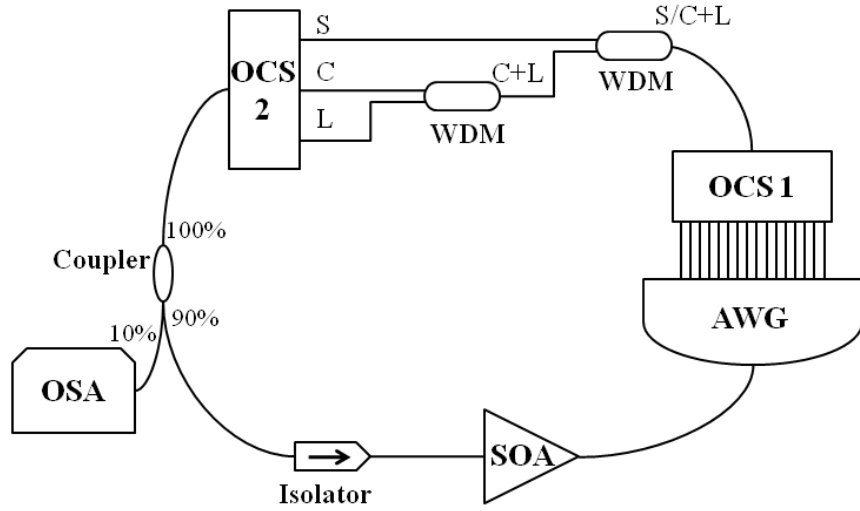


Figure 4. 1 Experimental setup for 120nm wideband tunable SOA fibre laser

The first chosen channel output of the OCS1 (i.e: channel 1) is then connected to a S/C+L bands wavelength division multiplexer (WDM) in order to split the signal into the S and C+L bands into two separate output ports. By using a similar kind of fused WDM coupler, the C+L portion is further divided into C and L outputs. All the individual outputs of S, C and L can be selected when they are connected to the 1, 2 and 3 channels of the second OCS (OCS 2) respectively, and this factor provides wavelength tunability to the laser resonator. If channel 1 of selected OCS 1 is $\lambda_{s1} = 1478.69$ nm, this will mean that the signal injected into the ring cavity through channel 2 of OCS 2, and subsequently amplified by the SOA, is λ_{s1} . This applies to any other channels of the AWG (channel 2 until channel 16) which provide the tunability characteristic within the S-band region. A very similar approach also applies to the C and L bands via choosing any channel of the channel 2 and 3 from the OCS 2. The optical isolator induces an anticlockwise unidirectional propagation of the emitted signal through the laser resonator. A 10% portion of the output signal is tapped out to

an optical spectrum analyzer (ANDO 6317C) by using a 90/10 broadband fused biconnical coupler. The resolution of the OSA is 0.02 nm. The results obtained are as shown in Figure 4.2 and described accordingly.

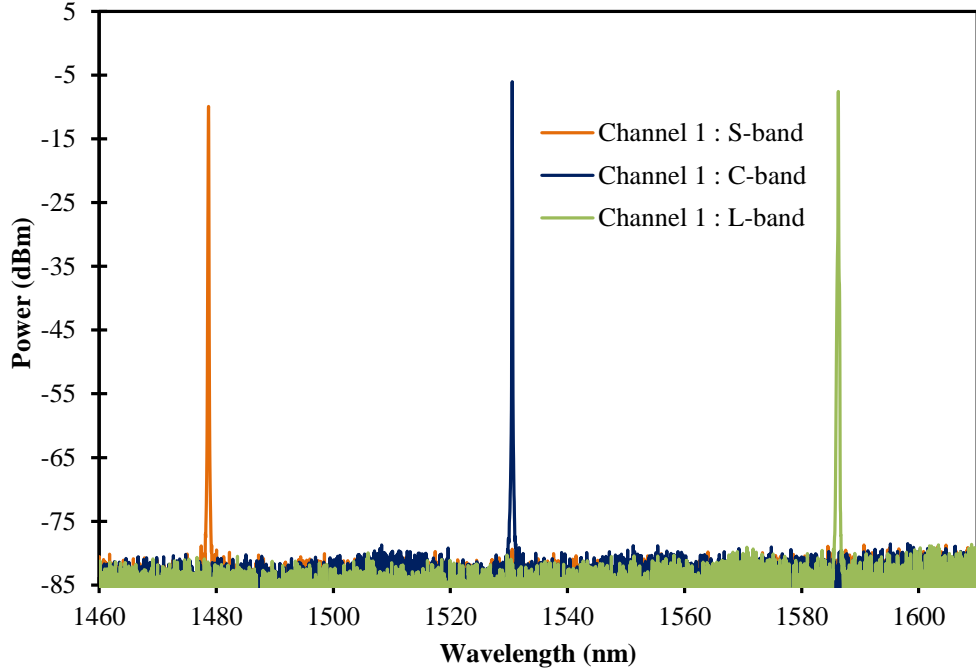


Figure 4. 2 Output spectrum of channel 1 of the AWG before it is split into three different bands by the S/C+L and C/L WDM splitter.

Figure 4.2 shows the spectrum emitted at channel 1 of OC1 where there are three different wavelength peaks produced at three different bands regions simultaneously. The peaks are produced as a result of transmitting the ASE power of the ultra-wideband SOA into the AWG where the effect of linear interference [14] contributes to multiplexing the ASE wide spectrum into many particular wavelengths. The measured peak powers are observed to be about -9.92 dBm for S-band of 1478.69 nm, -6.03 dBm for C-band of 1530.56 nm and -7.57 dBm for L-band of 1586.26 nm. The 4dB peak power variations can be improved by cleaning the connectors properly [13]. Note that the output wavelength will be in the similar range for the next channel

and so forth, but shifted by 0.8 nm (100 GHz) per channel. The shifting of the output wavelength is dependent on the interchannel spacing of the AWG utilized in the experiment.

The range of tuning of the single wavelength laser is as shown in Figure 4.3. It is shown that the widest tuning range is realized for the S-, C- and L-bands and superimposes the output wavelengths emitted from Channel 1 and Channel 16 of the AWG. The wavelength tuning range for S-band is observed from 1478.35 nm to 1490.09 nm, whilst covers from 1530.56 nm to 1542.34 nm for C-band. The L-band wavelength tuning range is observed to be from 1586.26 nm to 1598.42 nm. It is also measured that the linewidths of the three outputs of the respective S-, C- and L-bands are about 0.05 nm, 0.035 nm and 0.035 nm. A higher number of channels AWG can be used to attain a wider tuning range of the laser outputs. Since the AWG used in this experiment is a 1×16 AWG with 100 GHz frequency spacing (0.8 nm interchannel wavelength spacing), it is noted that the tuning range achievable is only as wide as 12 nm (15 spacings × 0.8 nm). This corresponds well with the measured value of 11.78 nm which is the maximum tuning range of the C-band region. Similar conditions apply to the S-band and the L-band region. For a higher number channel of AWG, say 1×64, the achievable maximum tuning range is about 50.4 nm [13], which shows the tuning range can be extended by utilizing a larger number of channel outputs. The narrowest interchannel spacing of 0.8 nm attained by the 50 GHz AWG is as shown in Figure 4.3.

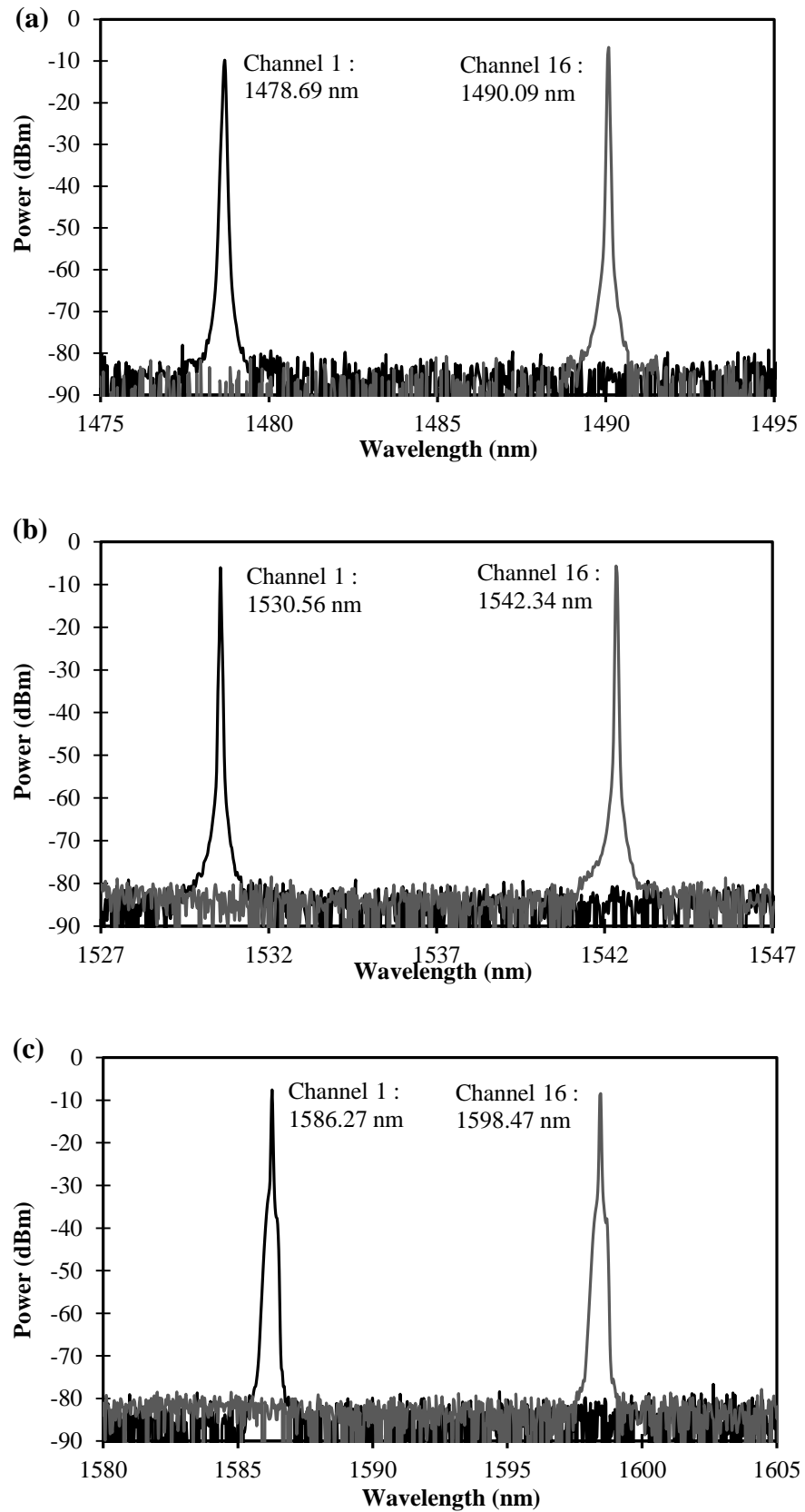


Figure 4. 3 Widest tuning range measured from channel 1 to channel 16 of the AWG for the (a) S-band, (b) C-band, and (c) L-band region.

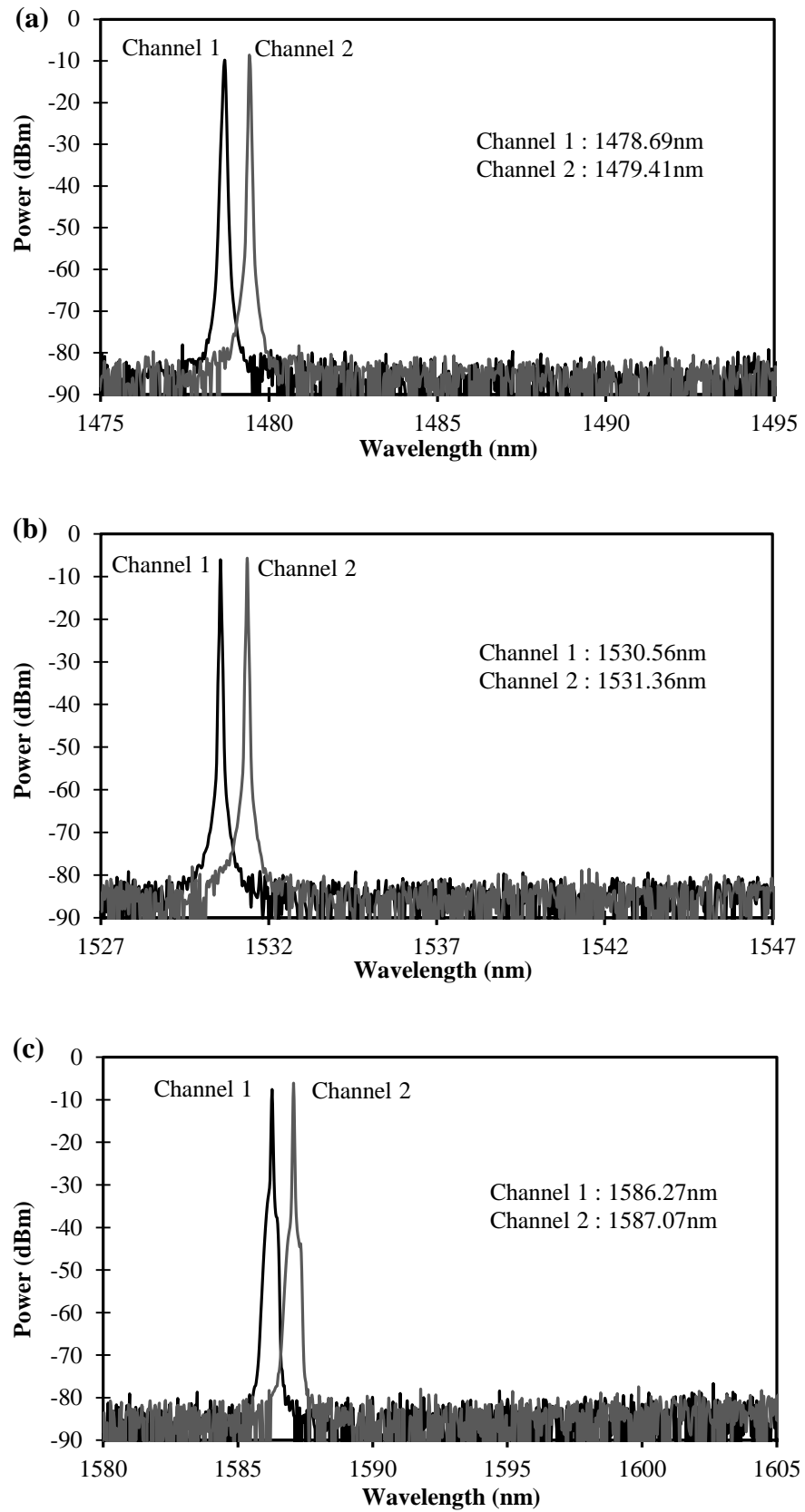


Figure 4. 4 Narrowest tuning range measured from consecutive channel of the AWG for (a) S-band, (b) C-band, and (c) L-band.

Figure 4.5 shows the results of the stability test conducted at the end of the experiment. The 2 hours stability test shows that the outputs of the laser system are very stable and well-controlled since there are no power fluctuations observed over the entire wavelength span for the entire period. The stability tests are taken at each channel of S-band (1478.64 nm), C-band (1530.52 nm) and L-band (1586.24 nm) and similar stability performances are observed through different region bands. Besides the power variations at different wavelengths, another crucial characteristic of an optical source is the side-mode-suppression-ratio (SMSR) of each output power wavelength [13]. The SMSR measurements of every output wavelengths for each band are plotted in Figure 4.6.

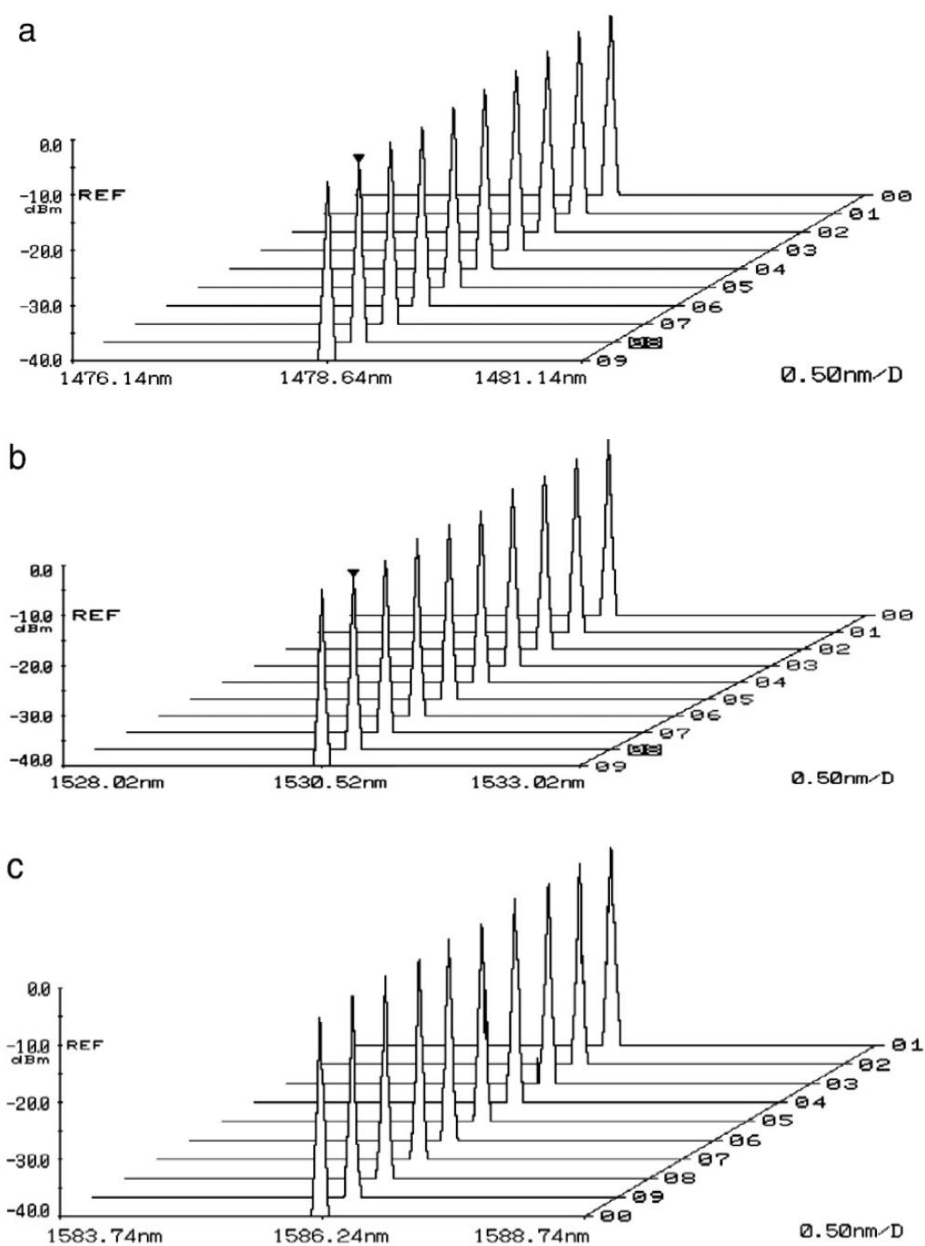


Figure 4. 5 Stability test for channel 1 for the (a) S-band, (b) C-band, and (c) L-band region.

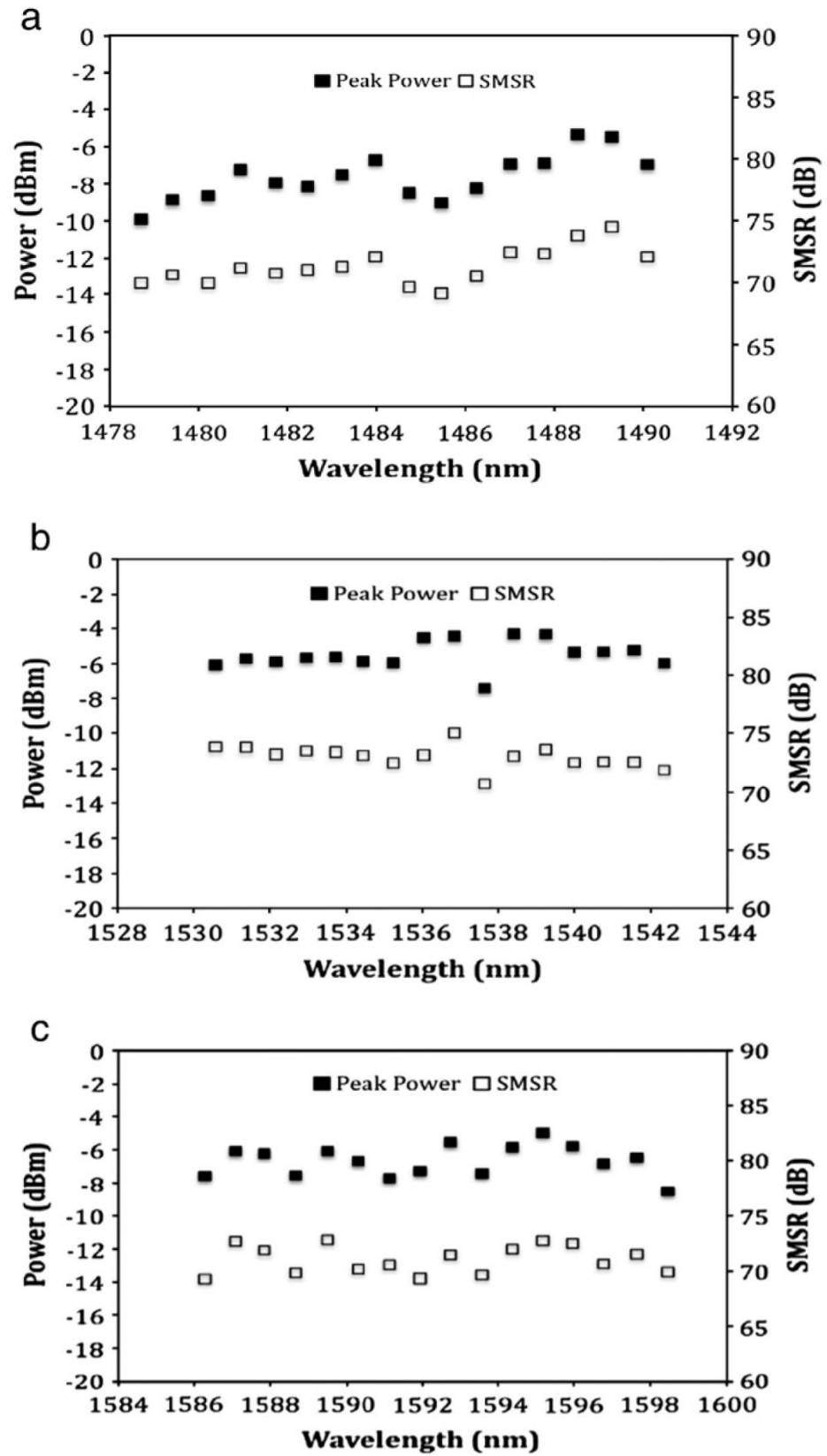


Figure 4. 6 Peak powers and SMSR values for all 16 channels of the AWG for (a) S-band, (b) C-band, and (c) L-band.

With the lowest value of 69.12 dB for 1485.45 nm and the highest value of 74.53 dB for 1489.29 nm, the SMSR value variations for the S-band region are shown in Figure 4.6 (a). The 5.41 dB variation, however, can be improved by optimizing the connections of the setup and by having an SOA with a flat ASE output power [13]. The SMSR values are measured as varying by about 69.95 dB for the S-band region wavelengths ranging from 1478.69 nm until 1490.09 nm. The average value of the SMSR is taken to be about 72 dB. With the slight output power variations between different wavelengths of the C-band region, the SMSR variation is observed to be about 4 dB with an average SMSR value of 72 dB. However, for wavelength of 1537.62 nm, the output peak power is slightly lower than that for the other wavelengths, and has a -7.37dBm value as shown in Figure 4.6 (b). As expected, the SMSR value measured is also lower than the other channels, and is measured as about 70.71 dB value for the respective wavelength. This lower value could be due to higher loss experienced by channel 10 as compared to other channels of the AWG [13]. According to Figure 4.6 (c), the observed fluctuations of the output peak powers are about 1.5 dB for the whole 16 wavelengths outputs. With an average value of 71.5 dB of SMSR, the values of each 16 wavelengths vary over a range of about 2.5 dB. The large values of SMSR measured for the S-, C- and L-bands indicates that a set of a high quality output signals has been realized.

With a possible tunable bandwidth of 120 nm, the whole bandwidth of switchable output power that can be switched is in the wavelength range of 1478.7 nm to 1598.47 nm as shown in Figure 4.7. As according to the figure, about 40 nm spacing of no output signals is observed between the last channel (channel 16) of the S-band and the first channel (channel 1) of the C-band (and similarly between the C- and L-bands). This is mainly due to the utilization of the 1×16 AWG, which has an

exploitable tuning range of 12 nm for each band. To rectify the exploitable tuning range, a higher number of channels of AWG can be used so as to provide a continuous tunability that covers the whole S-, C- and L-bands. For an example, each channel of a 1×64 AWG has about 51.2 nm width of frequency band. Generally, this demonstrated design represents a novel way to generate a switchable output that covers a very wide tuning range [13].

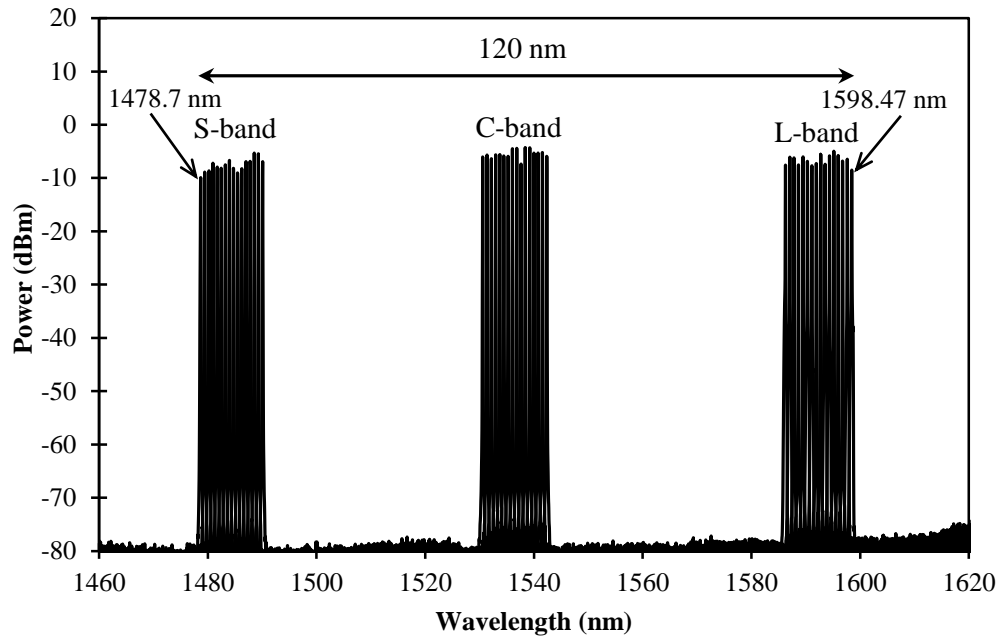


Figure 4. 7 16 channels AWG output laser spectrum for the S-, C- and L-bands with 120 nm bandwidth.

4.4 : Multi-wavelength SOA fibre laser

4.4.1 : Ultra-wideband SOA fibre laser by using FBGs

The next method of realizing the ultra-wideband multiwavelength SOA fibre laser is by employing a type of wavelength selective filter known as fibre Bragg grating (FBG). The ability of the FBG to select one or more wavelengths is important in

wavelength division multiplexing, or when pump and signal wavelength must be combined or separated [15]. Other optical devices can do the same thing, yet fibre gratings are selective over a narrow range of wavelengths with approximately 99% reflectivity, and fit naturally into the fibre optic systems [15]. The reflectivity of the FBGs play a major role in generating narrow reflected wavelengths, and provide an indication of the efficiency of the FBG. There are three different reflective wavelength profiles of FBGs used in this experiment. The FBGs with reflecting wavelengths of 1500 nm, 1540 nm and 1580 nm are used to attain a simultaneous triple band lasing output of the S-band, C-band and L-band regions. The experimental setup is as shown in Figure 4.8.

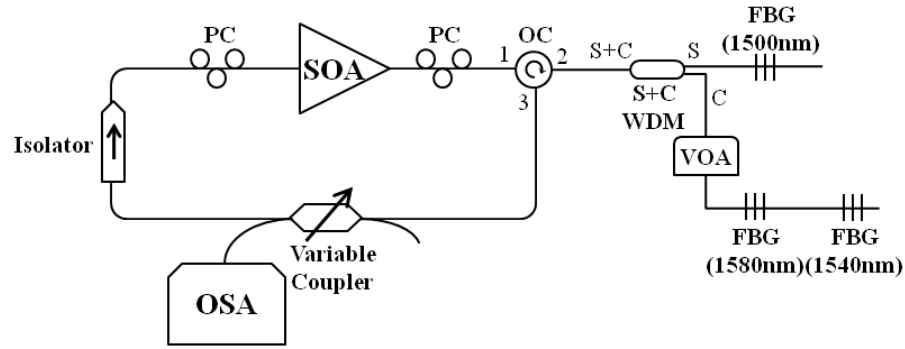


Figure 4. 8 Experimental setup for S-, C-, L-band fibre laser by using FBGs

The configuration consists of the ultra-wideband SOA as the gain medium that provides ultra-wideband amplified spontaneous emission (ASE), which is generated from the electron-hole pair recombination, to the ring cavity resonator. The ultra-wideband ASE is observed to range from 1460 nm to 1620 nm wavelength and covers the S-, C- and L-bands as discussed in chapter 3 of this thesis. Two polarization controllers (PCs) are attached to the input and output ports of the SOA to control the polarization state of the laser signal propagation in the laser resonator. The ASE

emitted by the SOA is then filtered by the wavelength selective filter, which consists of three FBGs connected through a three ports optical circulator with an S/C+L wavelength division multiplexer (WDM) coupler and a variable optical attenuator (VOA). The utilization of the S/C+L WDM coupler at the specified location in the cavity is to minimize the optical loss suffered by the triple band lasing output powers because of the different band region wavelengths, thus obtaining a high power lasing output with low noise which then contributes to a high signal-to-noise (SNR) ratio. The VOA also plays a significant role to support flat lasing output powers of 1540 nm and 1580 nm wavelengths. The filtered triple band lasing wavelengths then will propagate from port 2 to port 3 of the optical circulator and next pass through the SOA to be amplified. An optical isolator is located at the input port of the SOA in the cavity to force unidirectional propagation and to avoid back-reflected signal from the SOA. This process continuously repeat until the equilibrium state is achieved and lasing is observed at the Bragg wavelengths. To ensure high and flat output signals of the C- and L-bands (1580 nm and 1540 nm), the VOA is set up to a 6.64 dB value. As well as to maintain flatness of the three laser signal output of the S-, C- and L-bands wavelength, a variable coupler is also used to tap out a small portion of the oscillating laser from the cavity for analysis via the optical spectrum analyzer (OSA) possessing 0.02 nm resolution. A particular optimum ratio of the variable coupler is maintained throughout the experiment so as to attain stable and flat triple band lasing wavelengths.

The results of the experiment can be seen in Figure 4.9. It is observed that lasing is achieved at the three reflection wavelength of the FBGs; 1500.06 nm, 1540.02 nm and 1579.62 nm, which respectively correspond to the S-, C- and L-band wavelength regions at the SOA drive currents above 70 mA. At the low drive current of 70 mA, the lasing wavelengths are low in peak power values with low optical signal-

to-noise ratio (OSNR) due to the insufficient gain provided by the SOA amplification. As can be seen, the peak power values of the triple lasing wavelengths increase as the drive current of the SOA is increased. At the highest SOA drive current of 370 mA, a set of the highest peak power values is achieved. The lasing wavelength is attained at 1500.06 nm with peak power value of -6.66 dBm at the S-band region, while a lasing with peak power value of -11.28 dBm is attained at the C-band region of wavelength 1540.02 nm, and meanwhile at the L-band region, the lasing peak power value achieved is -8.53 dBm at wavelength 1579.62 nm. The optical signal-to-noise ratio (OSNR) of the three lasing wavelengths at the maximum drive current of SOA at room temperature are measured to be 65.35 dB for wavelength 1500.06 nm, 57.67 dB for wavelength 1540.02 nm and 63.02 dB for wavelength 1579.62 nm. The variation of the three lasing wavelengths peak powers, as well as the OSNRs, are mainly caused by the gain characteristics of the ultra-wideband SOA used.

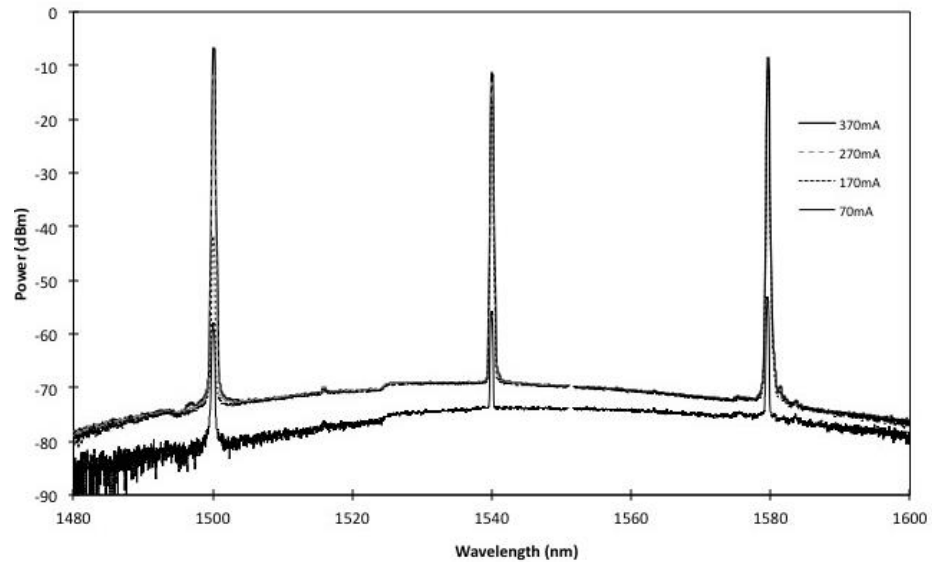


Figure 4. 9 Triple wavelength of S-, C-, L-band fibre laser in different injection currents of SOA

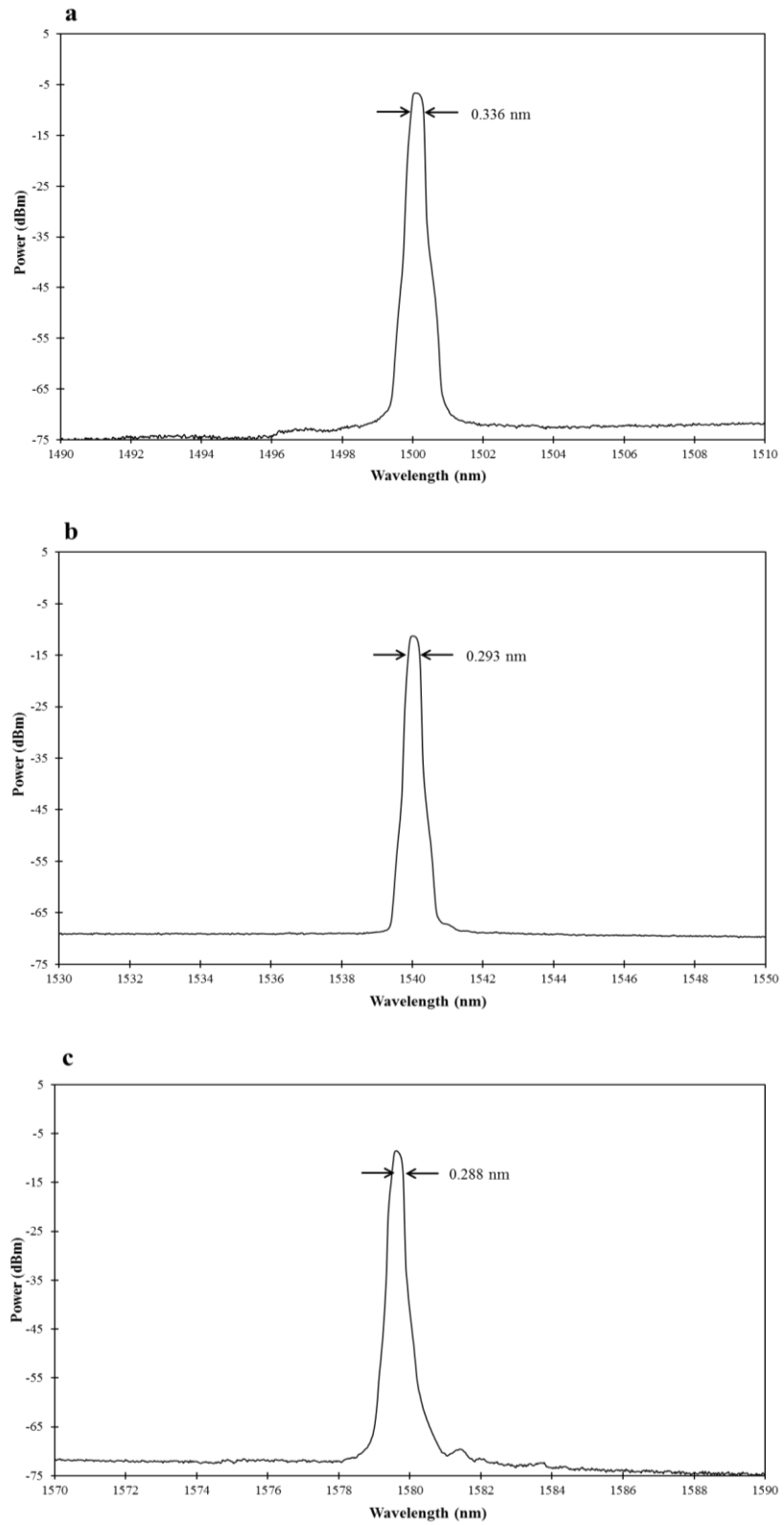


Figure 4. 10 Full-width half-maximum measurement of the triple band wavelengths fibre laser of the (a) S-band region at 1500.06 nm wavelength, (b) C-band region at 1540.02 nm wavelength, and (c) L-band region at 1579.62 nm wavelength.

Figure 4.10 (a), (b) and (c) show the full-width half-maximum measurement of the triple band wavelengths laser at the three Bragg reflected wavelengths of 1500.06 nm, 1540.02 nm and 1579.62 nm. The full-width half-maximum (FWHM) of a laser signal which is also known as the 3dB-linewidth, also known as *linewidth* or *spectral width*, which are simply defined exactly by the term; the width of the maximum spectrum that is cut by half, or in this case, represented by linewidth of which the peak power dropped by 3 dB, and FWHM is often measured in frequency units. An efficient laser signal should attain a small value of FWHM [18]. The size of the FWHM of the triple band lasing wavelength are measured to be 0.336 nm for the S-band region at wavelength 1500.06 nm, 0.293 nm for the C-band region at wavelength 1540.02 nm and 0.288 nm for the L-band region at wavelength 1579.62 nm.

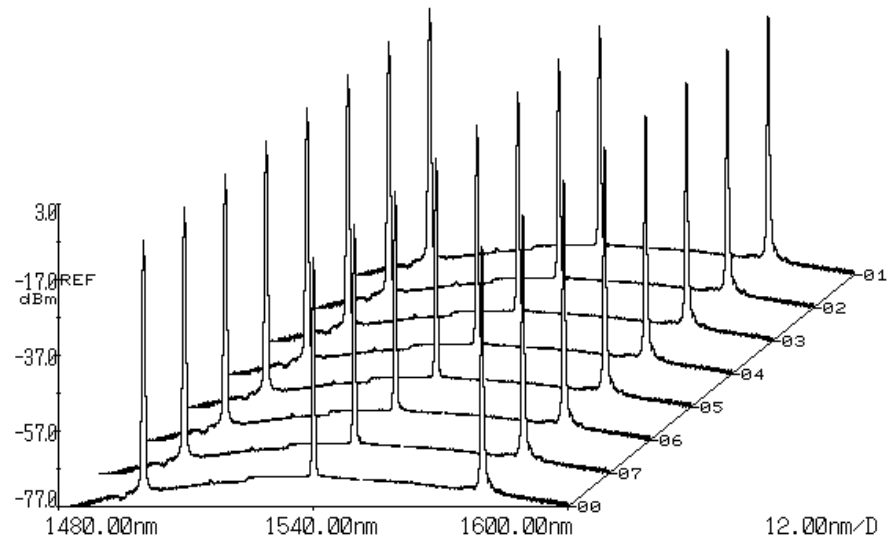


Figure 4. 11 Triple wavelength fibre laser in a stability test of 70 minutes duration

As according to Figure 4.11, the triple band wavelengths SOA fibre laser undergoes a stability test of 70 minutes duration. A very slight fluctuation in the peak

powers of the triple wavelengths can be observed from the 3D graph generated by the OSA, however the differences of the power values are smaller than 3 dB and thus can be neglected. The flat lasing output of the triple wavelength fibre laser can be attributed to the clamped gain in the SOA-based laser. Such triple band wavelengths SOA fibre lasers can be applied in communication network and sensor applications.

4.4.2 : Multi-wavelength SOA Brillouin fibre laser

The final method of generating an ultra-wideband SOA fibre laser lies in exploiting a non-linear optics principle of the stimulated Brillouin scattering (SBS) effect. However, the fibre has a low Brillouin optical gain in, and so it must be integrated with other amplifying medium in order to obtain high output power laser signals [23]. The amplified medium provides a primary gain to compensate for the cavity loss, and the SBS is utilized as the frequency-shifted mechanism [23]. This idea was successfully demonstrated by combining the SBS effect with the erbium doped fibre (EDF) as the gain medium, so as to create a fibre ring laser with reasonable output powers [23, 24]; this hybrid technique triggered the development of multi-wavelength Brillouin-erbium fibre lasers (BEFLs) [24-32]. Conventional EDFAs are particularly effective at the C-band (from 1525 nm to 1565 nm) or the L-band (from 1570 nm to 1610 nm) and can also be extended to the S-band (from 1460 nm to 1520 nm) by using depressed cladding erbium-doped fibre amplifiers (DC-EDFAs) [33]. On the other hand, the utilization of other rare earth doped fibre has been demonstrated to provide more bandwidth expansion outside the conventional C-band region of communication [34-38], but numerous research works have shown that the tuning range of multi-wavelength fibre lasers developed with the SBS technique are limited within a certain bandwidth of transmission [39-41]. Furthermore, in regards to the homogeneous

broadening property of the EDF, the production of a flat signal comb of the multi-wavelength BEFLs has been highly challenging. Other than being cheaper and easier to make, the semiconductor optical amplifier has comprehensive advantages over EDF by possessing a broad gain spectrum and dominant inhomogeneous broadening property [42].

The proposed setup for the ultra-wide band multi-wavelength Brillouin fibre laser (MBFL) is as shown in Figure 4.12. A 7.7 km long dispersion compensating fibre (DCF) is utilized in this experiment to act as a nonlinear gain medium. The DCF has a dispersion of -584 ps/nm and an insertion loss of about 6.66×10^{-3} dB/m. The MBFL resonator utilized an ultra-wide band SOA as a linear gain medium. The source of Brillouin pump (BP) in the experiment is realized by a tunable laser source (TLS) that injects 10.6 dBm of BP power into the system via one of the 50% ports of the 50/50 fused coupler. When the BP power penetrates into the DCF through the 50/50 optical coupler, the interaction of the high intensity of light with the nonlinear gain medium induces the creation of a multi wavelength laser comb output through the SBS process. The multi wavelength laser comb output exits the DCF and transmits into the linear laser resonator which is built by using two optical circulators designated as OC1 and OC2, as shown in Figure 4.5. The OCs are configured to act as a mirror by connecting port 1 to port 3 whilst port 2 is connected to the input and output of the MWBFL system. The SOA placed in the cavity is used to amplify the multi wavelength laser signal. A 90/10 fused coupler is placed in between port 1 and port 3 of OC2 to tap out 10% of the signal portion to be analysed via an OSA with 0.02 nm resolution.

The SBS process in the setups is explained as follows: the tunable laser source (TLS) emits the Brillouin pump (BP) power signal and travels through the optical isolator into the linear cavity via the 50% port of the optical coupler. The signal then

passes to the common port of the 50:50 fused coupler and onwards to the DCF, where it interacts with the nonlinear gain medium to generate the first Brillouin Stokes wavelength. The electrostriction process that arises inside the nonlinear gain medium results in the production of phonon waves, which then contribute to the backscattered signal [19]. This backscattered signal is corollary from the incidence of the BP with the phonon waves [19]. The first Stokes wavelength from the backscattered signal will travel in the opposite direction of the BP towards OC1, and is reflected back into the cavity whereupon it enters the DCF and the interaction process repeats so as to generate the second Stokes [19]. This process of oscillation continues, with each subsequent Stokes wavelength generated at a slightly lower power than the previous Stokes until the Stokes no longer generates the threshold power required for the SBS process to continue [19]. The obtained multi-wavelength comb makes many passes through the SOA via the linear cavity configuration, and is amplified to the point of lasing where it now functions as a multi-wavelength laser [19].

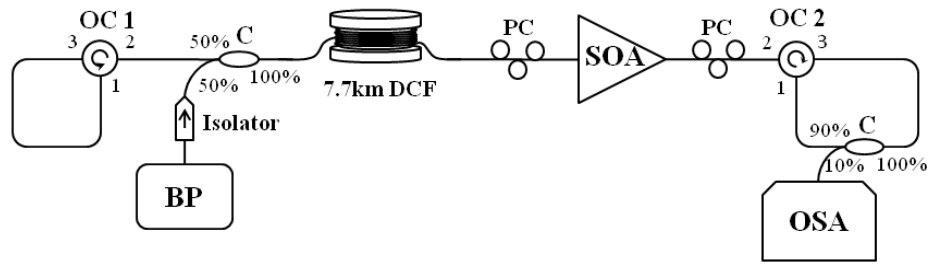


Figure 4. 12 Experimental setup for Brillouin fibre laser

The ultra-wide band characteristic of the SOA that has a very wide spectrum of ASE (as shown in Figure 3.3) can be used to estimate the pattern of the proposed MWBFL system. As can be seen in the respective figure, the peak power level of the ASE spectrum emitted by the SOA shifts towards the shorter wavelength region as the

injection current is increased. This attribute of the higher current filling more of higher energy states in the bands will induce gain at shorter wavelengths [7]. The following Figures 4.13, 4.14 and 4.15 show the multi-wavelength combs generated by BP wavelengths of 1510 nm, 1550 nm and 1580 nm respectively with 10.6 dBm BP power.

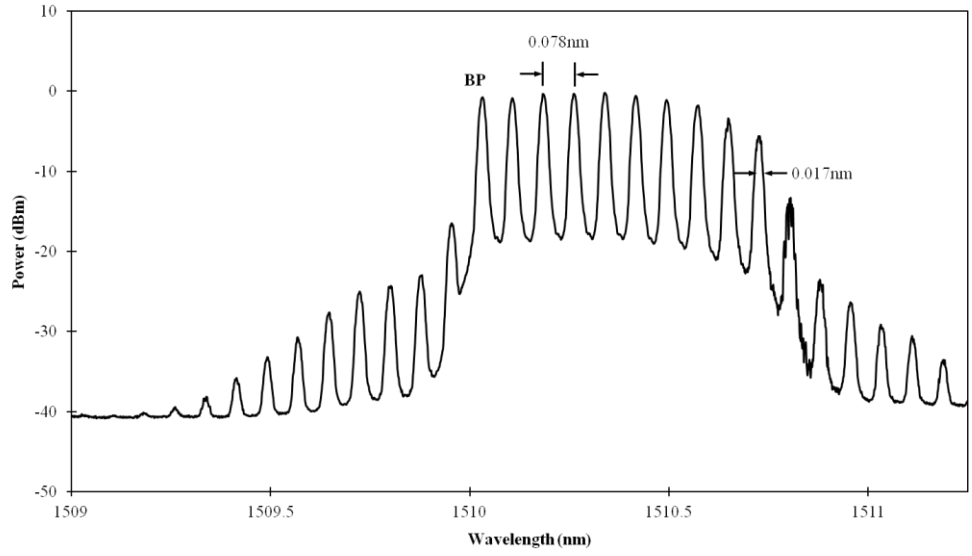


Figure 4. 13 Brillouin laser comb in S-band region of 1510 nm BP wavelength

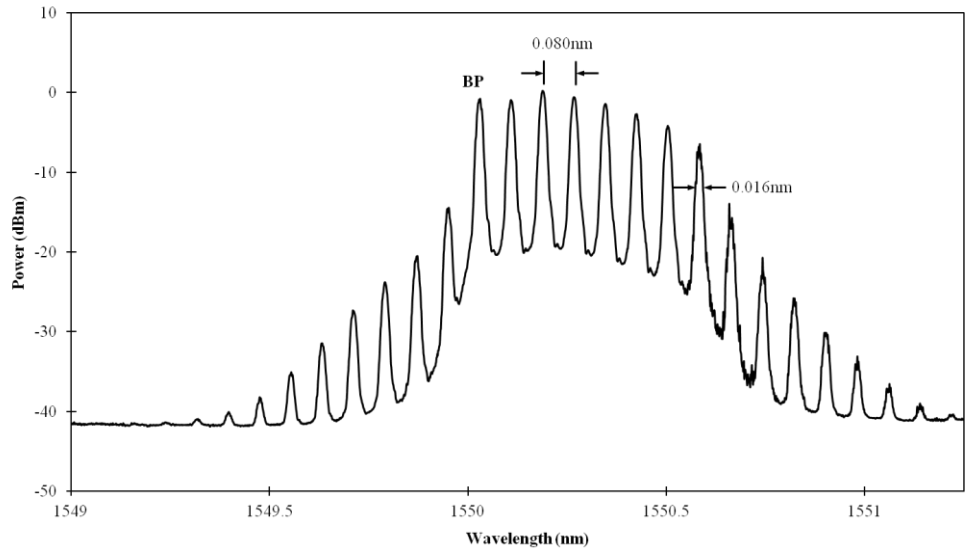


Figure 4. 14 Brillouin laser comb in C-band region of 1550nm BP wavelength

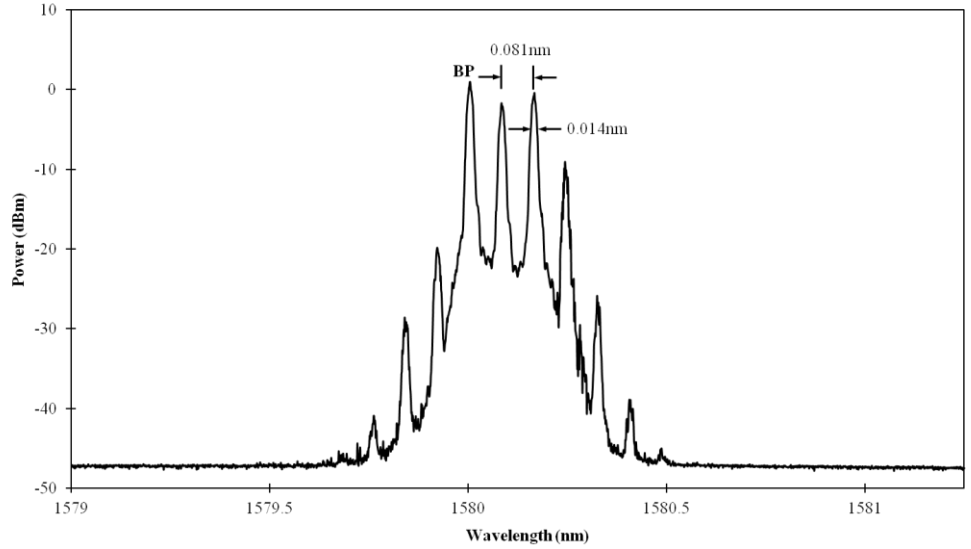


Figure 4. 15 Brillouin laser comb in L-band region of 1580nm BP wavelength

To achieve the widest linear amplification bandwidth of the multi-wavelength comb, the forward current injected into the SOA is set to 390 mA. At 1510 nm BP wavelength, 10 Brillouin Stokes are generated within the peak powers range of -5.94 dBm to -0.41 dBm. The observed wavelength spacings are about 0.078 nm and the 3-dB linewidth are about 0.017 nm as measured from the OSA. At 1550 nm BP wavelength, 8 Brillouin Stokes are obtained within the power range of -4.34 dBm to 0.02 dBm. The wavelength spacings and the 3-dB line-width are measured to be approximately 0.080 nm and 0.016 nm respectively. In the longer wavelength of L-band region, at a BP wavelength of 1580 nm, 3 Brillouin Stokes are attained. The peak powers obtained are ranging from -2.19 dBm to 0.39 dBm, with wavelength spacings of about 0.081 nm and 3-dB linewidth of about 0.014 nm.

From Figure 3.3 of the previous chapter, it can be seen that the low number of Brillouin Stokes achieved in the L-band region is due to the low ASE output power level (which contributed to low gain) in that particular wavelength region. The apparent higher number of Brillouin Stokes obtained in the shorter wavelength region

is basically due to the trait of the gain pattern of the ultra-wideband SOA used in the experiment. According to the ultra-wideband SOA gain pattern observed in Chapter 3 of this thesis, the higher gain in the shorter wavelength region generates higher peak powers. The higher peak powers achieved will eventually overcome the Brillouin threshold power of the system, hence generating further Stokes through the SBS effect.

The generated multi-wavelength combs of the anti-Stokes (which occur at wavelengths shorter than the BP wavelengths) in the proposed MWBFL output are also further analyzed. The high nonlinear properties of the SOA contribute to the anti-Stokes generation via the effect of four-wave mixing (FWM). It is observed that the spacing between adjacent wavelengths is figured to be approximately 0.08 nm, or approximately 10.7 GHz in the frequency domain: This is why there is less anti-Stokes generated by using EDFAs as compared to the SOA [5]. Figure 4.16 shows the number of Brillouin Stokes lines generated by the MWBFL system at different BP wavelengths. It can be inferred that the peak power of the lasing wavelengths obtained matches the ASE spectrum pattern for the corresponding wavelength range.

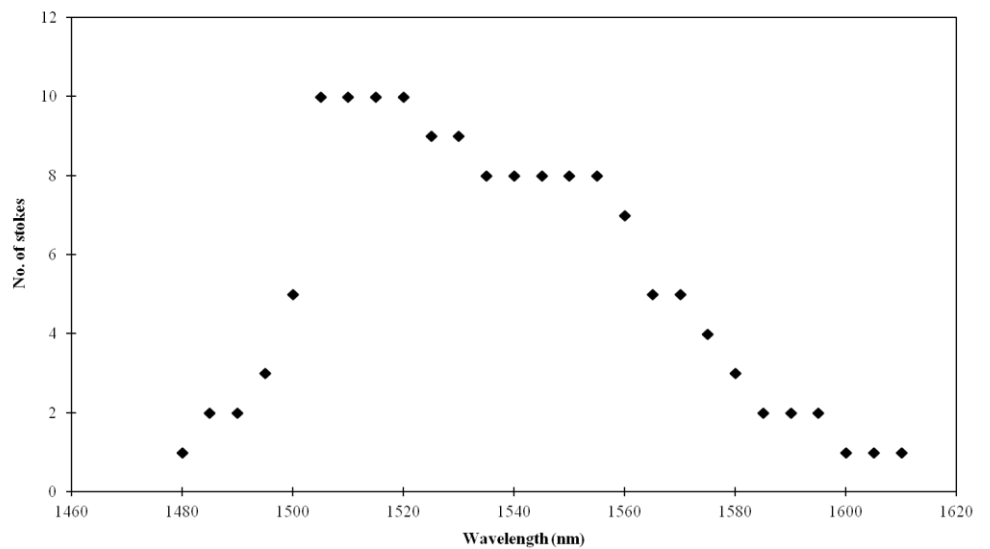


Figure 4. 16 Total number of Stokes versus BP wavelength graph

Since the operational wavelength of the ultra-wideband SOA used in the experiment is observed to cover the range of 1420 nm to 1620 nm, the SBS effect is also observed to be present within this wavelength region. This SBS occurrence is because of the character of the SOA in the MWBFL system, which supplies the required amplification for the SBS process to continue. As regards to Figure 4.16, it can be seen that the highest number of Stokes lines generated is within the BP wavelength range of 1500 nm to 1520 nm, which corresponds approximately 10 Stokes lines.

The stability of the MWBFL system is next tested by conducting a 70 minute stability test at room temperature. Note that the intended duration time of the system to be operated throughout applications is more than 10 hours. The results of the stability tests can be seen in Figures 4.17, 4.18 and 4.19 below. With almost no fluctuations or variations in the output power level, the multi wavelength laser output of each band is observed to be stable, and thus ensures reliability for various applications.

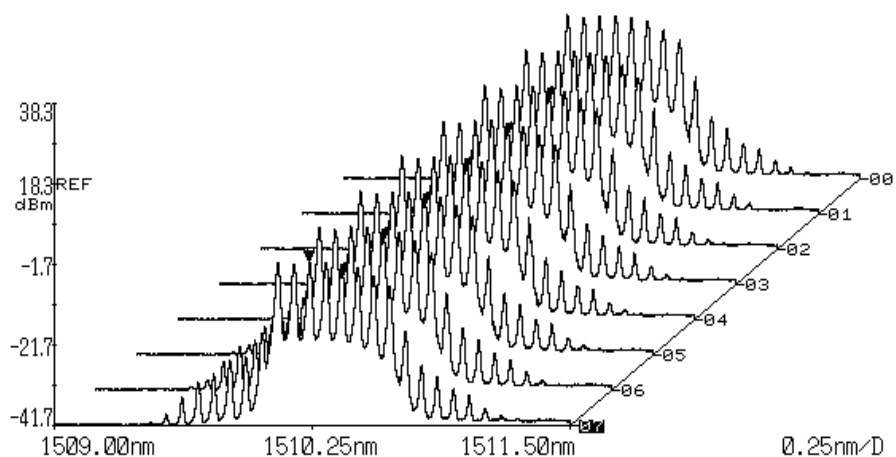


Figure 4. 17 A 70 minute stability test on 1510 nm BP wavelength Brillouin laser comb

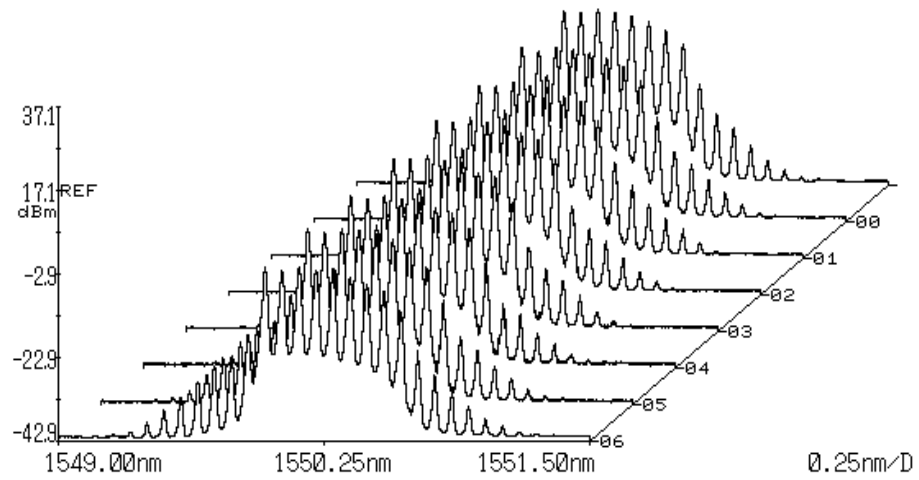


Figure 4.18 A 70 minute stability test on 1550 nm BP wavelength Brillouin laser comb

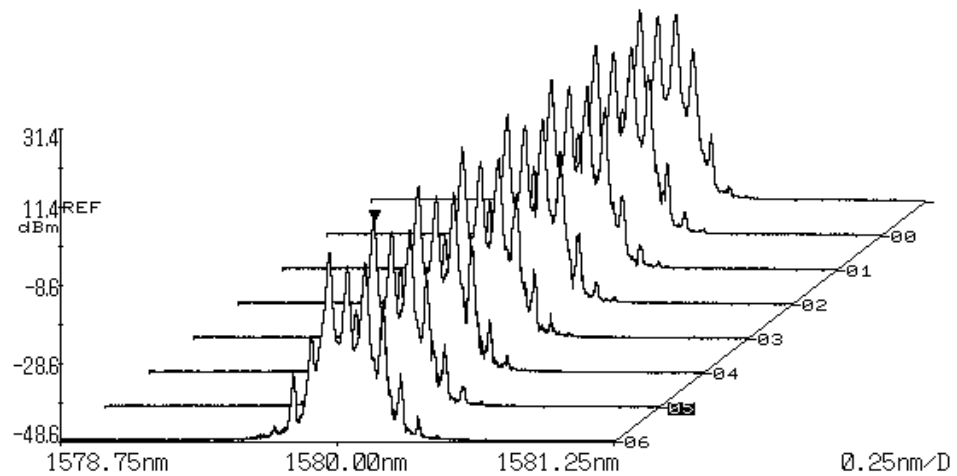


Figure 4.19 A 70 minute stability test on 1580 nm BP wavelength Brillouin laser comb

4.5 Summary

Throughout this chapter, three experiments for the objective of generating ultra-wideband SOA fibre laser are demonstrated. The first technique to generate the

ultra-wideband SOA fibre laser is by using AWGs as wavelength selective filter. The experiments attained laser output powers of as high as -9.92 dBm in S-band, -6.03 dBm in C-band and -7.57 dBm in L-band regions of channel 1 of the AWG. By superimposing the output wavelengths emitted from Channel 1 and Channel 16 of the AWG, a wide tuning range of about 12 nm for each S-, C- and L-band is demonstrated; 1478.69 nm to 1490.09 nm for S-band, 1530.56 nm to 1542.34 nm for C-band and 1586.27 nm to 1598.47 nm for L-band, which depends correspondingly on number of channel and interchannel spacing of the AWG used. The linewidth of the three laser outputs are measured to be 0.05 nm, 0.035 nm and 0.035 nm for the respective S-, C- and L-band. A stability test of 120 minutes duration time is conducted, and only slight fluctuations in the output power readings are observed at the end of the test. In the S-band region, the SMSR value is observed to be an average value of 72 dB with an overall fluctuation of about 4 dB, whilst in L-band region, fluctuations of the SMSR values are observed to be only about 2.5 dB with an average SMSR value of 71.5 dB.

The next method involves deploying three Fibre Bragg Gratings (FBGs) of each S-band (1500 nm), C-band (1540 nm) and L-band (1580 nm) into the cavity. At the highest drive current of SOA of 370 mA, a triple peak power of simultaneous S-, C- and L-band is observed. The laser peak power achieved is -6.66 dBm at wavelength of 1500.06 nm, -11.28 dBm achieved at 1540.02 nm, whilst -8.53 dBm is achieved at 1579.62 nm. The optical signal-to-noise ratios (OSNRs) of each reflected wavelength of the FBGs however is measured to be about 65.35 dB, 57.67 dB and 63.02 dB respectively. The 3-dB linewidth is measured to be about 0.792 nm wide at wavelength 1500.06 nm, 0.624 nm wide at wavelength 1540.02 nm and 0.672 nm wide at wavelength 1579.62 nm. The quality of the laser system is demonstrated by conducted

a stability performance test of 70 minutes duration, which resulted in negligible power fluctuation observed.

The final method exploits the nonlinear effect in an optical fibre undergoing a stimulated Brillouin scattering (SBS) effect, and utilizes a 7.7 km of dispersion compensating fibre (DCF) as the non-linear gain medium into the ultra-wideband SOA fibre laser cavity. With optimized Brillouin pump (BP) power of 10.6 dBm at each 1510 nm, 1550 nm and 1580 nm BP wavelength, 10, 8 and 3 Brillouin stokes are finally attained respectively. In the S-band region, the peak power of the Brillouin stokes obtained lies in the range of -5.94 dBm to -0.41 dBm with a 3-dB linewidth of 0.017 nm wide. In the C-band region, the peak power of the Brillouin Stokes are recorded to be in the range of -4.34 dBm to 0.02 dBm, with about 0.016 nm 3-dB linewidth. In the L-band region on the other hand, it is observed that the Brillouin Stokes' peak power are obtained in the range of -2.19 dBm to 0.39 dBm with about 0.014 nm wide 3-dB linewidth. The value of the wavelength spacing of each Brillouin comb attained is measured to be 0.078 nm for the S-band region, 0.080 nm for the C-band region and 0.081 nm for the L-band region. The viability of the multi-wavelength laser system is ensured by running a 70 minute stability test and observing negligible power fluctuation.

Although the objectives of this research project have been achieved in this chapter, the three successful methods are still in need of several improvements in order to be utilized in the network applications; approaches will be discussed further in the chapter five of the thesis.

REFERENCES

1. J. Hecht, (2002), Repeaters, Regenerators, and Optical Amplifiers In “Understanding Fibre Optics” (4th Edition), International Edition, (pp. 275-294), United States of America, Pearson – Prentice Hall.
2. L. F. Lester, A. L. Gray, L. Zhang, T. C. Newell, R. Wang, F. Nabulsi, L. Olona, P. M. Varangis, Z. Bakonyi, G. Onishchukov, A. Tunnermann, H. Su, A. Stintz, J. Zou, K. J. Malloy, “Quantum Dot Device Technology on GaAs: DFB Lasers, Tunable Lasers and SOA’s”, Optical Society of America, 2002.
3. Z. G. Lu, J. R. Liu, S. Raymond, P. J. Poole, P. J. Barrios, G. Pakulski, D. Poitras, F. G. Sun, S. Taebi, T. Hall, “Ultra-broadband Quantum-Dot Semiconductor Optical Amplifier and Its Applications”, Optical Society of America, 2007.
4. A. M. Odlyzko, I. Kaminov, T. Li, Optical Fibre Telecommunications IVB Components, Academic Press, San Diego, pp. 17-56, 2002.
5. Mohd Zamani Zulkifli, “S-band Multiwavelength Fibre Laser”, Master of Science Thesis, University of Malaya, 2008.
6. Mohd Zamani Zulkifli, “Study of S-band Optical Amplifiers and its Applications”, Doctor of Philosophy Thesis, University of Malaya, 2013.
7. S. Yamashita, T. Baba, K. Kashiwagi, “Frequency-shifted Multiwavelength FBG Laser Sensor”, Optical Fibre Sensors Conference Technical Digest, 2002. OFS 2002 15th, Vol. 1, pp. 285-288, May 2002.
8. P. C. Peng, H. Y. Tseng, S. Chi, “A Novel Fibre-Laser-based Sensor Network with Self-healing Function”, IEEE Photonics Technology Letters, Vol. 15, No. 2, pp. 275-2277, 2003.
9. S. Pradhan, G. E. Town, K. J. Grant, “Microwave Frequency generation using a Dual-wavelength DBR Fibre Laser”, Optical Fibre Technology/Australian

Optical Society, 2006 (ACOFT/AOS 2006) – Proceedings, pp. 104-105, July 2006.

10. Y. Yao, X. F. Chen, Y. T. Dai, S. Z. Xie, “Dual-Wavelength Erbium-doped Fibre Laser with a Simple Linear Cavity and its Application in Microwave Generation”, IEEE Photonics Technology Letters, Vol. 18, No. 1, pp. 187-189, 2006.
11. J. R. Qian, J. Su, X. X. Wang, B. Zhu, “Er-doped Fibre Ring Laser Gyroscopes Operating in Continuous Waves”, Chinese Optics Letters, Vol. 5, pp. 229-231, 2007.
12. A. A. M. Kok, S. Musa, A. Borreman, M. B. I. Diemeer, A. Driessen, “Completely Multimode Arrayed Waveguide Grating-based Wavelength Demultiplexer”, EURO CON 2003, Computer As a Tool, The IEEE Region 8, Vol. 2, pp. 422, 2003.
13. H. Ahmad, M. Z. Zulkifli, A. A. Latif, N. A. Hassan, Z. A. Ghani, S. W. Harun, “120nm wide band switchable fibre laser”, Optics Communications, Vol. 283, Issue 21, pp. 4333-4337, November 2010.
14. H. Okayama, M. Kawahara, “Waveguide Array Grating Wavelength Demultiplexer on LiNbO₃,” Integrated Photonics Research (IPR’95), Techn. Digest (Dana Point, CA, USA, 1995), pp. 296-298, 1995.
15. J. Hecht, (2002), Fibre Gratings: Wavelength Selection by Fibre Gratings In “Understanding Fibre Optics” (4th Edition), International Edition, (pp. 158-159), United States of America, Pearson – Prentice Hall.
16. J. Hecht, (2002), Fibre Gratings: Reflection and Transmission in Fibre Gratings In “Understanding Fibre Optics” (4th Edition), International Edition, (pp.), United States of America, Pearson – Prentice Hall.

17. J. B. Rosolem, A. A. Juriollo, M. A. D. Santos, M. A. Romero, "Comparative Analysis of Triple Band S-C-L Erbium-Doped Fibre and Semiconductor Optical Amplifier for CWDM Applications", *IET Optoelectron.*, Vol. 2, No. 3, pp. 115-121, 2008.
18. J. Hecht, (2002), *Wavelength and Frequency Measurements: Linewidth Measurements* In "Understanding Fibre Optics" (4th Edition), International Edition, (pp. 420), United States of America, Pearson – Prentice Hall.
19. M. Z. Zulkifli, H. Ahmad, N. A. Hassan, M. H. Jemangin, S. W. Harun, "An Ultra-wideband Tunable Multi-Wavelength Brillouin Fibre Laser based on a Semiconductor Optical Amplifier and Dispersion Compensating Fibre in a Linear Cavity Configuration", *Quantum Electronics*, Vol. 41, No. 7, pp. 602-605, 2011.
20. Mohammadreza Rezazadeh Shirazi, "Multiwavelength Brillouin Fibre Lasers", Thesis for the Degree of Doctor of Philosophy, University of Malaya, 2009
21. A. W. Al-alimi, M. H. Yaacob, A. F. Abas, M. A. Mahdi, M. H. Al-Mansoori, M. Mokhtar, "Simple Multiwavelength Brillouin-Erbium-doped Fibre Laser Structure Based on Short SSMF", *Optics Communications*, Vol. 300, pp. 8-11, 2013.
22. S. P. Smith, F. Zarinetchi, S. Ezekiel, "Narrow-linewidth Stimulated Brillouin Fibre Laser and Applications", *Optics Letters*, Vol. 16, No. 6, pp. 393-395, USA, March 1991.
23. N. M. Samsuri, A. K. Zamzuri, M. H. Al.Mansoori, A. Ahmad, M. A. Mahdi, "Brillouin-Erbium Fibre Laser with Enhanced Feedback Coupling using Common Erbium Gain Section", *Optics Express*, Vol. 16, No. 21, October 2013.
24. G. J. Cowle, D. Y. Stepanov, "Hybrid Brillouin/Erbium Fibre Laser", *Optics Letters*, Vol. 21, No. 16, pp. 1250-1252, August 1996.

25. M. R. Shirazi, M. Biglary, S. W. Harun, K. Thambiratnam, H. Ahmad, “Bidirectional Multiwavelength Brillouin Fibre Laser Generation in a Ring Cavity”, *J. Opt. A: Pure Appl. Opt.*, Vol. 10, 2008.
26. M. R. Shirazi, S. W. Harun, M. Biglary, H. Ahmad, “Linear Cavity Brillouin Fibre Laser with Improved Characteristics”, *Optics Letters*, Vol. 33, No. 8, pp. 770-772, April 2008.
27. B. Dong, D. Zhou, L. Wei, “Tunable Multi-wavelength Brillouin-Erbium Fibre Laser by Controlling Self-lasing Cavity Modes’ Oscillation”, *Optical Fibre Tech.*, Vol. 16, pp. 17-19, 2010.
28. Y. Tu, H. Gong, L. Zhang, Y. Jin, J. Wang, “Multiwavelength Brillouin Fibre Laser with EDFA”, *International Conference on Electronics and Optoelectronics (ICEOE)*, 2011.
29. Y. Li, Y. G. Liu, J. B. Xu, B. Y. Tai, Z. Wang, “Tunable Multiwavelength Brillouin-Erbium Ring-Cavity Fibre Laser with Short-Length Photonic Crystal Fibre”, *Laser Physics*, Vol. 20, No. 2, pp. 528-532, 2010.
30. T. F. Al-Mashhadani, M. H. Al-Mansoori, M. Z. Jamaludin, F. Abdullah, A. K. Abass, N. I. M. Rawi, “Tunable Multiwavelength L-Band Brillouin Fibre Laser Utilizing Passive EDF Absorber Section”, *Optics Fibre Tech*, Vol. 19, pp. 593-597, 2013.
31. N. A. M. A. Hambali, M. A. Mahdi, M. H. Al-Mansoori, A. F. Abas, M. I. Saripan, “Investigation on the Effect of EDFA Location in Ring Cavity Brillouin-Erbium Fibre Laser”, *Optics Express*, Vol. 17, No. 14, July 2009.
32. G. Mamdoohi, A. R. Sarmani, M. H. Yaacob, M. Mokhtar, M. A. Mahdi, “Multi-wavelength Brillouin-Raman Fibre Laser Utilizing Enhanced Nonlinear Amplifying Loop Mirror Design”, *Optics Express*, Vol. 21, No. 26, December 2013.

33. S. W. Harun, N. K. Saat, H. Ahmad, "An Efficient S-band Erbium-Doped Fibre Amplifier Using Double-Pass Configuration", *IEICE Electronics Express*, Vol. 2, No. 6, pp. 182-185, March 2005.
34. N. S. Shahabuddin, S. W. Harun, M. R. Shirazi, H. Ahmad, "A Linear Cavity Brillouin/Bismuth-Based Erbium-Doped Fibre Laser with Enhanced Characteristics", *Laser Physics*, Vol. 18, No. 11, pp. 1344-1348, 2008.
35. S. W. Harun, S. Shahi, H. Ahmad, "Brillouin Fibre Laser with 49cm Long Bismuth-based Erbium-doped Fibre", *Laser Physics Letters*, Vol. 7, No. 1, pp. 60-62, 2010.
36. S. Zheng, C. Zhang, S. Jian, "Compact Brillouin Bismuth-Gallium-Aluminum Co-Doped Erbium Doped Fibre Laser", *Optical Fibre Tech.* Vol. 18, pp. 161-166, 2012.
37. H. Ahmad, M. Z. Zulkifli, S. F. Norizan, A. A. Latif, S. W. Harun, "Controllable Wavelength Channels for Multiwavelength Brillouin Bismuth/Erbium Based Fibre Laser", *Progress In Electromagnetic Research Letters*, Vol. 9, 2009.
38. S. Shahi, S. W. Harun, H. Ahmad, "Multi-wavelength Brillouin Fibre Laser using a Holey Fibre and a Bismuth-Oxide based Erbium-Doped Fibre", *Laser Physics Letters*, Vol. 6, No. 6, pp. 454-457, 2009.
39. D. Zhou, P. R. Prucnal, I. Glesk, "A Widely Tunable Narrow Linewidth Semiconductor Fibre Ring Laser", *IEEE Photonics Technology Letters*, *IEEE Photonics Technology Letters*, Vol. 10, No. 6, pp. 781-783, 1998.
40. Y. Huang, L. Zhan, J. H. Ji, S. Y. Luo, Y. Xia, "Multiwavelength self-seeded Brillouin-Erbium Fibre Laser with 45-nm Tunable Range", *Optics Communication*, Vol. 281, No. 3, pp. 452-456, 2008.

41. M. H. Al-Mansoori, M. K. Abd-Rahman, F. R. Mahamd Adikan, M. A. Mahdi, "Widely Tunable Linear Cavity Multiwavelength Brillouin-Erbium Fibre Lasers", *Optics Express*, Vol. 13, Issue 9, pp. 3471-3476, 2005.
42. C. H. Yeh, S. Chi, "Fibre-fault Monitoring Technique for Passive Optical Networks based on Fibre Bragg Gratings and Semiconductor Optical Amplifier", *Optics Communication*, Vol. 257, No. 22, pp. 306-310, 2005.
43. T. Akiyama, M. Ekawa, M. Sugawara, K. Kawaguchi, H. Sudo, A. Kuramata, H. Ebe, Y. Arakawa, "An Ultrawide-band Semiconductor Optical Amplifier Having an Extremely High Penalty-Free Output Power of 23dBm Achieved with Quantum Dots", *IEEE Photonics Technology Letters*, Vol. 17, No. 8, August 2005.
44. G. Ortner, C. N. Allen, C. Dion, P. Barrios, D. Poitras, D. Dalacu, G. Pakulski, J. Lapointe, P. J. Poole, W. Render, S. Raymond, "External Cavity InAs/InP Quantum Dot Laser with a Tuning Range of 166nm", *Applied Physics Letters*, Vol. 88, pp. 0121119(1-3), Canada, March 2006.
45. Q. Wang, Q. X. Yu, "Continuously Tunable S and C+L bands Ultra Wideband Erbium-doped Fibre Ring Laser", *Laser Physics Letters*, Vol. 6, No. 8, pp. 607-610, April 2009.
46. A. Mori, H. Masuda, K. Shikano, K. Oikawa, K. Kato, M. Shimizu, "Ultra-wideband Tellurite-based Raman Fibre Amplifier", *Electronics Letters*, Vol. 37, No. 24, November 2001.
47. J. B. Rosolem, A. A. Juriollo, R. Arradi, A. D. Coral, J. C. R. F. De Oliveira, M. A. Romero, "S-C-L Triple-band Double-Pass Erbium-Doped Silica Fibre Amplifier with an Embedded DCF Module for CWDM Applications", *Journal of Lightwave Tech.* Vol. 24, No. 10, October 2006.

CHAPTER 5

FUTURE WORKS AND CONCLUSION

5.1 Future works

The ultra-wideband semiconductor optical amplifier (SOA) has more potential compared to other rare earth-doped fibers mostly because of its compactness and the ability to cover S-, C- and L-band of transmission regions just by utilizing a single chip component within an amplifier. Achieving the high potential of the ultra-wideband SOA in generating multi-wavelength fiber lasers still requires several improvements. The focus of this research is to design and develop an ultra-wideband fiber laser by using the SOA; it has been fulfilled but there are many other routes in which the research can continue. Some of the targets of future works would be:

1. To enhance the output power of the existing design. Basically, the enhancement should focus on the output power of the ultra-wideband SOA fiber laser to meet the ITU and IEEE standard requirements. In addition, the research should be focusing more on how to produce an ultra-wideband multi-wavelength SOA fiber laser with the same values of peak powers throughout the S-, C- and L-bands. Other than that, improving the noise level problem in the laser cavity could indirectly improve the side-mode-suppression ratio (SMSR) values of the attained laser signals.
2. To enhance the current ultra-wideband SOA fiber laser to have wider tuning range, so that more wavelength channels can be attained. Another idea is to allow the channel spacing between the wavelengths to be adjusted as necessary.

3. To produce a Brillouin multi-wavelength comb that covers all the S-, C- and L-band continuously. A hybrid with a Raman amplifier could make it possible as the high intensity power of the Raman amplifier is sustainable for continuous Brillouin Stokes generation, leading to production of an ultra-wide comb Brillouin fibre laser.

Other than that, efforts to reduce the polarization dependent gain (PDG) effect on the ultra-wideband SOA can be put into consideration by carefully protecting the fiber setup within a suitable case on the optical table. Such protection can minimize disruptions and so reduce the PDG effect. Furthermore, attaching a polarization controller in each input and output port of the SOA also reduces the PDG effect.

5.2 Conclusion

In conclusion, this thesis has shown that the ultra-wideband SOA can efficiently act as the gain medium that provides ultra-wideband amplification covering the short (S-), conventional (C-) and long (L-) bands of transmission in communication. Furthermore, the inhomogeneity characteristic exhibited by the ultra-wideband SOA containing an inhomogeneous broadening gain medium has made it possible to generate multi-wavelength fiber laser systems with no dependency on mode competition effect, thus proving to work better than the majority of other doped fibre mediums. The proposed ultra-wideband SOA fiber lasers will have many applications, especially in optical communications where multiple channels with smaller spacing are necessary to achieve high transmission capacity, and also for optical sensing where multiple channels with larger spacing is useful to accommodate for wavelength shift in response to the tested phenomena of the experiments. With more study and further research in the future, the ultra-wideband SOA fiber laser is anticipated to enhance many existing applications in

optical fibre technologies, and also spur new developments of applications so as to bring many significant advantages to the nation and to the world.

Other than that, many research findings were published in internationally referred journals in the course of completing this research. Several publications are based on the experiments done that are directly related to this thesis and some of them are extensions of the research work done within the same project study. There are also publications that are indirectly related to the thesis which are very useful in improving other skills, such as splicing and device handling, that could be beneficial to researcher skill development. All the publications are listed in Appendix 2 of the thesis.

APPENDIX 1



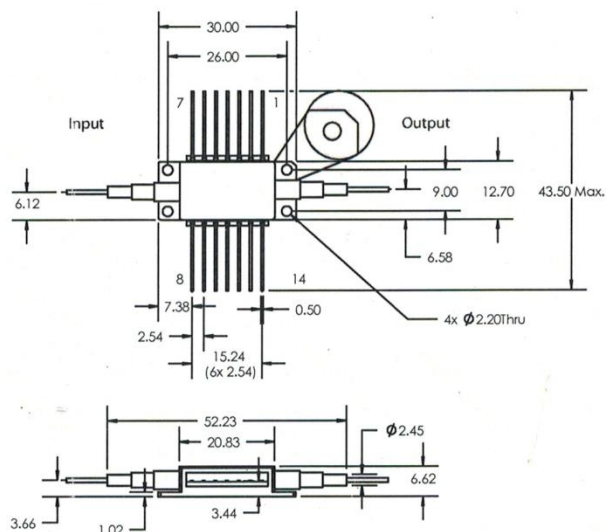
Alphion SA_H Devices Operating Specifications

Absolute Maximum Ratings*

Parameter	Symbol	Min	Typ	Max	Unit	Note
Operating Temperature	T_{case}	0		70	°C	Case Temperature
Storage Temperature	T_{store}	-40		85	°C	
Operating Bias Current	I_f			600	mA	
Optical Amplifier Reverse Bias	V_{rev}			2	V	
Thermistor Current	I_{therm}			5	mA	
TEC Current	I_{TEC}			1.8	A	
TEC Voltage	V_{TEC}			3.4	V	

* Stresses in excess of the Absolute Maximum Ratings can cause permanent damage to the device. These are absolute stress ratings only. Functional operation of the device is not implied at these or any other conditions in excess of those given in the operational section of the datasheet. Exposure to Absolute Maximum Ratings for extended periods can adversely affect the device reliability.

Pin Assignments			
1	TEC (+)	14	TEC (-)
2	Thermistor	13	NC
3	NC	12	NC
4	NC	11	Chip (-)
5	Thermistor	10	Chip (+)
6	NC	9	NC
7	NC	8	NC



*Note: Pin #1 is marked by a bevel (notch) at the base of the housing

* Warning *

Alphion SOA devices are designed for normal operation from 0 to 70°C.

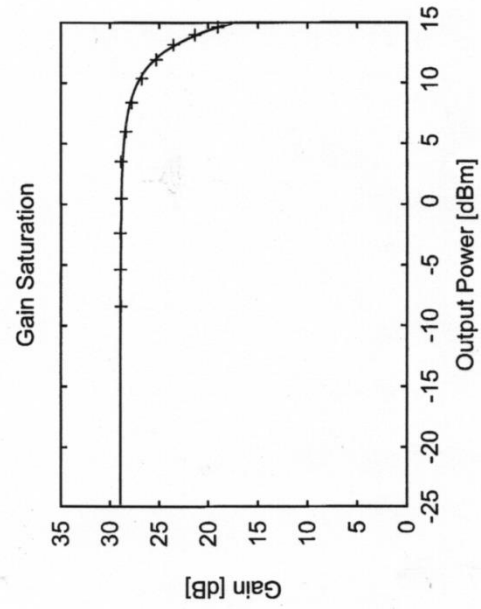
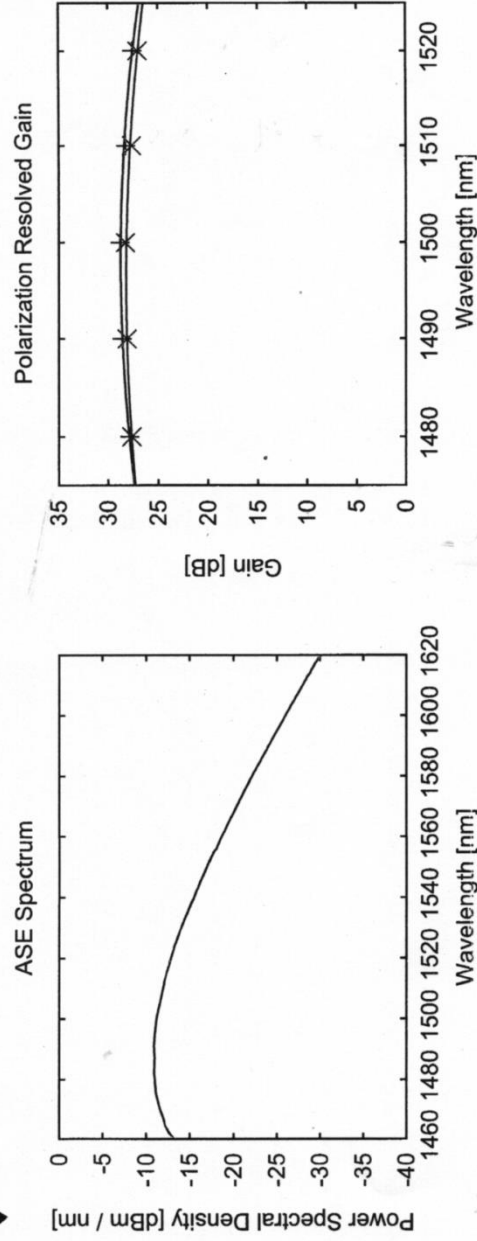
To ensure safe operation, certain precautions should be followed:

- Do not set chip temperature lower than 25°C
- Ensure proper heat sinking or mounting on Alphion SET-II Board
- Do not expose device to case temperatures higher than 70°C during operation
- Do not expose device to storage temperatures greater than 85°C

Alphion®...enabling the photonic future™



Alphion SAS26p 01P020



I	420	mA
T chip	25	°C
P ase, out	7.6	dBm
P ase, in	7.6	dBm
Peak wl	1487	nm
BW ase, fwhm	70.6	nm
Peak gain	28.8	dB
Max PDG	0.6	dB
Avg NF	7.0	dB
P sat, 3dB	+11.5	dBm
ASE ripl	0.8	dB

APPENDIX 2

LIST OF ISI PUBLICATIONS

1. H. Ahmad, M. Z. Zulkifli, **N. A. Hassan**, S. W. Harun, "S-band Multiwavelength Ring Brillouin/Raman Fiber Laser with 20GHz Channels Spacing", Applied Optics, Vol. 51, No. 11, 10 April 2012.
2. H. Ahmad, M. Z. Zulkifli, **N. A. Hassan**, S. W. Harun, "Enhancement of Brillouin Stokes Generation in the S-band Region Using a Combination S-Band Depressed Cladding Erbium Doped Fiber and Semiconductor Optical Amplifier", Laser Physics Letters, Vol. 22, No. 3, pp. 1-7, 2012.
3. H. Ahmad, M. Z. Zulkifli, **N. A. Hassan**, A. A. Latif, S. W. Harun, "High Gain S-Band Semiconductor Optical Amplifier with Double-Pass Configuration", Laser Physics Letters, Vol. 21, Issue 7, pp. 1208-1211, 2011.
4. M. Z. Zulkifli, H. Ahmad, **N. A. Hassan**, M. H. Jemangin, S. W. Harun, "An Ultra-wideband Tunable Multi-Wavelength Brillouin Fibre Laser Based On A Semiconductor Optical Amplifier and Dispersion Compensating Fiber in a Linear Cavity Configuration", Quantum Electronics, Vol. 41, Issue 7, pp. 602-605, 2011.
5. H. Ahmad, M. Z. Zulkifli, A. A. Latif, **N. A. Hassan**, Z. A. Ghani, S. W. Harun, "120nm Wide Band Switchable Fiber Laser", Optics Communications, Vol. 283, Issue 21, pp. 4333-4337, 2010.
6. M. Z. Zulkifli, **N. A. Hassan**, N. A. Awang, Z. A. Ghani, S. W. Harun, H. Ahmad, "Multiwavelength Fiber Laser in the S-Band Region using a Sagnac Loop Mirror as a Comb Generator in an SOA Gain Medium", Laser Physics Letters, Vol. 7, Issue 9, pp. 673-676, 2010.

7. A. A. Latif, M. Z. Zulkifli, **N. A. Hassan**, S. W. Harun, Z. A. Ghani, H. Ahmad, "A Compact O-plus C-band Switchable Quad-Wavelength Fiber Laser using Arrayed-Waveguide Grating", *Laser Physics Letters*, Vol. 7, Issue 8, pp. 597-602, 2010.
8. H. Ahmad, M. Z. Zulkifli, **N. A. Hassan**, F. D. Muhammad, S. W. Harun, "S-C-L triple wavelength supertluminescent source based on an ultra-wideband SOA and FBGs", *Quantum Electronics*, 43 (10), pp. 923-926, 2013.



120 nm wide band switchable fiber laser

H. Ahmad ^{a,*}, M.Z. Zulkifli ^a, A.A. Latif ^a, N.A. Hassan ^a, Z.A. Ghani ^c, S.W. Harun ^{b,1}

^a Photonics Laboratory, Department of Physics, University of Malaya, 50603 Kuala Lumpur, Malaysia

^b Department of Electrical Engineering, Faculty of Engineering, University of Malaya, 50603 Kuala Lumpur, Malaysia

^c Faculty of Applied Sciences, MARA University of Technology, 40450 Shah Alam, Malaysia

ARTICLE INFO

Article history:

Received 10 March 2010

Received in revised form 9 June 2010

Accepted 10 June 2010

ABSTRACT

A novel method of producing switchable tunable output that spans the S-, C- and L-bands is presented. The achievable tuning range is about 120 nm. The design consists of a wide band SOA, 1×16 AWG and an optical selectable switch in a ring configuration. The measured average output powers for S-, C- and L-bands for different output wavelengths are -7.0 dBm, -6 dBm and -6.5 dBm respectively. The SMSR for these wavelengths is about 72 dB.

© 2010 Elsevier B.V. All rights reserved.

1. Introduction

Currently there is a need for Switchable Multiwavelength Fiber Laser (SMWFL) to support the Dense Wavelength Division Multiplexing (DWDM) network as a replacement part for the optical source. The advantages of the switchable multiwavelength laser are its ability to select a single channel from a multiwavelength comb [1] and its generally stable output with narrow linewidth emission line which is compatible with existing optical network systems. Besides its application in the telecommunication, the SMWFL can be a source for spectroscopy and for use in the fiber sensor. This flexibility spurs intense research in developing a stable switchable wavelength that can have a wide tuning range. There are various methods of realizing switchable outputs such as that based on polarization dependent device in the cavity [2], the use of high-birefringence fiber loop mirror (HiBi-FLM), cascaded Fiber Bragg Grating (FBG) cavities and cavities with birefringence FBG or cascaded Birefringence FBGs [3–6]. The development of the SMWFL using Sagnac Loop Mirrors (SLM) [7] and compression strain FBG for tunable wavelength has also been demonstrated [8,9]. This system is capable of generating a wide range of tunability specification within the C-band and C- plus L-band. However, the usage of SLMs requires a fixed length of fiber for a particular wavelength which has to be manually adjusted.

As a result of this shortcoming in SLMs based system, use of Arrayed Waveguide Grating (AWG) provides a switchable alternative. The use of the AWG as a wavelength slicing mechanism has generated new interests in developing the Multiwavelength Fiber Laser (MWFL,

operating at fixed spacing of 50 GHz, 100 GHz or 200 GHz) that fits well with the DWDM network. This technique has been demonstrated using Amplified Spontaneous Emission (ASE) output of a Semiconductor Optical Amplifier (SOA) or Erbium Doped Fiber Amplifier (EDFA) into AWG [10–14].

Most of the reported works are concentrated within the C- plus L-band and it would be interesting to extend this coverage to include the S-band. Recent migration into the metro-network based or Coarse Wavelength Division Multiplexing (CWDM) would require a switchable fiber laser that can be tuned from the S- to L-band. Recent works to cover all the three bands have been done using thulium doped fiber together with erbium doped fiber in a hybrid configuration [15]. It consists of two components of 20 m in length thulium doped fiber connected in parallel with 12 nm of erbium doped fiber pumped by numerous laser diodes. Although the tunability range is wide, reaching as large as 145 nm, the complexity and usage of many laser diodes can be a hindrance to realizing a commercial unit. A similar approach is also being undertaken by Foroni et al. [16] to achieve a tuning range of 120 nm using three components of erbium doped fibers connected in parallel and multiplexed to generate the tunability range. The tuning for the entire range is not clearly stated but a tunable C-band filter is used in the C-band. The approach in the design is based on a double pass technique as reported in an earlier paper by Harun et al. [17].

As an alternative approach in generating a wide tuning range, a single semiconductor optical amplifier (SOA) is used in place of the many pump lasers and it provides a tuning range of 120 nm covering the S-, C- and L-bands as proposed in this paper. The tunability is performed using an arrayed waveguide grating (AWG) in conjunction with optical channel selector (OCS) providing electronically tuned selectable output. This is illustrated and demonstrated in the following section.

* Corresponding author.

E-mail address: harith@um.edu.my (H. Ahmad).

¹ Tel.: +603 79674290; fax: +603 79676770.

2. Experimental setup

The experimental setup, as shown in Fig. 1, consists of an SOA, an AWG and two OCSs connected in a ring configuration. The SOA is from Alphion (SAS26P) with output characteristics that cover a wavelength range from 1400 nm to 1650 nm which acts as the gain medium. The Amplified Spontaneous Emission (ASE) emitted from it is connected to the 1×16 AWG which slices the ASE output spectrum into 16 different wavelength outputs which can be referred to 16 different channels. Since the ASE output of the SOA is broad, which covers the S-, C- and L-bands, each channel will contain output components from S-, C- and L-bands due to the diffraction effect of the AWG. Each individual wavelength will diffract and focus at different angles at the AWG output plane according to Eq. (1) below [18],

$$\theta_m \approx \frac{N_{eff} \Delta L - m \lambda_g}{N_f d_a} \quad (1)$$

where θ_m is the tilt angle, ΔL is the optical path difference, $\lambda_g = \frac{\lambda}{N_{eff}}$, m is an integer (diffraction order), d_a is the pitch between the array waveguide, and N_{eff} and N_f are the effective refractive indices in the waveguide array and in the free propagation region respectively. AWG used is optimized for the C-band operation from wavelength 1530.56 nm to 1542.34 nm. However, when a broadband source (S-, C- and L-bands) is passing through the AWG, each channel will have 3 components, one each for S-, C- and L-bands. This is due to the various diffraction order which now includes $m-1$, m and $m+1$ which satisfied the condition $\theta_{m-1} = \theta_m = \theta_{m+1}$ for different wavelengths. θ_{m-1} is for L-band, θ_m is for C-band, and θ_{m+1} is for S-band. Since they focus at the same spot, they will be reproduced together in a single output although the AWG is designed to have single output for C-band only. These output channels are connected to the 16 outputs of the 1×16 optical switch which is referred to as the optical channel selector (OCS1). For instance, channel 1 contains outputs in S-, C- and L-bands at wavelengths that satisfy Eq. (1). (As an example, channel 1 contains $\lambda_s = 1478.69$ nm, $\lambda_c = 1530.56$ nm and $\lambda_L = 1586.26$ nm). The optical Switch is a commercial unit (ANDO AQ3540) with a switching speed of 500 m/s between channels and a transmission bandwidth that ranges from 1200 nm to 1650 nm. This bandwidth is large enough to cover the experimental bandwidth of this work.

The output of channel 1 (similarly for the other channels) is then connected to a S/C+L bands Wavelength Division Multiplexer (WDM) that splits the S and C+L bands into different output ports. The C+L is further split into C and L outputs using a similar type fused WDM coupler as shown in Fig. 1. These individual outputs, S, C and L, are then connected to channels 1, 2 and 3 of the second OCS (OCS 2). From OCS 2, the individual output, S, C or L, can be chosen as a means to provide the tunability. For instance, if the S output of

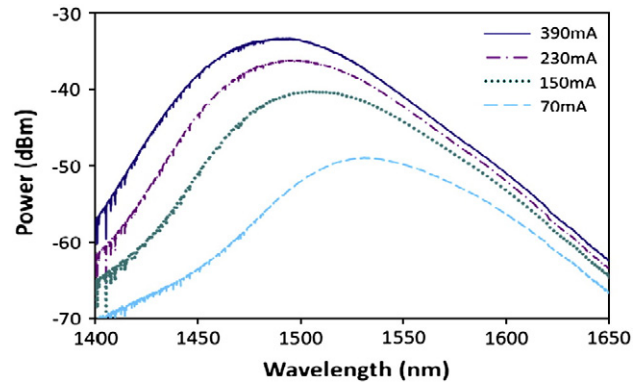


Fig. 2. ASE spectrum of wideband SOA.

channel 1 from OCS 1 is chosen ($\lambda_{s1} = 1478.69$ nm), then this will be injected into the ring cavity via channel 1 of OCS 2 to be amplified by the SOA. Similarly, for channel 2 of the AWG ($\lambda_{s2} = 1479.41$ nm), channel 3 until channel 16 can be chosen and this provides the tunability within the S-band region. This similar approach is also applicable for the C- and L-bands by choosing channel 2 and 3 of OCS 2. The injected light will traverse into the ring cavity in an anticlockwise direction set upon by the optical isolator. The output signal is taken from a 90/10 broadband fused biconnical coupler with the 10% port connected to the optical spectrum analyzer (ANDO 6317 C) with a resolution of 0.02 nm. The tunability spans over the S-, C- and L-bands providing a very well controlled and simple design that provides a laser source that can be utilized for WDM, CWDM network and also for application in optical sensors, optical spectroscopy and many others.

3. Results and discussion

Fig. 2 shows the ASE output spectrum of wideband SOA with different driven current. The bandwidth of ASE is increased when the driven current is increased. The bandwidth of the ASE is about 250 nm that ranges from 1400 nm to 1650 nm at 390 mA drive current. The wideband ASE is important in providing a wide tuning range of the fiber laser.

Fig. 3 shows the spectrum taken by using OSA at channel 1 of OCS1 with three peaks produced at three different bands simultaneously. However, this is not yet to be considered as a laser source since there is no cavity and the peaks are produced only by the ASE source which comes from the SOA. As illustrated in the figure, the measured peak powers are -9.92 dBm, -6.03 dBm and -7.57 dBm for wavelengths

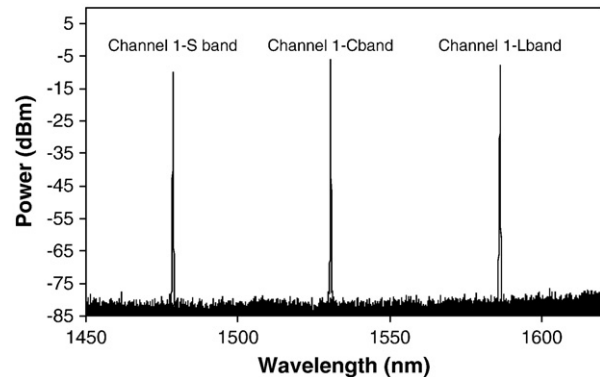


Fig. 3. Spectrum of the output wavelength from channel 1 before it is split into three different bands by the S/C+L and C/L splitter.

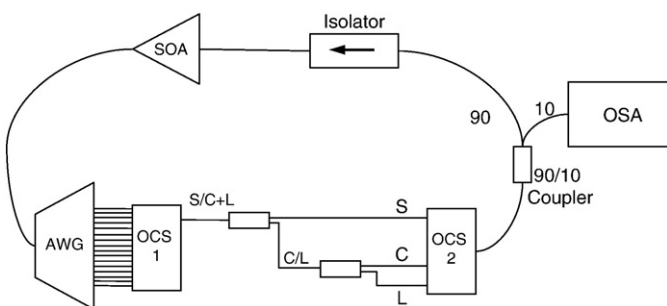


Fig. 1. Experimental setup for SMWFL.

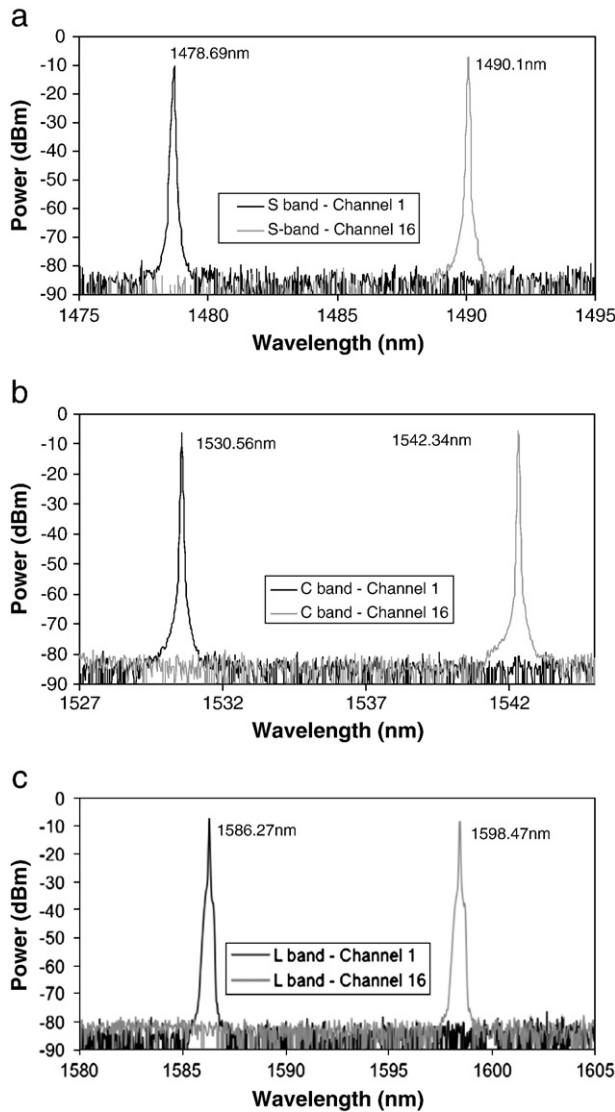


Fig. 4. Widest tuning range for (a) S-band (b) C-band (c) L-band.

1478.69 nm(S-band), 1530.56 nm (C-band) and 1586.26 nm (L-band), respectively. The peak powers have power variations within 4 dB and they can be made equal by proper cleaning of the connectors and having an AWG with equal response at these wavelengths. For channel 2 and the rest of the channels the output will be similar, representing the various bands, but shifted by 0.8 nm (100 GHz) which is the interchannel spacing of the AWG.

The tuning range of the single wavelength laser is as given in Fig. 4 which shows the widest tuning range that can be realized for the S-, C- and L-bands by superimposing the output wavelengths coming from Channels 1 and 16 of the AWG. The range for S-band is from 1478.35 nm to 1490.09 nm, for C-band it is from 1530.56 nm to 1542.34 nm and for L band from 1586.26 nm to 1598.42 nm. The measured linewidths of the outputs in the S-, C- and L-bands are about 0.05 nm, 0.035 nm and 0.035 nm. A wider tuning range can be achieved by using an AWG with more channel outputs. In the case of 1×16 AWG with 100 GHz (0.8 nm) interchannel spacing, the maximum tuning range that can be realized in the C-band is $15 \text{ (spacing)} \times 0.8 \text{ nm}$ which equals 12 nm. This value corresponds well with the measured value of 11.78 nm. The situation is similar for the S- and L-band. For a higher channel count, such as 1×64 AWG, the tuning spacing range will be about 50.4 nm. This shows that the

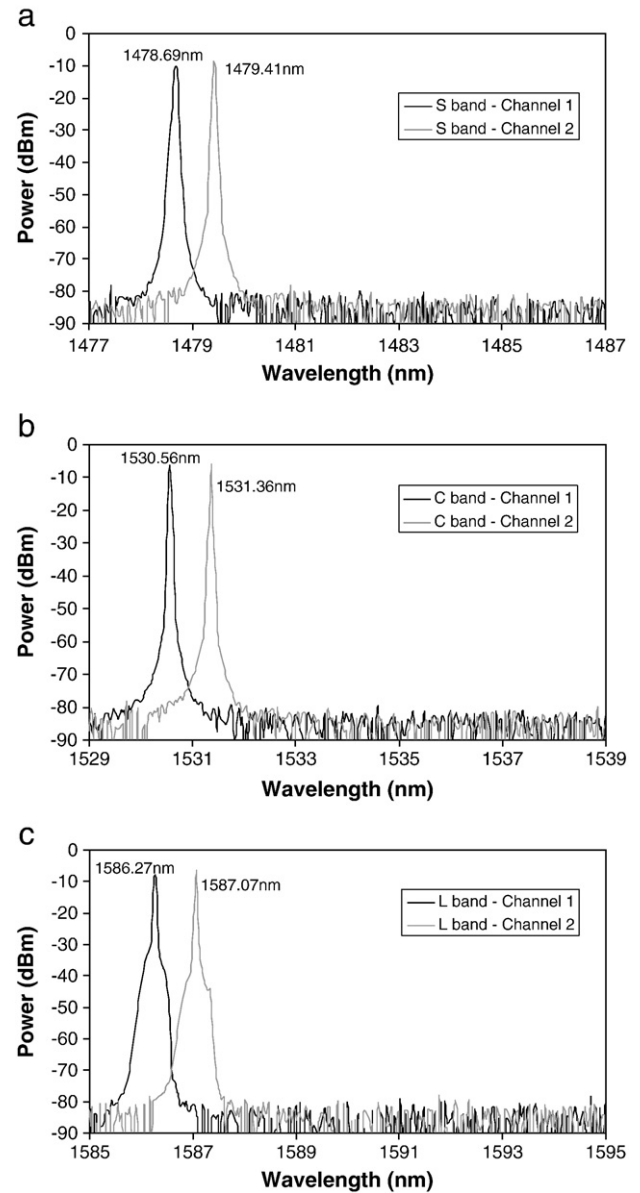


Fig. 5. Narrowest tuning ranges for (a) S-band (b) C-band and (c) L-band.

experimental approach can be extended to a wider tuning range by having a larger number of channel outputs.

Fig. 5 shows the narrowest spacing achievable for the various bands with 0.8 nm of interchannel spacing that can be attained for AWG with 50 GHz. Fig. 6 shows the stability of the output wavelength taken over a 2 hour period. This is taken for each single channel where for S-band it is at 1478.64 nm, C-band at 1530.52 nm and L-band at 1586.24 nm. Similar stabilities are observed for other wavelengths in the different bands. As shown in the figure, there are no power fluctuations for the entire wavelengths, indicating a very stable and well-controlled output.

Other important characteristics of the optical source are the power variations at different wavelength outputs and the Side Mode Suppression Ratio (SMSR) as presented in Fig. 7.

Fig. 7(a) shows the output wavelength variations for the S-band with the lowest value of 69.12 dB for 1485.45 nm and the highest value of 74.53 dB for 1489.29 nm. The variation is about 5.41 dB which can be improved by optimizing the connection and also having an SOA with flat ASE output. The SMSR varies by about 69.95 dB for

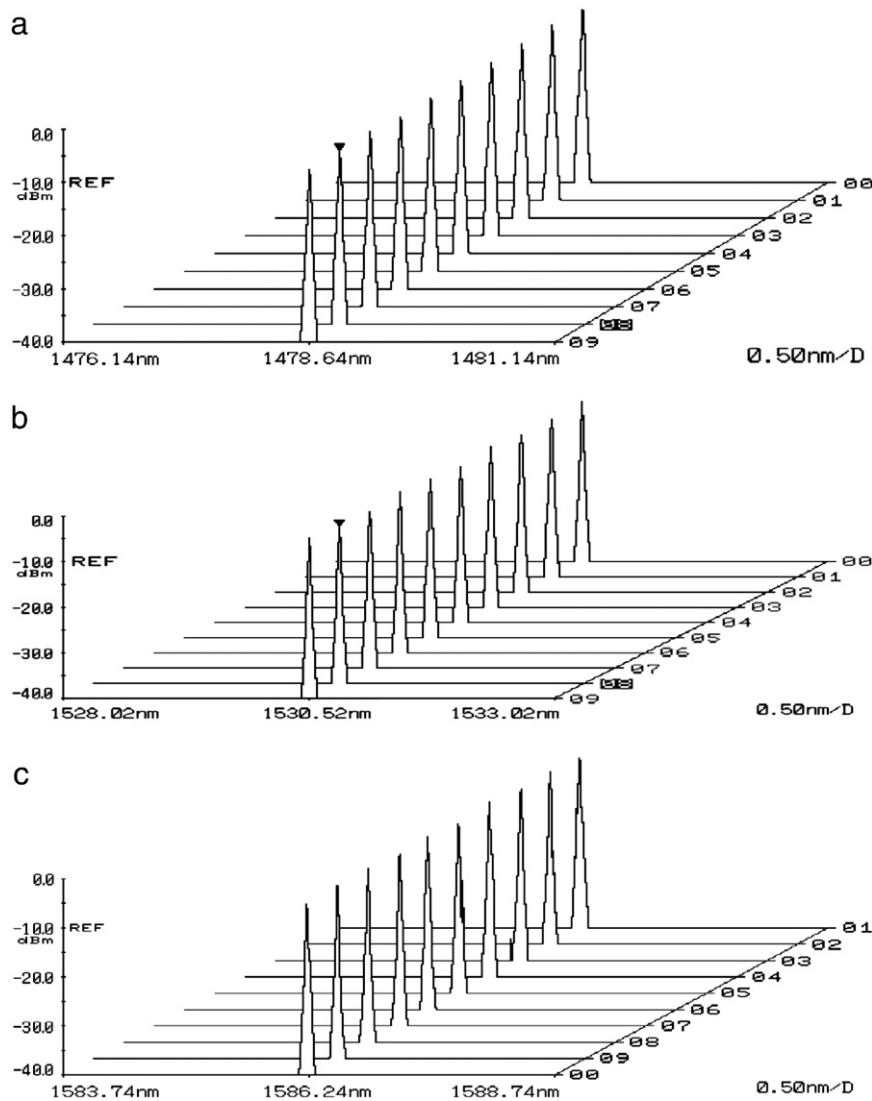


Fig. 6. Stability of Channel 1 for the (a) S-band, (b) C-band and (c) L-band.

wavelengths of between 1478.69 nm (Channel 1) to 1490.09 nm (Channel 16). On average, the SMSR is about 72 dB. Fig. 7(b) shows a better result for the C-band with little power variations at different wavelengths except for wavelength of 1537.62 nm which has a peak power of -7.37 dBm.

Similarly, for the SMSR, the variation is about 4 dB with an average value of 72 dB except at wavelength 1537.62 nm (Channel 10) which has an SMSR of 70.71 dB. This could be due to higher loss at channel 10 as compared with other channels in the AWG. This can also be seen in Fig. 7(a) which shows a slightly lower output power and a lower SMSR.

For the L-band region as in Fig. 7(c), the peak power fluctuation is about 1.5 dB for the 16 wavelengths outputs. The SMSR varies by about 2.5 dB with an average value of 71.5 dB. Large values of SMSR are observed for the three bands indicating the output signals are of high quality.

The entire bandwidth of switchable output that can be switched from 1478.7 nm to 1598.47 nm is shown in Fig. 8 with a possible tunable bandwidth of 120 nm. The switching process is very stable and repeatable providing a wide selection of outputs within the S-, C- and L-bands. As shown in the figure, the spacing between the last channel (channel 16) of the S-band and the first channel (channel 1) of the C-band (similarly between the C- and L-bands) is about 40 nm

with no outputs, which is largely due to the usage of 1×16 AWG. The usable tuning range in each band is about 12 nm. This can be rectified by having a higher channel count, giving a continuous tunability that covers the S-, C- and L-bands. For instance, in a 1×64 channel, the frequency band for each band would be about 51.2 nm. On the whole, this proposed design provides a novel way of generating switchable output that covers a wide tuning range.

4. Conclusion

A design of a wide band switchable fiber laser with a tunability span of 120 nm is successfully demonstrated. It consists of an SOA that provides the ASE output which is then sliced into individual outputs using a 1×16 AWG. This is then amplified by the SOA to generate a stable switchable output that covers the S-, C- and L-bands. The switchable output of the S-band can be tuned from 1478.35 nm to 1490.09 nm, for C-band from 1530.56 nm to 1542.34 nm, and for L-band from 1586.26 nm to 1598.42 nm. The average output powers for each of the S-, C- and L-bands are -7 dBm, -6 dBm and -6.5 dBm, respectively. The SMSR for the various bands is about 72 dB indicating a good signal-to-noise ratio. The output wavelengths are stable over time and have been tested for 2 h with negligible power change. Although the usable tuning range is about 12 nm, this range can be

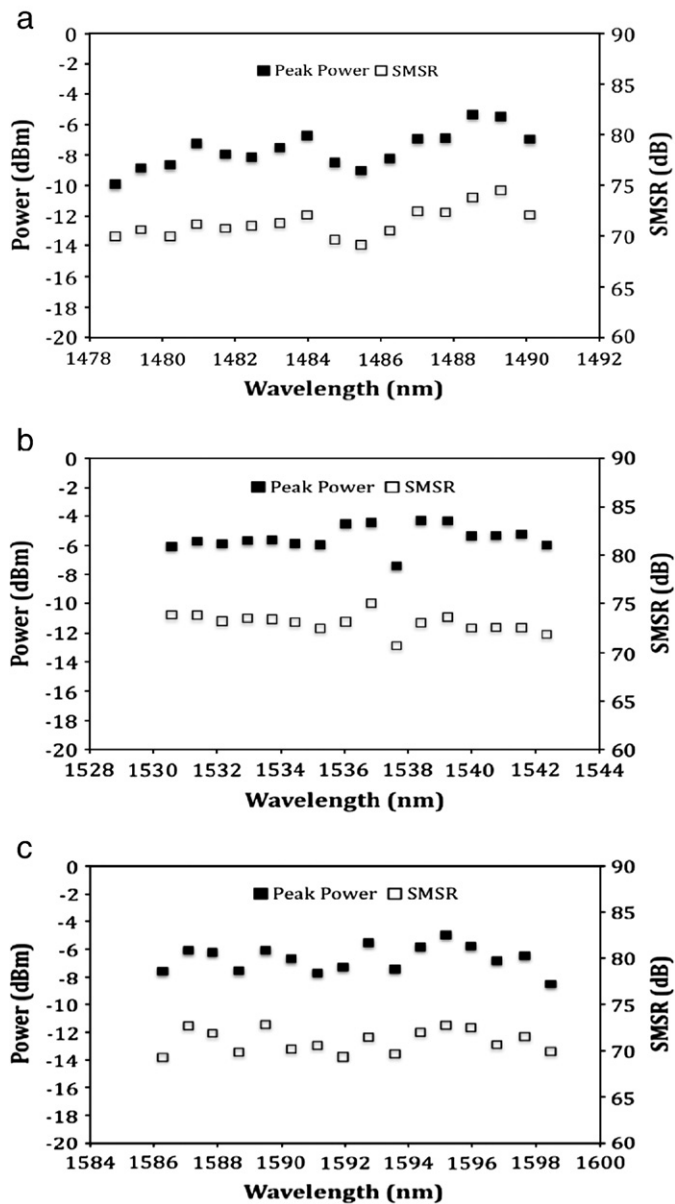


Fig. 7. Peak powers and SMSR for all channels of the entire bands, (a) S-band, (b) C-band and (c) L-band.

improved by having a higher number of output channels in the AWG such as 1×64 . Nevertheless, this work demonstrates an important

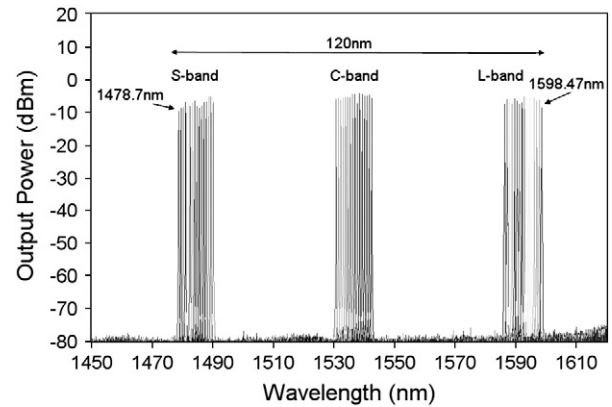


Fig. 8. Spectrum of output lasers for S-, C- and L-bands with 120 nm bandwidth.

technique in realizing a tunable switchable output that can span the entire S-, C- and L-bands.

References

- [1] Suchun Feng, Ou, Xu, Shaohua Lu, Tigang Ning, Shuisheng Jian, *Opt. Commun.* 281 (24, 15) (2008) 6006.
- [2] Y.W. Lee, B. Lee, *IEEE Photon. Technol. Lett.* 15, no.6 (June 2003) 795.
- [3] S. Hu, L. Zhan, Y.J. Song, W. Li, S.Y. Luo, Y.X. Xia, *IEEE Photon. Technol. Lett.* 17 (7) (July 2005) 1387.
- [4] Q. Mao, J.W.Y. Lit, *IEEE Photon. Technol. Lett.* 14 (5) (May 2002) 612.
- [5] C. Zhao, X. Yang, C. Lu, J.H. Ng, X. Guo Xin, P.R. Chaudhuri, X. Dong, *Opt. Commun.* 230 (4) (2004) 313.
- [6] T.V.A. Tran, K. Lee, S.B. Lee, Y. Han, *Opt. Express* 16 (3) (2008) 1460.
- [7] G. Das, J.W.Y. Lit, *IEEE Photon. Technol. Lett.* 16 (1) (Jan. 2004) 60.
- [8] C.S. Goh, M.R. Mokhtar, S.A. Butler, S.Y. Set, K. Kikuchi, M. Ibsen, *IEEE Photon. Technol. Lett.* 15 (4) (Apr. 2003) 557.
- [9] S.-K. Liaw, K.-L. Hung, Y.-T. Lin, C.-C. Chiang, C.-S. Shin, *Opt. Laser Technol.* 39 (2007) 1214.
- [10] H. Ahmad, K. Thambiratnam, A.H. Sulaiman, N. Tamchek, S.W. Harun, *Laser Phys. Lett.* 5 Issue 10 (2008) 726.
- [11] Y. Tachikawa, K. Okamoto, *Proc. Inst. Elect. Eng., Optoelectron.* 143 (5) (1996) 322.
- [12] Y. Tachikawa, K. Okamoto, *Electron. Lett.* 31 (19) (1995) 1665.
- [13] R. Kasahara, M. Ishii, Y. Inoue, S. Sohma, H. Takahashi, S. Suzuki, T. Shibata, T. Kitagawa, Integrated 32ch dynamic wavelength channel selector using AWG and 32X1 PLC switch, *Optical Fiber Communication Conference OFC 2004*, vol. 1, 2004, p. 2602.
- [14] M.Z. Zulkifli, N. Tamchek, A.A. Latif, S.W. Harun, H. Ahmad, *Opt. Commun.* 282 (2009) 2576.
- [15] H. Chen, F. Babin, G. He, G.W. Schinn, S-, C- and L-band continuously tunable fiber laser using thulium- and erbium-doped fibers, *CLEO'05*, vol. 3, 2005, p. 55.
- [16] M. Foroni, L. Ruggeri, F. Poli, A. Cucinotta, S. Selleri, S+C+L Band Double-Pass EDFA, in *Optical Amplifiers and Their Applications/Coherent Optical Technologies and Applications*, OSA Technical Digest Series(CD) (Optical Society of America, 2006), paper JWB44.
- [17] S.W. Harun, P. Poopalan, H. Ahmad, *IEEE Photon. Technol. Lett.* vol. 14 (Mar. 2002) 296.
- [18] A.A.M. Kok, S. Musa, A. Borreman, M.B.I. Diemeer, A. Driessen, Completely multimode arrayed waveguidegrating-based wavelength demultiplexer, *EUROCON 2003. Computer as a Tool*, The IEEE Region 8, vol. 2, 2003, p. 422.

High Gain S-Band Semiconductors Optical Amplifier with Double-Pass Configuration¹

H. Ahmad^a, M. Z. Zulkifli^a, N. A. Hassan^a, A. A. Latif^a, and S. W. Harun^b

^a Photonics Laboratory, Department of Physics, University of Malaya,
50603 Kuala Lumpur, Malaysia

^b Department of Electrical Engineering, Faculty of Engineering, University of Malaya,
50603 Kuala Lumpur Malaysia

e-mail: harith@um.edu.my

Received January 14, 2011; in final form, January 21, 2011; published online June 4, 2011

Abstract—In this paper we propose and demonstrate a double-pass configuration of a compact high gain short wavelength (S-) band amplifier based on a semiconductor optical amplifier (SOA) operating from 1480 to 1520 nm. The proposed system provides gain value of 31.07 dB at a signal power level of -40 dBm taken at 1500 nm. The measure gain profile of the double-pass configuration over different power levels and at different signal wavelengths outperforms that of the single-pass configuration. The noise figure of both configurations averages out to 10 dB. This system provides a good alternative as a high-gain and compact amplifier in the S-band region.

DOI: 10.1134/S1054660X11130019

INTRODUCTION

Increasing demands for communication and information transmission capabilities has recently seen the need for optical communications systems to further expand their transmission windows. Current systems operate at a wavelength range that covers the conventional (C-) band and long-wavelength (L-) bands of 1530 to 1565 nm and 1565 to 1625 nm, respectively has reached its maximum capacities. As such, there is a need to further expand the transmission window so as to incorporate the short-wavelength (S-) band region of 1480 to 1520 nm.

This need has initiated new research into the development of optical amplifiers operating in the S-band region, such as those based on thulium doped fibers (TDFs) [1–3] or co-doping existing erbium doped fibers (EDFs) with ytterbium [4–6]. Hybrid optical amplifiers comprising of EDF based amplifiers with a Raman gain medium [7, 8] have also been explored. These initial avenues of research have met with success, and are able to provide suitable amplification in the S-band region. Now, the research efforts have begun to look towards fully utilizing these new developments by developing a wide-band optical amplifier that covers the complete range of the S-, C-, and L-bands in a single amplifier, focusing specially on the development of a simple, low-cost and highly compatible design (current designs typically involve a number of different components to be made to function together, thus increasing the cost and complexity of the system as well as limiting its compatibility to systems already in use).

In addressing the above issue, semiconductor optical amplifiers (SOAs) provide a viable solution to the development of an ultra-wide bandwidth amplifier capable of operating in the S-, C-, and L-bands simultaneously [9, 10]. Furthermore, SOAs typically possess a wider bandwidth as compared to erbium doped fibre amplifiers (EDFAs), although its gain profile is generally lower than that of the EDFA. In this paper, we propose and demonstrate a double-pass configuration of a compact high gain S-band amplifier based on a SOA operating from 1480 to 1520 nm. The gain value of the proposed setup shows a better performance as compared to other type of S-band Optical Amplifier [11, 12].

EXPERIMENTAL SETUP

Figure 1a below shows the experimental setup of the high-gain S-band SOA in a double-pass configuration. It consists of an SOA (Alphion SAS28p) with an amplified spontaneous emission (ASE) spectrum covering 1420 to 1600 nm.

The S-band band SOA is driven by an ILX laser diode controller at a current of 460 mA, while a Yokogawa AQ2211 tunable laser source (TLS) with a tunability range of 1440 to 1530 nm and a resolution of 0.001 nm was used to provide the S-band input signal. An optical isolator is immediately placed after the TLS to force the signal to propagate in a unidirectional path and also prevent any back-reflected signals that can cause damage to the TLS. The S-band signal generated from the TLS first travels to port 1 of the first optical circulator (OC1), where it then continues via port 2 towards the polarization controller and onwards to the SOA. The use of the polarization controller is to

¹ The article is published in the original.

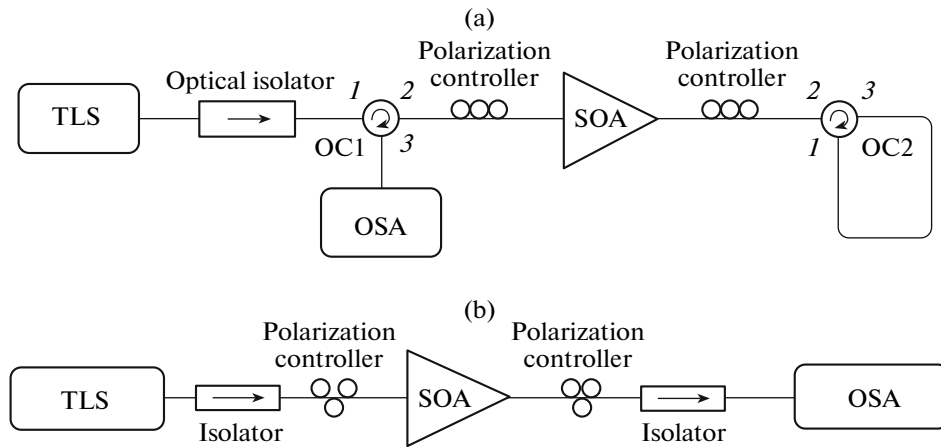


Fig. 1. Experimental setup of high gain S-band SOA in (a) the double pass configuration and (b) the single pass configuration.

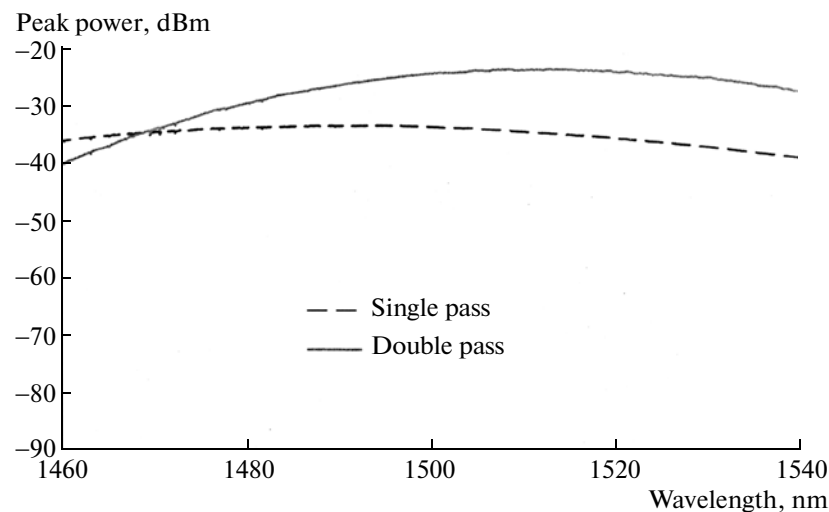


Fig. 2. ASE spectra comparison between single pass and double pass configurations at a 460 mA injection current.

provide a means to optimize the gain. The amplified signal will then exit the SOA and enter another polarization controller, after which it enters the second optical circulator (OC2) where ports 1 and 3 are connected, acting as a “mirror”. This back-reflected amplified signal will then be re-amplified by the SOA and now will be emitted at port 3 of OC1 (entering OC1 at port 2) and be analyzed by an optical spectrum analyzer (OSA) (Ando AQ6317C). For the case of the single pass configuration, there are no optical circulators that act as “mirrors” unlike in the double-pass. Instead the signal is measured directly after the SOA as shown in Fig. 1b. The characteristics of the double-pass SOA are discussed in the next section.

RESULTS AND DISCUSSIONS

Figure 2 below shows the compared ASE spectra of the SOA in the single- and double-pass configurations.

From Fig. 2, the ASE power level is observed to be -24 dBm at a wavelength of 1500 nm when the SOA is driven at a current of 460 mA. At a similar condition the single-pass configuration only yields an ASE power of -32 dBm, 8 dB lower than that of the double-pass configuration. However, the optimum ASE bandwidth for the double pass configuration is observed to be limited to a wavelength range of 1440 to 1540 nm whilst the single pass configuration ASE shows wider bandwidth coverage from 1400 until 1540 nm. As can be seen in Fig. 2, the ASE of the single-pass and double-pass configuration experiences a very distinct shape difference. The ASE for double pass configuration is observed to be slightly concentrated at the longer transmission wavelength region that fits well in the S-band region; whilst the single-pass ASE disperses over a wider transmission wavelength range. The distinct difference in the ASE shape of the double-pass configuration is influenced by the inhomoge-

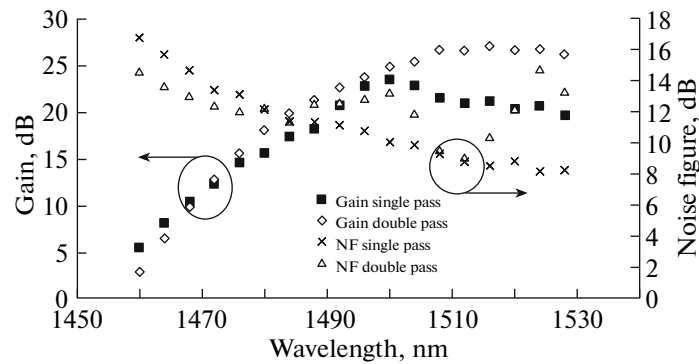


Fig. 3. Gain and NF performance with different input wavelengths at input power -30 dBm.

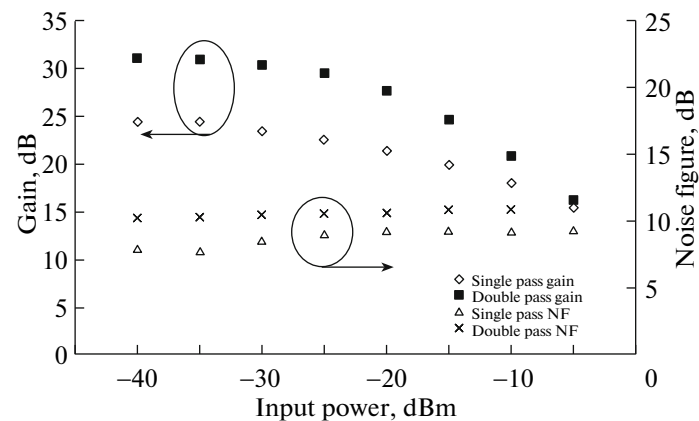


Fig. 4. Gain and NF performance against different input powers at a wavelength of 1500 nm.

neous broadening property of the SOA material gain, InGaAsP [13–17].

The gain and noise figure (NF) performance for both configurations against different input wavelengths at signal input power -30 dBm is shown in Fig. 3.

As can be seen from Fig. 3, the initial gain values of both the single- and double-pass systems are almost similar, with the difference between the gain achieved by the two systems amounting to approximately 2 to 3 dB until an input wavelength of 1500 nm. However, at longer wavelengths the gain of the single-pass systems drops, whereas the gain of the double-pass system continues to increase to a maximum value of 27.06 dB at a wavelength of 1516 nm, and improvement of 6.01 dB over that of the single-pass configuration. This gain performance can be explained from the ASE spectra of the two systems as given in Fig. 2. The NF of the single-pass system fares better from 1480 until 1520 nm in comparison to the double-pass system that has a better NF from 1460 to 1480 nm. The NF for the single-pass configuration at 1490 nm is about 11 dB and reduces to 8 dB at around 1520 nm.

Normally, the NF of an SOA is always high, and as such the values obtained can be considered a good achievement. The fluctuating NF of the double-pass system at the longer wavelength region is attributed to the polarization dependence gain (PDG) effect in the SOA.

Besides the above, the SOA characteristics of gain and NF at different signal input power levels from -40 to -5 dBm (simulating low to high powered input signals) are also measured at a fixed wavelength, in this case 1500 nm.

This is shown in Fig. 4 whereby the double-pass configuration shows a higher gain performance with respect to the single-pass configuration, having a maximum gain of 31.07 dB at an input signal power of -40 dBm. This is about 6.7 dB higher than the maximum gain of the single-pass configuration at this condition.

As the signal power level increases, the gain of the double-pass can be seen to always exceed that of the single-pass system, but at higher signal powers such as -5 dB, they tend to merge, which is largely due to saturation. The measured NF at different power levels

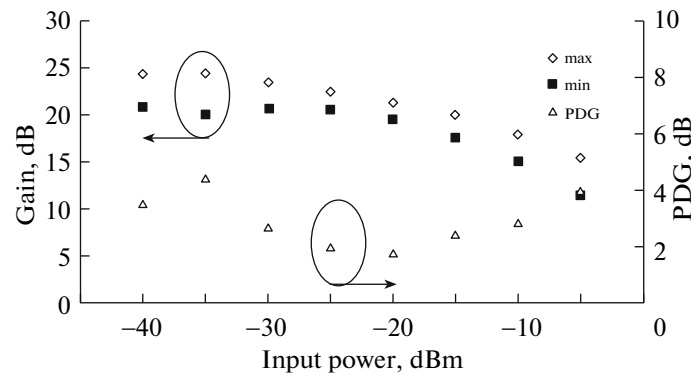


Fig. 5. The maximum and minimum gain obtained by changing the polarization controller and also the pdg at different input powers.

averages out to 10 dB with a similar profile to that of the single-pass configuration, which has a slightly lower noise figure of between 8 to 9 dB (a difference of only 1 to 2 dB). On the whole, this specific SOA can function as a good alternative for obtaining high gain amplification in the S-band region. As also observed in Fig. 4, the gain difference measured at 1500 nm and taking a particular case of an input power of -30 dBm does not correspond well with that of Fig. 3, where for the case of the input signal wavelength of 1500 nm and input signal power of -30 dBm. This difference is largely due to the PDG of all types of SOAs. This can be avoided by the careful adjustment of the polarization controllers.

The PDG characteristics against the input signal power are shown in the Fig. 5 by measuring the maximum and minimum gain of the SOA via the adjustment of the polarization controllers. The maximum and minimum gain is about 23.41 dB and 20.73 dB, respectively, whilst the PDG is 2.68 dB, taken at a signal power of -30 dBm for the case of a single-pass SOA configuration. This value can be larger for a double-pass configuration.

CONCLUSIONS

In conclusion this paper has demonstrated a high gain amplifier covering the S-band region from 1480 to 1520 nm. Within this range, the gain of the double-pass configuration obtained is higher than that of the single-pass configuration, with a gain value of 31.07 dB at an input signal power level of -40 dBm and a wavelength of 1500 nm. The NF of the double-pass system also fares better from 1480 until 1520 nm at 11 to 8 dB in comparison to the single-pass system, although the single pass system has a better NF at wavelengths shorter than 1480 nm. This system provides a good alternative for a high-gain and compact

amplifier in the S-band region, and this is the first of its demonstration to the knowledge of the authors.

REFERENCES

1. H. Chen, F. Babin, M. Leblanc, G. He, and G. W. Schinn, *J. Lightwave Technol.* **21**, 1629 (2003).
2. S. Aozasa, H. Masuda, M. Shimizu, and M. Yamada, *J. Lightwave Technol.* **25**, 2108 (2007).
3. G. G. Du, D. J. Li, H. W. Li, J. S. You, and S. C. Ruan, *Chin. Phys. Lett.* **23**, 2108 (2006).
4. J. Chang, Q. Wang, X. Zhang, Z. Liu, Z. Liu, and G. Peng, *Opt. Express* **13**, 3902 (2005).
5. S. W. Harun, N. K. Saat, and H. Ahmad, *IEICE Electron. Express* **2**, 182 (2005).
6. H. Ahmad, N. K. Saat, and S. W. Harun, *Laser Phys. Lett.* **2**, 369 (2005).
7. H. Seo, J. T. Ahn, B. J. Park, and W. J. Chung, *ETRI J.* **29**, 779 (2007).
8. M. H. Abu Bakar, M. A. Mahdi, M. Mokhtar, A. F. Abas, and N. Md. Yusor, *Laser Phys Lett.* **6**, 602 (2009).
9. H. Ahmad, A. H. Sulaiman, S. Shahi, and S. W. Harun, *Laser Phys.* **19**, 1002 (2009).
10. Q. Wang and Q. X. Yu, *Laser Phys. Lett.* **6**, 607 (2009).
11. S. W. Harun, M. Z. Zulkifli, M. R. Tamjis, and H. Ahmad, *J. Mod. Opt.* **55**, 3035 (2008).
12. C. H. Yeh, C. N. Lee, F. Y. Shih, and S. Chi, *Laser Phys. Lett.* **5**, 51 (2008).
13. S. Ritchie, in *Semiconductor Optoelectronic Materials, Proceedings of the IEEE Colloquium on Optoelectronic Materials* (1990), p. 411.
14. Y. H. Zhong, Z. X. Zhang, and X. Y. Tao, *Laser Phys.* **20**, 1756 (2010).
15. H. Ahmad, M. Z. Zulkifli, K. Thambiratnam, A. A. Latif, and S. W. Harun, *Laser Phys. Lett.* **6**, 539 (2009).
16. M. Z. Zulkifli, N. A. Hassan, N. A. Awang, Z. A. Ghani, and S. W. Harun, *Laser Phys. Lett.* **7**, 673 (2010).
17. J. E. Im, B. K. Kim, and Y. Chung, *Laser Phys.* **20**, 1918 (2010).

An ultra-wideband tunable multi-wavelength Brillouin fibre laser based on a semiconductor optical amplifier and dispersion compensating fibre in a linear cavity configuration

M.Z. Zulkifli, H. Ahmad, N.A. Hassan, M.H. Jemangin, S.W. Harun

Abstract. A multi-wavelength Brillouin fibre laser (MBFL) with an ultra-wideband tuning range from 1420 nm to 1620 nm is demonstrated. The MBFL uses an ultra-wideband semiconductor optical amplifier (SOA) and a dispersion compensating fibre (DCF) as the linear gain medium and nonlinear gain medium, respectively. The proposed MBFL has a wide tuning range covering the short (S-), conventional (C-) and long (L-) bands with a wavelength spacing of 0.08 nm, making it highly suitable for DWDM system applications. The output power of the observed Brillouin Stokes ranges approximately from –5.94 dBm to –0.41 dBm for the S-band, from –4.34 dBm to 0.02 dBm for the C-band and from –2.19 dBm to 0.39 dBm for the L-band. The spacing between each adjacent wavelengths of all the three bands is about 0.08 nm, which is approximately 10.7 GHz for the frequency domain.

Keywords: Brillouin fibre laser, ultra-wideband semiconductor optical amplifier, linear cavity, lasing comb, Stokes lines.

1. Introduction

One of the primary goals of continued research in optical communications systems is to increase the total transmission bit rate over long communication links in dense wavelength division multiplexing (DWDM) systems. Whilst the DWDM technology saves cost in terms of transmission infrastructure, multiple wavelength sources are still required to fully exploit the increased capacity of the DWDM-enabled system, and this can incur a significant cost (this would therefore negate any cost savings from the DWDM systems).

Multi-wavelength sources provide a viable cost-effective alternative over the use of multiple single-wavelength sources in DWDM systems, thus allowing the full capabilities of the DWDM system to be realised. Many linear and nonlinear methods can be employed to generate multiple wavelength sources from various gain media, including conventional erbium-doped fibre amplifiers (EDFAs), semiconductor optical amplifiers (SOAs) or via such nonlinear phenomenon as stimulated Brillouin scattering (SBS) [1–6]. The operational bandwidths of DWDM systems are determined by the operating regions of the optical amplifiers used in these systems.

Conventional EDFAs are particularly effective at the C-band (from 1525 to 1565 nm) or the L-band (from 1570 to 1610 nm) and can also be extended to the S-band (from 1460 to 1520 nm) using depressed cladding erbium-doped fibres (DC-EDFs) [7, 8]. Small signal gain amplifiers in the form of SOAs also allow for amplification in all three bands. S-band amplification can also be realised using fluoride doped fibres [such as in thulium-doped fibre Amplifiers (TDFAs)] or by such nonlinear methods as Raman amplification [9, 10]. They can also be used for fabrication of multi-wavelength sources when combined with such techniques as the Sagnac loop mirror (SLM), Brillouin's effect and also tunable band-pass filters (TBFs) in a fibre laser configuration to generate a multi-wavelength output. SLM techniques typically make use of a polarisation maintaining fibre (PMF) of a particular length as a mirror in order to attain a multi-wavelength lasing comb [2, 5, 6], whilst the SBS effect can be used by inserting a high intensity source signal into a high-nonlinear fibre, thus generating Brillouin Stokes which are then amplified by a linear gain medium, for example, by a fibre amplifier [3, 4, 11]. The SBS technique is the most common method employed in developing multi-wavelength sources; however, it suffers from certain shortcomings in terms of generating a wide tuning range for the multi-wavelength output due to the homogeneous broadening effect experienced by the fibre amplifier. Many research works have shown that the tuning range of multi-wavelength fibre lasers developed with the SBS technique are limited to within a certain bandwidth of transmission [12–14].

To overcome this limitation, we propose a multi-wavelength Brillouin fibre laser (MBFL) with an ultra-wide tuning range. An SOA is used in the proposed MBFL as the linear gain medium to amplify the generated Brillouin Stokes from the nonlinear gain medium, because the inhomogeneous broadening characteristics of the SOA are well-known to be able to overcome the limitations of fibre-based optical amplifiers in terms of the range of wavelengths that can be amplified [1].

2. Experimental setup

Figure 1 shows the proposed setup for the ultra-wide band MBFL. The MBFL consists of a 7.7-km-long dispersion compensating fibre (DCF) that acts as a nonlinear gain medium. The DCF has a dispersion of -584 ps nm^{-1} and an insertion loss of approximately $6.66 \times 10^{-3} \text{ dB m}^{-1}$. An ultra-wide bandwidth SOA is used as a linear gain medium to the MBFL system. A tunable laser source (TLS) acts as a Brillouin pump (BP). The BP enters the system through one of the 50% ports of 50:50 fused coupler. Upon entering the 50:50 coupler, the TLS signal then travels to the DCF, where it interacts with the nonlinear gain medium and generates a multi-wavelength out-

M.Z. Zulkifli, H. Ahmad, N.A. Hassan, M.H. Jemangin Photonics Research Center (Department of Physics), University of Malaya, 50603 Kuala Lumpur, Malaysia; e-mail: mohdzamani@um.edu.my; S.W. Harun Department of Electrical Engineering, Faculty of Engineering, University of Malaya, 50603 Kuala Lumpur Malaysia

Received 19 January 2011

Kvantovaya Elektronika 41 (7) 602–605 (2011)

Submitted in English

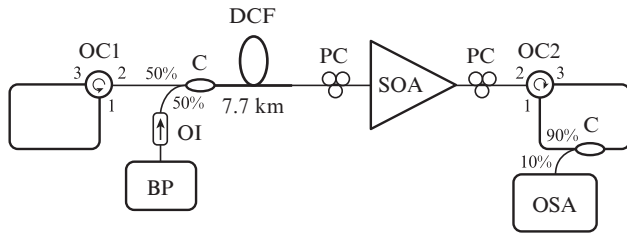


Figure 1. Experimental setup of the proposed MBFL: (BP) Brillouin pump; (OI) optical isolator; (OC) optical circulator; (DCF) dispersion compensating fibre; (PC) polarisation controller; (SOA) semiconductor optical amplifier; (C) coupler; (OSA) optical spectrum analyser.

put comb through the SBS process. The multi-wavelength output comb exits the DCF and enters the linear laser cavity [which is constructed using two optical circulators (OCs) with both ends connected to the BFL system designated as OC1 and OC2] as shown in Fig. 1. The OCs are configured to act as mirrors by connecting port 1 to port 3 whilst port 2 is connected to the input and output of the BFL system. The multi-wavelength signal is amplified by the SOA placed within the linear cavity. The SOA is manufactured by Alphion and has an operational amplification bandwidth of 1460 nm to 1620 nm, which is able to cover the S-, C- and L-band regions. A 90:10 fused coupler is placed between port 1 and port 3 of OC2 to extract a 10% portion of the signal for analysis by an optical spectrum analyser (OSA) with a resolution of 0.02 nm.

The SBS process is as follows: the BP signal is emitted by the TLS and travels into the linear cavity via the 50% port of the optical coupler. It then passes to the common port of the 50:50 fused coupler and continues onward to the DCF, where it will interact with the nonlinear gain medium to generate the first Brillouin Stokes. The electrostriction process that arises inside the nonlinear gain medium results in the production of phonon waves, which then contribute to the backscattered signal. This backscattered signal is corollary from the incidence of the BP with the phonon waves. The first Stokes from the backscattered signal will travel in the opposite direction of the BP towards OC1 and is then reflected back into the cavity where it enters the DCF and the interaction process repeats to generate the second Stokes. This process of oscillation continues, with each subsequent Stokes wavelength generated at a slightly lower power than the previous Stokes until the Stokes generates no longer the threshold power required for the SBS process to continue. The obtained multi-wavelength comb makes many passes through the SOA via the linear cavity configuration, and will be amplified to the point of lasing where it now becomes a multi-wavelength laser.

3. Results and discussions

Figure 2 shows the amplified spontaneous emission (ASE) spectrum of the ultra-wide band SOA at different injection currents. The observed ASE spectrum covers the region from 1400 nm to 1650 nm and can be used to gauge the gain pattern of the proposed MBFL.

It can be seen that the ASE output power generated by the SOA shifts towards the shorter wavelength region as the injection current is increased. This is attributed to the energy absorbed by the excited electrons from the lower energy level state to the higher energy level state, which is then de-excited

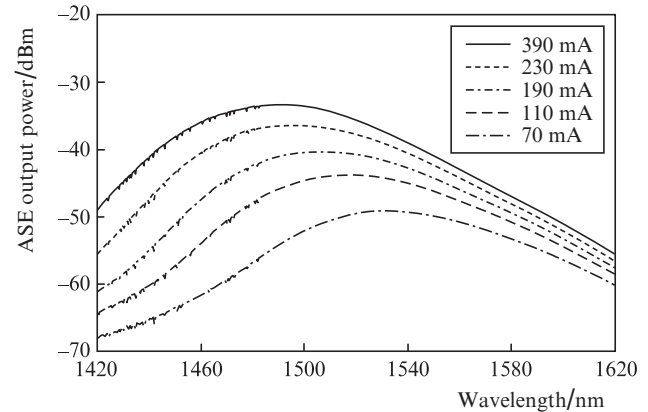


Figure 2. ASE output power spectrum of the SOA at different injection currents.

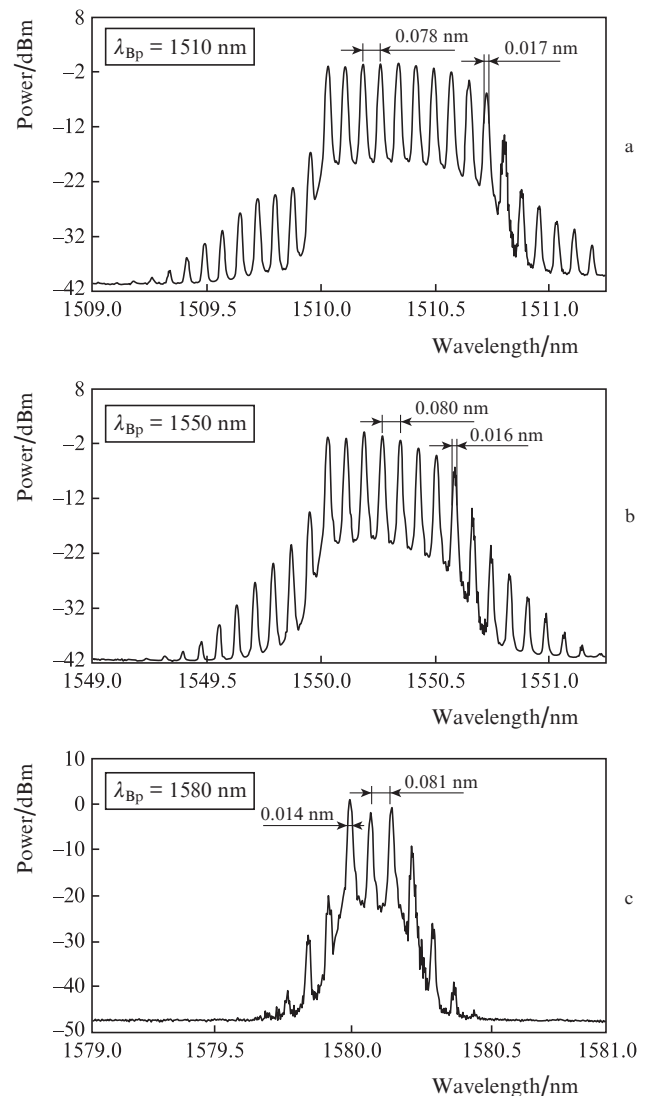


Figure 3. Lasing combs generated with a Brillouin pump wavelength of (a) 1510, (b) 1550, and (c) 1580 nm at 10.6 dBm.

and emitted as a photon with the same energy as the excited electron. The increase in the energy of the photon results in shorter wavelengths. Figure 3 shows multi-wavelength comb

spectrum generated by BP wavelengths of 1510 nm, 1550 nm, and 1580 nm with a power of 10.6 dBm.

The injection current of the SOA is set to 390 mA as to provide the maximum linear amplification width (see Fig. 2). At a BP wavelength of 1510 nm, 10 Brillouin Stokes are generated. The peak powers of the lasing wavelengths in the S-band are observed to be in the range from -5.94 dBm to -0.41 dBm, with wavelength spacings of approximately 0.078 nm and a 3-dB linewidth of approximately 0.017 nm as obtained from the OSA. In the C-band, 8 Brillouin Stokes with peak powers of -4.34 dBm to 0.02 dBm and wavelength spacings of approximately 0.080 nm with a 3-dB linewidth of approximately 0.016 nm are observed. In the L-band, 3 Brillouin Stokes with peak powers ranging from -2.19 dBm to 0.39 dBm are obtained with wavelength spacings of approximately 0.081 nm between each consecutive Stokes line observed and a 3-dB linewidth of approximately 0.014 nm. The low number of Brillouin Stokes in Fig. 3c is attributed to the low ASE output power (and henceforth low gain) in that region (Fig. 2). One can see that the number of generated Brillouin Stokes is higher in the shorter wavelength region but reduces towards the longer wavelength region. This is attributed to the gain pattern of the ultra-wide band SOA, where the higher gain in the shorter wavelength region generates higher peak powers, and thus generates Stokes via the Brillouin effect. Essentially, this shows that the higher the gain, the higher the peak power achieved so as to overcome the threshold power and generate more Stokes via the Brillouin effect.

Further analysis of the output of the proposed MBFL shows that the generated multi-wavelength combs with the wavelengths shorter than the BP wavelengths (anti-Stokes) are caused by effect of four-wave mixing (FWM) as shown in the three cases. This is largely due to the high nonlinear properties of the SOA. The spacing between each adjacent wavelength is computed to be approximately 0.08 nm or approximately 10.7 GHz in the frequency domain. As a point to note, less anti-Stokes are generated using EDFAs as compared to the SOA. Figure 4 shows the number of lasing lines in the generated multi-wavelength comb at different BP wavelengths, and it can be inferred that the peak power of the lasing wavelengths from the generated multi-wavelength comb closely matches the ASE spectrum within the same wavelength range.

Since the ultra-wideband SOA used in this experiment covers a range of 1480 nm to 1610 nm, the Brillouin effect is

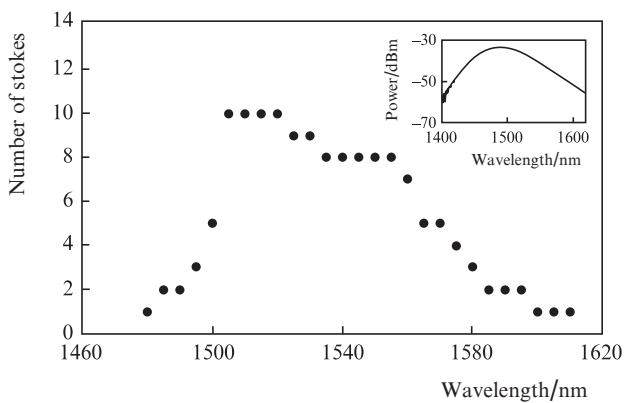


Figure 4. Total number of Stokes in the lasing comb, observed within 1480 nm and 1610 nm at a BP power of 10.6 dBm. The inset is the ASE spectrum of the ultra-wideband SOA with an injection current of 390 mA.

also observed to be present within this wavelength region, as the SOA can provide the necessary amplification for the SBS process to continue. The total number of Stokes lines for each BP wavelength is plotted in Fig. 4. It can be inferred that the most Stokes lines are generated at a wavelength range from 1500 nm to 1520 nm, which is approximately 10 Stokes lines.

The MBFL system is tested at intervals of 10 min for a period of 70 min at room temperature to determine its stability and reliability. Actually, this system was left running for more than 10 h during the total duration of this experiment. The output of the system for different bands is presented in Fig. 5. It can be seen from Fig. 5 that the output of the MBFL is stable, with almost no fluctuations or variations in the output power. This ensures that the system is stable and can be used for various applications.

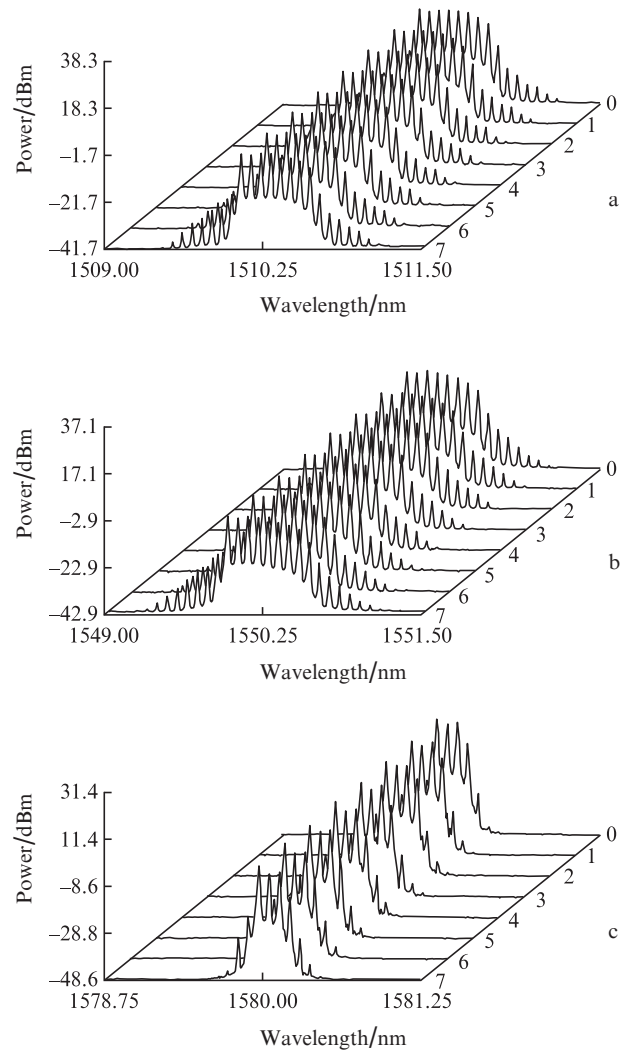


Figure 5. Spectra of the proposed MBFL at 10-min intervals over a testing period of 70 min for the (a) S-, (b) C- and (c) L-bands.

4. Conclusions

In this paper, we have proposed and demonstrated a novel MBFL with a wide tuning range from 1480 nm to 1620 nm that covers the S-, C- and L-bands for optical communications. A laser comb with 10 Brillouin Stokes has been achieved in the S-band, with a wavelength spacing of 0.078 nm and a

3-dB linewidth of 0.017 nm. The output powers from peak to peak vary from -5.94 dBm to -0.41 dBm. For the C-band region, 8 Stokes lines are generated with a wavelength spacing of 0.080 nm and 3-dB linewidth of 0.016 nm. The peak to peak output power varies between -4.34 dBm to 0.02 dBm. In the L-band region, 3 Stokes lines are observed which is due to the low ASE output power because of the gain distribution of the SOA. The wavelength spacing between these lines is approximately 0.081 nm with a 3-dB linewidth of 0.014 nm. The values of the output power are noted to be within the range of -2.19 dBm to 0.39 dBm. Continued running of the systems from 70 min to more than 10 h demonstrates the stability and reliability of the system, with power fluctuations of less than 2 dB.

References

1. Connelly M.J. *Semiconductor Optical Amplifiers* (Dordrecht: Kluwer Academic Publishers, 2004).
2. Zulkifli M.Z., Hassan N.A., Awang N.A., Ghani Z.A., Harun S.W., Ahmad H. *Laser Phys. Lett.*, **7**, 1 (2010).
3. Huang Y., Zhan L., Ji J.H., Luo S.Y., Xia Y.X. *Opt. Commun.*, **281**, 452 (2008).
4. Ahmad H., Zulkifli M.Z., Latif A.A., Thambiratnam K., Harun S.W. *Laser Phys.*, **19** (12), 2188 (2009).
5. Dong X.P., Li S., Chiang K.S., Ng M.N., Chu B.C.B. *Electron. Lett.*, **36** (19), 1609 (2000).
6. Ahmad H., Shahabuddin N.S., Rahman A.A., Thambiratnam K., Harun S.W. *J. Modern Opt.*, **55** (14), 2179 (2008).
7. Harun S.W., Saat N.K., Ahmad H. *IEICE Electron. Express*, **2** (6), 182 (2008).
8. Caspary R., Unrau U.B., Kowalsky W. *Proc. 5th Intern. Conf. on Transparent Optical Networks* (Warsaw, 2003) Vol. 1, pp 236–242.
9. Aozasa S., Masuda H., Shimizu M. *J. Lightwave Technol.*, **24** (10), 3842 (2006).
10. Tanabe S., Tamaoka T. *J. Non-Cryst. Sol.*, **326–327**, 283 (2003).
11. Shahi S., Harun S.W., Shahbuddin N.S., Shirazi M.R., Ahmad H. *Opt. Laser Technol.*, **41**, 198 (2009).
12. Zhou D., Pruchal P.R., Glesk I. *IEEE Photon. Technol. Lett.*, **10** (6), 781 (1998).
13. Huang Y., Zhan L., Ji J.H., Luo S.Y., Xia Y.X. *Opt. Commun.*, **281**, 452 (2008).
14. Al-Mansoori M.H., Abd-Rahman M.K., Mahamd Adikan F.R., Mahdi M.A. *Opt. Express*, **13** (9), 3471 (2005).

S–C–L triple wavelength superluminescent source based on an ultra-wideband SOA and FBGs

H. Ahmad, M.Z. Zulkifli, N.A. Hassan, F.D. Muhammad, S.W. Harun

Abstract. We propose and demonstrate a wide-band semiconductor optical amplifier (SOA) based triple-wavelength superluminescent source with the output in the S-, C- and L-band regions. The proposed system uses an ultra-wideband SOA with an amplification range from 1440 to 1620 nm as the linear gain medium. Three fibre Bragg gratings (FBGs) with centre wavelengths of 1500, 1540 and 1580 nm are used to generate the lasing wavelengths in the S-, C- and L-bands respectively, while a variable optical attenuator is used to finely balance the optical powers of the lasing wavelengths. The ultra-wideband SOA generates an amplified spontaneous emission (ASE) spectrum with a peak power of –33 dBm at the highest SOA drive current, and also demonstrates a down-shift in the centre wavelength of the generated spectrum due to the spatial distribution of the carrier densities. The S-band wavelength is the dominant wavelength at high drive currents, with an output power of –6 dBm as compared to the C- and L-bands, which only have powers of –11 and –10 dBm, respectively. All wavelengths have a high average signal-to-noise ratio more than 60 dB at the highest drive current of 390 mA, and the system also shows a high degree of stability, with power fluctuations of less than 3 dB within 70 min. The proposed system can find many applications where a wide-band and stable laser source is crucial, such as in communications and sensing.

Keywords: ultra-wideband semiconductor optical amplifier, S-, C-, L-band superluminescent source.

1. Introduction

Multi-wavelength fibre lasers (MWFLs) have recently attracted significant interest as compact and cost-effective transmission sources for a variety of applications in optical communications [1–3], optical sensing [4, 5], optical instrumentation [6] and even microwave photonic systems [7]. Conventionally, erbium doped fibres (EDFs) are employed as the gain media for MWFLs due to their large gain, high saturation power and relatively low noise figure, thus generating high quality signals.

Currently, most EDF-based MWFLs are optimised to operate at the C-band region of 1530 nm to 1565 nm [8]. However, the recent expansion of the communications bandwidth into the L-band region of 1565 nm to 1625 nm has necessitated the development of cost effective wavelength

sources for this bandwidth. For the EDF-based MWFL to operate at the L-band region, an additional length of an EDF must be added to the MWFL. The drawback of this approach is the lower gain and higher noise figure encountered by the system, thereby reducing the overall quality of the lasing wavelength generated [9, 10]. Furthermore, the simultaneous lasing of both C- and L-band signals in the MWFL cannot be achieved by conventional means, and requires special techniques such as the four-wave-mixing effect [11] or the use of specialty fibres such as bismuth-doped fibres [12] and highly nonlinear fibres [13] as well as complex configurations such as an EDF-Raman hybrid [14]. In addition, researchers are now looking towards the S-band region of 1480 nm to 1530 nm for future transmission needs, and S-band MWFLs have therefore attracted significant interest as low-cost sources for transmission in the S-band region. However, as was the case with the L-band MWFL, the S-band MWFL cannot be implemented by conventional means, and requires specialised fibres such as depressed-cladding EDFs [15] or special techniques such as Brillouin scattering [16] in order to generate lasing wavelengths. As a result, it is very difficult to develop an ultra-wideband MWFL capable of generating simultaneous lasing wavelengths in the S-, C- and L-band regions using a single gain medium.

Besides MWFLs, there is also a need for multi-wavelength superluminescent sources (MWSS) that can find useful applications in the areas of sensors and also act as a source of probe signals for the S-, C- and L-bands. This will complement the existing fibre lasers and provide a low-cost, ultra-wideband signal source. The semiconductor optical amplifier (SOA) is a highly suitable candidate for the generation of an ultra-wide band MWSS, particularly because of its inhomogeneous broadening properties. Unlike the EDF, which has homogenous broadening properties, the SOA allows for the simultaneous amplification of multiple wavelengths without the detrimental effects of mode-competition and unstable signal outputs, covering a range of 1440 nm to 1620 nm. This range covers the S-, C- and L-bands and allows for the development of compact and low cost SOA-based MWSS without the need for complex configurations or special techniques.

In this work, a triple wavelength MWSS is proposed and demonstrated utilising an ultra-wideband SOA as the linear gain medium and fibre Bragg gratings with centre wavelengths of 1500, 1540 and 1580 nm, respectively, as wavelength filters for the simultaneous generation of the S-, C- and L-band superluminescent outputs. The proposed system is analysed for its performance in terms of power and signal-to-noise ratio (SNR), and also for its stability over extended periods of time. The proposed triple-wavelength MWSS will have many potential applications in communications and sensing tasks.

H. Ahmad, M.Z. Zulkifli, N.A. Hassan, F.D. Muhammad, S.W. Harun
Photonics Research Centre, University of Malaya, 50603 Kuala Lumpur, Malaysia; e-mail: harith@um.edu.my;

Received 24 October 2012; revision received 31 March 2013
Kvantovaya Elektronika 43 (10) 923–926 (2013)
Submitted in English

2. Experimental setup

Figure 1 shows the experimental setup of the proposed S–C–L MWSS. The MWSS consists of two main components: a ring cavity which provides gain for the superluminescent output and a filtering mechanism to obtain the S-, C- and L-wavelengths.

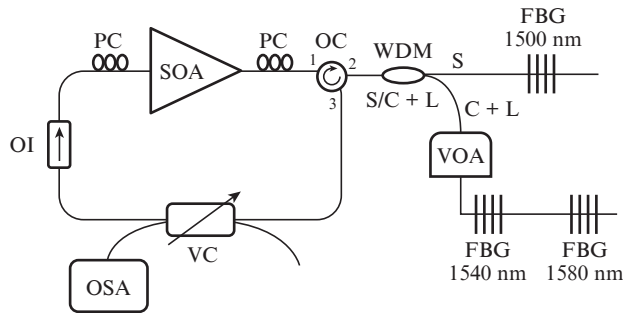


Figure 1. Experimental setup for a triple wavelength S–C–L-band superluminescent source:

(PC) polarisation controller; (OC) optical circulator; (WDM) wavelength division multiplexer; (OI) optical isolator; (VOA) variable optical attenuator; (VC) variable coupler; (OSA) optical spectrum analyser.

The gain medium of the S–C–L MWSS is an ultra-wideband SOA, with an amplification bandwidth of more than 220 nm from 1400 nm to 1620 nm. The active layer of the SOA is an InGaAsP substrate, which provides a gain bandwidth of 160 nm and a polarisation dependent gain of 1.5 dB. Initially, the SOA generates the amplified spontaneous emission (ASE) spectrum, which then travels from the output of the SOA through a polarisation controller (PC) and then to port 1 of the optical circulator (OC). The ASE spectrum is then emitted at port 2 of the OC, where it now encounters the common port of an S/C + L wavelength division multiplexer (WDM). Here, the ASE spectrum is split into two spectral components, with one spectral component covering the S-band region, while the second spectral component covering the C- and L-band regions. The S-band spectrum is channelled to a 1500-nm fibre Bragg grating (FBG), which reflects only a single superluminescent output at a wavelength of 1500 nm. The FBG has a reflectivity of 99%, with a spectrum width of about 1.5 nm (Fig. 2), which is shown for wavelength of

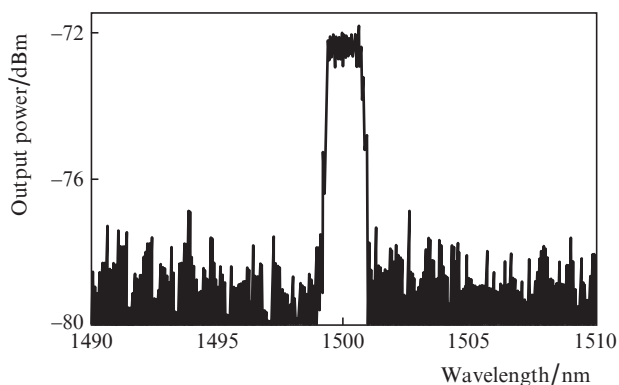


Figure 2. FBG reflectivity at 1500 nm, having a linewidth of about 1.5 nm and a reflectivity close to 99%.

1500 nm. A similar profile is seen for wavelengths of 1540 and 1580 nm.

In the same manner, the second spectral component (which is the C- and L-band) is channelled through a variable optical attenuator (VOA) towards two FBGs, which reflect two superluminescent wavelengths at 1540 and 1580 nm. The VOA is used to control the power of the two superluminescent wavelengths at 1540 nm and 1580 nm so that it is the same as that of the 1500-nm signal. The VOA is used to allow for power adjustments because there is a tendency of having a higher oscillation power in the C- and L-band region, even though peak ASE of the SOA is higher in the S-band region. The reflected signals at 1500, 1540 and 1580 nm now travel to the S/C + L WDM and are combined to form a triple superluminescent wavelength spectrum which then travels towards port 2 of the OC, which is then emitted at port 3. This triple wavelength will then oscillate in the ring cavity through the 2×2 variable coupler (VC) and the optical isolator (OI), which will force the oscillation in a clock-wise direction as well as another PC. The variable coupler will allow for different coupling ratios, where a portion of the oscillating signal is then extracted for analysis using an optical spectrum analyser (OSA) with a resolution of 0.02 nm.

3. Result and discussions

Figure 3 shows the ASE spectra of the ultra-wideband SOA at different drive currents. As can be seen, the power of the ASE spectrum obtained at a drive current of 70 mA forms a bell shape, rising gently from approximately –65 dBm at 1440 nm to a peak value of about –49 dBm at 1540 nm, before slowly decreasing to –60 dBm at a wavelength of 1620 nm. As the drive current increases to 150 mA, the same spectral shape is obtained, rising from –54 dBm at 1440 nm to –40 dBm at 1507 nm before dropping to about –57 dBm at 1620 nm. At 270 mA, the ASE spectrum obtained has a power of –45 dBm at 1440 nm, rising to –35 dBm at 1492 nm before dropping again to –55 dBm at 1620 nm, while at the highest drive current of 390 mA, the spectrum obtained has a power of –41 dBm at 1440 nm, rising to –33 dBm at 1486 nm before dropping again to approximately –55 dBm at 1620 nm.

From the spectra of Fig. 3, two important observations can be made, which will in turn determine the behaviour of the superluminescent source during the later stages of this work. The first observation is that at lower drive currents, a

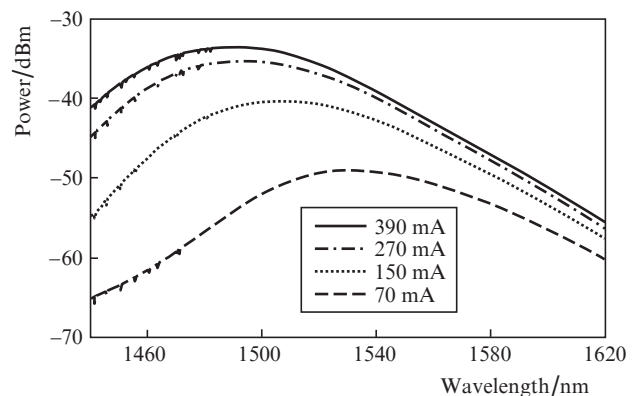


Figure 3. ASE spectra of the ultra-wide band SOA at different injection currents.

small increase in the drive current will result in a large jump in the power of the ASE spectrum generated. However, as the drive current is increased, the resulting increase in the ASE spectra becomes smaller and smaller; this is because of the limited number of carriers that the SOA can sustain at any given time. As such, at the lower drive currents, an increase in the drive current will translate into the significant generation of carriers in the SOA. However, at higher drive currents (approaching the maximum drive current of the SOA) any increase in the drive current generates only few additional carriers. This causes the SOA to operate in a saturated condition and allowing only a slight increase in the power of the ASE spectrum [3]. The second important observation is the shifting of the peak wavelength of the ASE spectra towards the shorter wavelength region as the drive current increases. For instance, at 70 mA, the peak wavelength is approximately 1530 nm, with a higher output power from 1530 nm towards 1620 nm as compared to the power obtained in the shorter wavelength region of 1440 nm to 1530 nm. As the current increases, the peak wavelength shifts towards a shorter wavelength, moving towards 1500 nm and for further increases the wavelength peaks around 1480 nm, with lower output power at the longer wavelengths (from 1520 nm to 1620 nm). This occurs as a result of the distribution of the carrier densities; at lower input powers, the carrier density has a symmetrical spatial distribution, peaking at the centre of the SOA and tailing off towards the input and output facets, thus causing the ASE to peak at the centre region. This is the same characteristic as observed in the case of black body radiation [17].

Figure 4 shows the power of the superluminescent output wavelengths in the S-C-L superluminescent source at different drive currents. The generation of the three, well defined superluminescent wavelengths is achieved when the SOA is operated at a high drive current, for instance at 270 mA, and the VOA is used to adjust the output power of the C- and L-band wavelengths such that the power level is the same as that of the S-band wavelength. Subsequently, the characteristic measurements are done by driving the SOA at low drive currents and increasing the current. It must be noted that the VOA can be fine-tuned to have all three wavelengths with equal power. At the lowest drive current of 70 mA, three superluminescent wavelengths are obtained at 1500, 1540 and 1580 nm, with respective peak powers of -58, -56 and -53 dBm.

As the SOA drive current is increased to 170 mA, the superluminescent wavelength obtained at the S-band (1500 nm) increases only marginally to -42 dBm, whereas the super-

luminescent wavelengths at the C-band and L-band (1540 and 1580 nm) increase significantly, to -16 and -12 dBm, respectively. A further increase in the SOA drive current to 270 mA brings the three superluminescent wavelengths to -12, -11 and -10 dBm respectively for the wavelengths of 1500, 1540 and 1580 nm. At the highest SOA drive current of 390 mA, there is an increase in the S-band output power, from -12 dBm (270 mA) to -6 dBm, whereas for the case of the C- and L-bands the power remains relatively unchanged. These results are taken without any adjustment to the VOA. The increase in the output power in the shorter wavelength region is due to the ASE spectrum as given in Fig. 3, which has a broad peak towards the shorter wavelength as the drive current increases. The average signal-to-noise ratios (SNRs) of the three generated wavelengths at the lowest drive current of 70 mA is approximately 20 dB, and as the drive current increases to 170, 270 and finally 370 mA, the average SNR also increases to 48, 60 and 62 dB respectively. This correlates with the increase in the superluminescent wavelengths output power at different drive currents. It can also be inferred that the change in the SNR is not linear: It faster at low drive currents, whereas its increase at higher drive currents is only marginal.

Figure 5 shows the measured power as a function of the SOA drive current at different wavelength regions. It can be seen that the C- and L-bands have a lower threshold current of 70 mA, whereas the threshold current for the S-band region is higher at 170 mA.

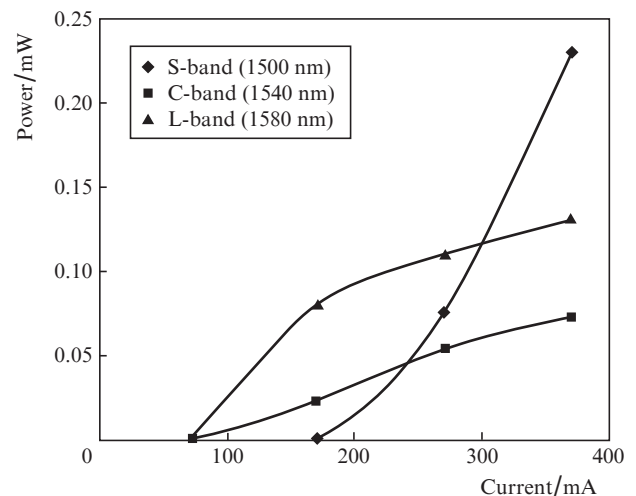


Figure 5. Output power of the SOA as a function of the drive current at different operating wavelengths.

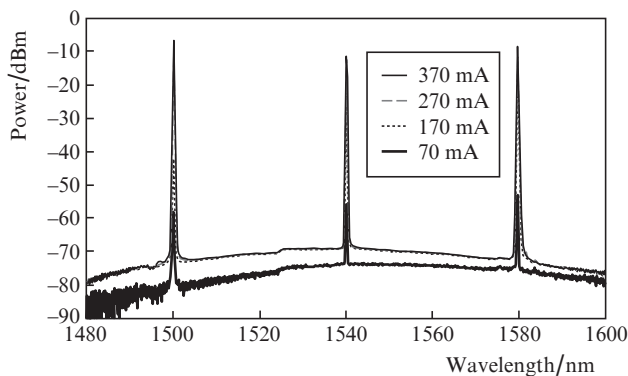


Figure 4. Simultaneous generation of the triple wavelength output at the S-, C- and L-band at different SOA drive currents.

Also, the L-band signal shows a steeper power slope of $8.0 \times 10^{-4} \text{ mW mA}^{-1}$ as compared to the plot of the C-band signal, which has a slope of $2.4 \times 10^{-4} \text{ mW mA}^{-1}$. However, at about 170 mA, the slope of the L-band signal plateaus off with a value of about $2.5 \times 10^{-4} \text{ mW mA}^{-1}$. The S-band signal on the other hand has a higher threshold value of 170 mA as compared to the C- and L-band signals, as well as a slope of approximately $7.5 \times 10^{-4} \text{ mW mA}^{-1}$ for the region between 170 and 270 mA. However, the slope efficiency of the S-band signal increases significantly to $1.5 \times 10^{-3} \text{ mW mA}^{-1}$ after a drive current of 270 mA. At the lower drive currents, the L-band signal initially gives the highest output power, followed by the C-band signal and finally the S-band signal. However, at approxi-

mately 235 mA, the power of the S-band signal increases to equal the power of the C-band signal. At about 280 mA, the S-band signal now becomes as strong as the power of the L-band signal, and at higher drive currents the S-band signal now becomes the dominant signal, with a peak power of almost double the L-band signal and three times larger than that of the C-band signal.

Figure 6 shows the stability of the proposed triple wavelength superluminescent source over a period of 70 minutes, with the spectrum of the lasing wavelengths obtained in 10-minute intervals.

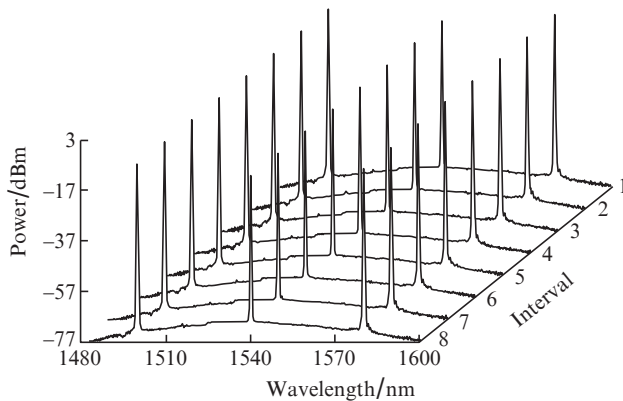


Figure 6. Stability test for the triple wavelength superluminescent source in 10 min time interval. $P_{\text{REF}} = -17$ dBm.

It can be seen that the proposed system is highly stable, with minimal fluctuations of less than 3 dB over the test period. As such, the proposed superluminescent source can be used as a viable source for applications such as communications and sensing.

4. Conclusions

A triple-wavelength superluminescent source based on a wide-band SOA and operating in the S-, C- and L-band regions is proposed and demonstrated. The proposed superluminescent source utilises a wide-band SOA with a broad amplification range of 1440 to 1620 nm as the gain medium, and three FBGs at 1500, 1540 and 1580 nm to generate the superluminescent wavelengths. The ASE generated by a ultra-wideband SOA which has a peak power of -49 dBm at 1540 nm at the lowest drive current and a peak power of -33 dBm at 1486 nm at the highest SOA drive current, thereby indicating a wavelength down-shift as the drive current increases. This is attributed to the distribution of the carrier densities in the SOA, akin to black-body radiation. The power of the lasing wavelengths also increases as the drive current is increased, with the wavelengths at 1540 nm and 1580 nm initially increasing faster than the lasing wavelength at 1500 nm. However, at high drive currents, the 1500 nm wavelength is observed to have the highest output power of -6 dBm, while the 1540 and 1580 nm wavelengths have output powers of -11 and -10 dBm respectively, thereby becoming the dominant wavelength. All wavelengths show a good average SNR of more than 60 dB at the highest drive current of 390 mA. The system also shows a high degree of stability, with power fluctuations of less than 3 dB over a time period of 70 minutes. Therefore, the proposed system will have many applications in tasks such as

communications and sensing, where a wide-band and stable SOA-based MWSS can be applied.

Acknowledgements. We would like to thank the University of Malaya for providing the funding this project under the UMRG Grants RP019-2012A and RG143-12AET.

References

1. Lee S.L., Jang I.F., Wang C.Y., Pien C.T., Shih T.T. *IEEE J. Sel. Top. Quantum Electron.*, **6**, 197 (2000).
2. Zhang A., Liu H., Demokan M.S., Tam H.Y. *IEEE Photonics Technol. Lett.*, **17**, 2535 (2005).
3. Ahmad H., Thambiratnam K., Sulaiman A.H., Tamchek N., Harun S.W. *Laser Phys. Lett.*, **5**, 726 (2008).
4. Achaerandio E., Jarabo S., Abad S., Amo M.L. *IEEE Photonics Technol. Lett.*, **11**, 1644 (1999).
5. Chaudhari A.L., Shaligram A.D. *Sensors and Actuators A: Phys.*, **100**, 160 (2002).
6. Ye W., Liu W., Chen T., Yang D.Z., Shen Y.H. *Laser Phys.*, **20**, 1636 (2010).
7. Fu J., Chen D., Sun B., Gao S. *Laser Phys.*, **20**, 1907 (2010).
8. Harun S.W., Rahman F.A., Dimyati K., Ahmad H. *Laser Phys. Lett.*, **3**, 495 (2006).
9. Islam M.N., Hwang S., Song K.W., Song K.U., Park S.H., Nilsson J., Cho K. *Electron. Lett.*, **37**, 1539 (2001).
10. Zhou Y.W. *Laser Phys.*, **22**, 753 (2012).
11. Liu X., Zhao W., Liu H., Zou K., Zhang T., Lu K., Sun C., Wang Y., Ouyang X., Chen G., Hou X. *J. Opt. A: Pure Appl. Opt.*, **8**, 601 (2006).
12. Shahabuddin N.S., Harun S.W., Zulkifli M.Z., Thambiratnam K., Ahmad H. *J. Modern Opt.*, **55**, 1345 (2008).
13. Im J.E., Kim B.K., Chung Y. *Laser Phys.*, **21**, 540 (2011).
14. Chen D., Qin S. *Microwave Opt. Technol. Lett.*, **49**, 2339 (2007).
15. Zulkifli M.Z., Jemangin M.H., Harun S.W., Ahmad H. *Laser Phys.*, **21**, 1633 (2011).
16. Ahmad H., Saat N.K., Harun S.W. *Laser Phys. Lett.*, **2**, 369 (2005).
17. Connelly M.J. *IEEE J. Quantum Electron.*, **37**, 439 (2001).